Advances in Electrospun Nanofibers

Guest Editors: Niranjan Patra, Miroslav Cernik, and Marco Salerno

Advances in Electrospun Nanofibers

Advances in Electrospun Nanofibers

Guest Editors: Niranjan Patra, Miroslav Cernik, and Marco Salerno

Editorial Board

Contents

Editorial
Advances in Electrospun Nanofibers

Niranjan Patra,[1] Miroslav Cernik,[2] and Marco Salerno[3]

[1]*Department of Materials, Imperial College London, London SW7 2AZ, UK*
[2]*Centre for Nanomaterials, Technical University of Liberec, 461 17 Liberec, Czech Republic*
[3]*Nanophysics Department, Istituto Italiano di Tecnologia, 16163 Genova, Italy*

Correspondence should be addressed to Niranjan Patra; n.patra@imperial.ac.uk

With this special issue of *AENF* we are pleased to present contributions to the exciting field of electrospinning of nanofibers and its applications. Among different methods for producing one-dimensional (1D) nanostructures, electrospinning is the simplest, most economically viable, and commercially successful process of generating nanofibers and is continuously rising in research and developments. Rapid progress is being made especially in the area of electrospun nanofiber applications forming a bridge among materials science, biomedicine, and electronics. In this special issue, we have seven excellent contributions forming an interesting collection of works on nanofibers spinning and its disparate applications in biomedicine, decontamination process, and materials science.

A review article "Carbon Nanotube and Graphene Based Polyamide Electrospun Nanocomposites" comes from F. Navarro-Pardo et al., where the authors present a nice overview of the process of forming amide electrospun nanocomposites fibers using two well-known carbon nanostructures, namely, CNTs or graphene, as the fillers, which qualify for diverse field of applications like drug delivery system, biosensors, solar cells, electronic devices, transparent electrodes, or membrane filtration. This review elaborates the process parameters, especially how the selection of solvent is important for the dispersion of carbon nanostructures in the matrix to form nanofibers. The authors also discuss electrical, optical, and mechanical properties as well as crystallinity of the composite obtained by a number of research groups. The comprehensive picture given by F. Navarro-Pardo et al. may help to understand the structure-property relationship of polyamide/CNT/graphene based spun fiber composites

from which in the future new applications would probably stem given their exceptional properties.

The use of NaCl solution as shell fluid to prepare medicated nanofibers in a modified coaxial electrospinning is presented by Y. Wu et al. These authors have modified and developed a coaxial electrospinning to produce medicated nanofibers with the help of NaCl as shell fluid for ease of preparation. They found that the shell-to-core ratio of the fluid flow rate plays an important role in controlling the fiber diameter and morphology, as observed by optical and scanning electron microscopy. The fabricated nanofibers have a fine compatibility with sodium Diclofenac and can elute the drug in neutral condition, suggesting potential application in colon targeted drug release. Y. Wu et al. have also carried out ex vivo tests to prove that the mats enhance the transmembrane delivered drug. Based on the above facts, the authors claim development of a potential medicated nanomaterial with tunable diameters and improved functional performance.

S. Seo et al. present an overview of the applications of spun nanofibers in dentistry. They have especially focused on polymeric nanofibers or bioceramic nanoparticle-incorporated nanofibers. The article shows how these advanced materials have contributed to highly promotive cell homing behavior and improved dental tissue regeneration. It also describes how the spun nanofibers play a versatile role in controlled release of biomolecule therapeutics (i.e., growth factors) or modification with adhesive biomolecules (i.e., fibronectin and RGD sequence) and contributes to further improved dental regeneration. Whereas a number of experiments on nanofibrous scaffolds in the in vitro and in vivo study

have already been conducted, clinical customization to each patient's defect is still difficult. Additionally, since dental tissue degeneration may come from biological disorders, further studies of biological interplay between electrospun nanofiber and cells derived from compromised dental tissue are essential. Further studies will help to understand the biological effect of nanofibers, which can conclusively elaborate techniques to customize nanofiber scaffolds and categorize clinical defects into several groups for their customization. The work of S. Seo et al. sheds light on recently applied spun nanofibers in dentistry from process to applications.

The work of T. Jiříček et al. entitled "Flux Enhancement in Membrane Distillation Using Nanofiber Membranes" studied the membrane distillation. Spun PVDF nanofibers were tested under various conditions on a direct contact MD unit to find the optimum conditions for flux, which is compared with the commercially available membrane of PTFE, PE, and PES. Membrane thickness proved to be a crucial parameter when fluxes are concerned. They have found that the thinner membranes have higher fluxes and lower distillate purity. Also higher energy losses via conduction are found for thinner membranes. The authors suggest that since mass and heat transfers are connected, it is best to develop new membranes with a target application in mind for the specific membrane module and operational conditions. It is also shown that flux, energy efficiency, and distillate purity are closely connected, and one cannot be increased without sacrificing the other two. Therefore, nanofiber membranes suggest a solution but further improvement of membrane hydrophobicity in terms of *LEP* would be required for most future large scale applications.

On the other hand, A. Vojtěch et al. studied the organochlorinated pesticides decontamination using polyetherimide nanofibers as a sorbent, fixed on a solid phase microextraction (SPME) assembly made of steel wire, and compared with three commercial available SPME fibers, that is, PDMS $7 \mu m/100 \mu m$ and DVB/Carboxene/PDMS, in which extraction time variability parameter was solely focused. Organochlorinated pesticides hexachlorocyclohexanes (HCH) and chlorobenzenes (ClB) were chosen as model water pollutants. The work presents the thermal, morphological, and adsorption properties of the nanofibers. In particular the authors observed that the polyetherimide (PEI) fibers show improved response for the target compound compared to other commercial available fibers, which allows shortening the extraction time from 50 to 10 mins, while maintaining the required sensitivity. This fast sorption and economical and easy production of PEI nanofibers would be most beneficial for using them as sorbent in the SPME fibers. The authors also suggest further research in polyetherimide nanofibers as a sorbent in analytical chemistry.

I. Veverkova and I. Lovětinská-Šlamborová present a study based on antibacterial activities using modified silica nanofibers. The authors have developed a functionalized organic-inorganic nanofibrous material which has biomedical application as wound dressing material for skin regeneration. Nanofibrous membrane of a combination of water-soluble polymer PVA with silica was electrospun and stabilized by heat-treatment before being functionalized with nanoparticles of silver and copper. Cut to the chase, the prepared functionalized nanofibrous membrane shows good antibacterial activities, having high potential as a wound dressing material favoring tissue regeneration.

I. Lovětinská-Šlamborová et al. developed a nontoxic silica nanofiber which is immobilized with topical antibiotic (tetracycline) in two different methods (spectrophotometric analysis and HPLC analysis) for quantification onto silica fibers. They have found that covalent functionalization works better than the simple physisorption in immobilization of tetracycline into the silica fibers. The tetracycline immobilized nanofibers membrane shows excellent antibacterial behavior which is intended for biomedical application. The tested quantity of antibiotics is much less than the commercial available tetracycline which ruled out the fear of antibiotics resistance to human body when used in higher quantity.

While the papers in this special issue illustrate some interesting applications which can open up new windows for the scientific community and for the betterment of the mankind, there is still much room for further development and improvement of the properties of these materials, to maximize their utility and spread their use further. This may be regarded as a small step towards a much bigger and systematic investigation of electrospun nanofibrous materials for new applications.

Acknowledgments

Niranjan Patra
Miroslav Cernik
Marco Salerno

Research Article

Silica Nanofibers with Immobilized Tetracycline for Wound Dressing

Irena Lovětinská-Šlamborová,[1] Petr Holý,[2] Petr Exnar,[3] and Ivana Veverková[4]

[1]*Institute of Health Studies, Technical University of Liberec, Studentská 1402/2, 46117 Liberec, Czech Republic*
[2]*Faculty of Science, Humanities and Education, Technical University of Liberec, Studentská 1402/2,*
 46117 Liberec, Czech Republic
[3]*Institute for Nanomaterials, Advanced Technologies and Innovation, Technical University of Liberec, Studentská 1402/2,*
 46117 Liberec, Czech Republic
[4]*Faculty of Textile Engineering, Technical University of Liberec, Studentská 1402/2, 46117 Liberec, Czech Republic*

Correspondence should be addressed to Ivana Veverková; ivana.veverkova@tul.cz

Local antibiotic treatment has its justification for superficial infections. The advantage of this treatment is that the antibiotic has effects on bacterial agent directly at the application site. Skin infections which are intended for the local antibiotic treatment are superficial pyoderma, some festering wounds, burns of second and third degree, infected leg ulcers, or decubitus of second and third degree. Tetracyclines are available topical antibiotics with a broad bacterial spectrum. At present, ointments containing tetracycline are also used for the treatment, which rarely can lead to skin sensitization. In this paper, a development of novel nanofibrous material with immobilized tetracycline is presented. Two different methods of immobilized tetracycline quantification onto silica nanofibers are employed. It was proven that the prevailing part of tetracycline was bound weakly by physisorption forces, while the minor part was covalently bound by NH_2 groups formed by the preceding functionalization. The silica nanofibers with immobilized tetracycline are promising material for wound dressing applications due to its antibacterial activity; it was proved by tests.

1. Introduction

In recent years, the properties of nanofibers are intensively studied due to their suitability for biomedical applications [1, 2]. The advantage of this nanomaterial is the surface chemical modification possibility and subsequent immobilization of suitable biomolecules.

In literature, many methods of biomolecules immobilization onto a silica matrix are described. Primarily, it is the formation of covalent bond between the biomolecule and the silica substrate; the noncovalent interactions and adsorption are also often utilized [3, 4]. For biomedical applications, these nanomaterials are studied as effective drug delivery systems for a wide group of substances such as the drugs for the diabetes and cancer treatment or drugs for bones and tendons regeneration [5].

Pure silica nanofibers are convenient for medical applications because they are able to satisfy a number of very stringent criteria, such as low toxicity, relatively high porosity, and a suitable surface for subsequent functionalization. With formed Si-OH bonds on the surface, this material provides an attractive matrix for the binding and a controlled release of biomolecules, this for several reasons. First, the highly porous silica matrix is stable in an aqueous solution for a period which is identical to the normal short-term administration of the drug (from 20 minutes to several days). Furthermore, the silica nanofibers are prepared without using of stabilizing agents [6]; they do not exhibit any toxicity and immunogenicity. When longer stability in the aqueous medium is required (to prolong drug release, e.g.), the matrix is stabilized at higher temperatures (about 500˚C) [7].

The gradual release of the drug is a key aspect to increase efficiency and reduce potential side effects of drugs such as antibiotics. In the first phase, the noncovalently attached biomolecules are released; in the second phase, the covalent bonds between biomolecules and the substrate are broken and the remaining drug is gradually released. Therefore, the silica nanofibers with immobilized broad-spectrum antibiotic appear to be the ideal wound dressing material for the chronic wounds treatment. The material completely adheres to the wound bed; it copies its surface and thus no air bubbles are created between the nanomaterial and the surface of the wound. In the wound bed, gradual release of an antibiotic occurs and the antibiotics directly affect the bacterial microflora in the wound. Relatively small concentration of antibiotics leads to cleaning of the wound and healing process is initiated. Very important fact is that the silica nanofibers are gradually dissolved in body fluids; this phenomenon also occurs in the wound and it is not necessary to remove wound dressing residues [6].

Tetracyclines belong to a group of broad-spectrum bacteriostatic antibiotic. Good to medium sensitivity to this antibiotic exhibits streptococci, *Listeria*, pneumococci, *Vibrio cholerae*, *Campylobacter jejuni*, *Treponema pallidum*, and others. Variable sensitivity is reported for enterococci, staphylococci, *Escherichia coli*, *Klebsiella*, *Salmonella*, or *Clostridia*. Their antibacterial mechanism consists in affecting the protein synthesis; binding of transfer-RNA at the m-RNA-ribosome complex is averted in a bacterial cell. This leads to blockage of protein synthesis [8].

Another side effect of tetracycline is irritation of the digestive tract mucosa and inhibition of intestinal and pancreatic enzymes. Tetracyclines have negative influence on the normal microflora in the oral cavity, in the vagina, or in the intestine. pathogenic bacteria, fungi, or yeasts can settle. Sometimes this can lead to rare infections disease that can occur as a septic disease ending in death for some patients [9].

Pharmaceutical forms of tetracyclines (Doxycycline and Minocycline) are tablets, suspension, or syrup for children or injection. Established Doxycycline per os dosage is 200 mg/24 hours in the first day and then 100 mg/24 hours. Intravenous dosage is 1×200 mg/24 hours (initial dose), followed by 100–200 mg/24 hours (maintenance dose) [10]. Bacteriostatic activity of tetracycline does not depend on concentration, but on the time of exposure. Doxycycline elimination half-life $t_{1/2}$ is approximately 20 hours in favor of biliary excretion; Minocycline half-life $t_{1/2}$ is approximately 16 hours with the same ratio of biliary and renal excretion. Locally, tetracyclines are applied in concentrations of 2-3% (lower concentration can cause resistance). Moreover, it can also lead to photosensitization of the skin (pigmentation). Doxycycline and Minocycline drawbacks are an increasing number of resistant gram-negative rods and gram-positive cocci bacterial strains and the absence of bactericidal activity when using pharmacotherapeutic concentrations in plasma [9].

Silicon dioxide (SiO_2) or silica exhibits properties which make it potential ideal material for scaffolds or grafts. SiO_2 is widely considered as basic material in a form of nanoparticles, nanofibers, or thin films for biomedical applications [11, 12]. Direct physical adsorption of bioactive factors onto inorganic scaffolds such as mesoporous silica scaffold [13] is a commonly utilized method for bone tissue engineering.

2. Materials and Methods

2.1. Materials of Experiment. The materials used in this research were tetraethoxysilane (TEOS ≥ 98%, Sigma Aldrich), (3-aminopropyl)triethoxysilane (APTES ≥ 98%, Sigma Aldrich), isopropyl alcohol (p.a., Penta, Czech Republic), tetracycline (TC ≥ 98%, Sigma Aldrich), absolute ethanol (Penta, Czech Republic), fluorescein 5(6)-isothiocyanate (≥90% for HPLC, Sigma Aldrich), sodium hydroxide (NaOH, p.a., Penta, Czech Republic), hydrochloric acid (HCl, p.a., 35%, Penta, Czech Republic), hydrofluoric acid (HF, p.a., 40%, Penta, Czech Republic), ammonium-acetate (p.a. Penta, Czech Republic), methanol (p.a. Penta, Czech Republic), and trifluoroacetic acid (99%, Sigma Aldrich).

For antibacterial tests, the gram-negative *Escherichia coli* (*E. coli*, ATCC 9637) and the gram-positive *Staphylococcus aureus* (*S. aureus*, ATCC 12600) were purchased from the Czech Collection of Microorganisms, Masaryk University in Brno. As a solid base for antibacterial tests, the blood agar (Biorad s.r.o., Prague) and Müeller-Hinton agar (OXOID CZ s.r.o.) were used. Antibiotic discs were purchased from ITEST plus s.r.o., Hradec Králové (tetracycline content 10 μg/piece).

2.2. Silica Nanofibers Preparation. Preparation of the silica nanofibers is fully described in patent [3]. The initial sol was prepared by the sol-gel method; controlled hydrolysis and polycondensation of tetraethoxysilane (TEOS) are carried out, where isopropyl alcohol was used as a solvent and HCl as a catalyst. TEOS was dissolved in isopropyl alcohol, and water and HCl were added so that the molar ratio $k = [H_2O]/[TEOS]$ was $k = 2.3$ and the molar ratio $m = [HCl]/[TEOS]$ was $m = 0.01$. After the hydrolysis and polycondensation reaction, the sol was concentrated by evaporation of the solvent to a final content of 36 wt% SiO_2. No auxiliary polymer or wetting agents were used for the electrospinning.

Silica nanofibers were produced by electrospinning of the sol using a technology called Nanospider in the pilot plant Superlab of the Elmarco Liberec Company [15] and on the pilot plant laboratory device at the Department of Nonwovens, Technical University of Liberec. For the electrospinning, strings electrode in a length of 50 cm was used. By using this system, the nanofibrous layer is wider and the yield is higher; it is favorable for mass production. Prior to use, the silica nanofibers were thermally stabilized at 180°C for 2 hours.

The stabilized silica nanofibers comprise analytically more than 90% of SiO_2. The rest are retained alcohols from preparation process (isopropyl alcohol and ethanol) and water (in the form of Si-OH groups and adsorbed water). Alcohol content is gradually decreased with storage time, but it does not affect other properties of the nanofibers.

2.3. Characterization of Silica Nanofibers. The prepared silica nanofibers were visualized and characterized by a scanning electron microscope (SEM) Carl Zeiss ULTRA plus. The measurement of specific surface area was carried out by the
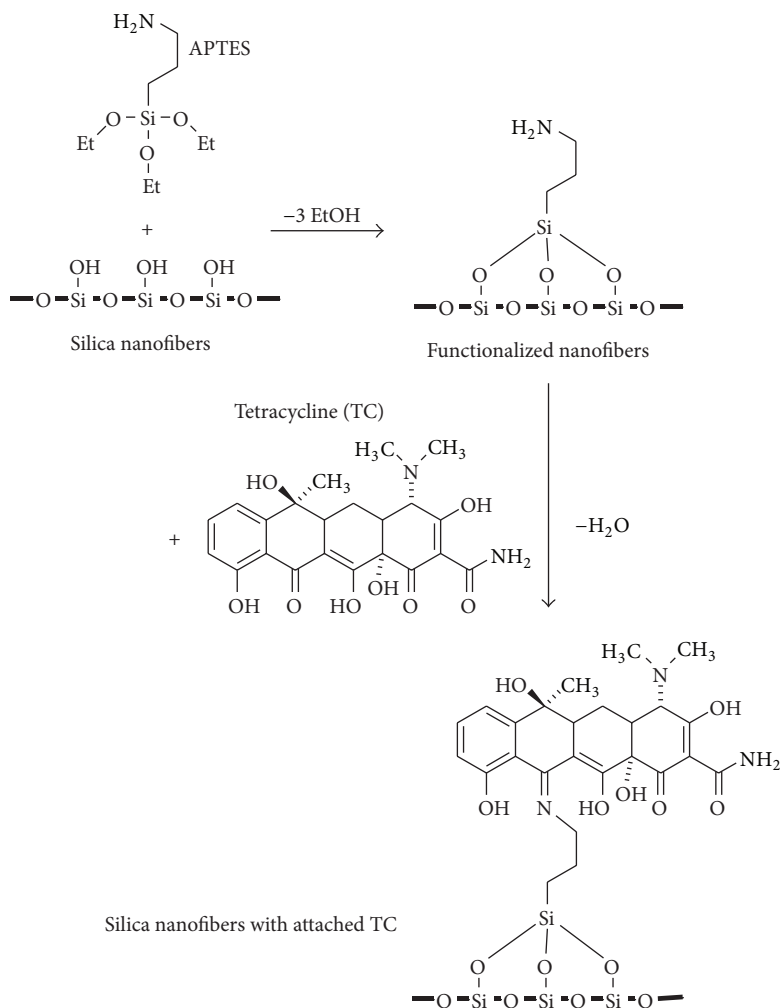
SCHEME 1: Reaction of silica nanofibers with APTES and the subsequent coupling reaction with tetracycline [14].

method of krypton adsorption on the Autosorb IQ-KR/MP instrument.

2.4. Silica Nanofibers Functionalization by Amino Groups.
Amino groups on the silica nanofiber matrix were introduced by reaction with (3-aminopropyl)triethoxysilane (APTES) (Scheme 1). A sample of the nanofibrous sheet was dipped in 0.08% APTES solution in aqueous isopropyl alcohol (6% H_2O v./v.) for 1 hour. After removal from APTES solution, the samples were washed twice with water and once with 0.1% acetic acid and dried at 30°C for 3 hours.

2.5. Quantification of Amino Groups on Silica Nanofibers.
Determination of formed amino groups on the surface of the functionalized nanofibers in APTES was performed according to the method developed by Ritter and Brüwiller [16]; the method was slightly modified for our purpose.

Samples of silica nanofibers (weight approximately 5 mg) were incubated with 2 mL of stock solution of fluorescein isothiocyanate in absolute ethanol (1 mg/mL) overnight in the dark, under gentle shaking. After removing from fluorescein isothiocyanate solution, the samples were exhaustively washed with ethanol and dried. Afterwards, dried nanofibers were dissolved in 0.2 M NaOH and the absorbance of the resultant solution was measured by spectrophotometric analysis. Measurements were performed on the double-beam UV-Vis spectrophotometer Cintra 202 in 10 mm quartz cuvettes; used wavelength was 490 nm ($\varepsilon = 75000$ mol^{-1}·cm^{-1}).

These measurements of reactive (accessible) amino group quantity were confronted with elemental analysis of functionalized nanofibers. Elemental analysis of the samples was performed on the PE 2400 Series II CHNS/O Analyzer.

2.6. Silica Nanofibers Functionalization by Tetracycline.
Amino groups on the surface of functionalized nanofibers are usable for immobilization of tetracycline by formation of a covalent bond (see Scheme 1). Samples of functionalized nanofibers were left in the action of tetracycline solution in absolute ethanol (0.1% or 1% w./v.); the reaction was carried out in a covered Petri dish placed in the dark for 24 hours at

room temperature. Subsequently, the samples were eluted in absolute ethanol and dried at 35°C for 30 min.

2.7. Tetracycline Quantification. The quantity of tetracycline (TC) entrapped in nanofibrous net was determined by spectrophotometric analysis (see Section 2.5). The quantity of adsorbed TC was calculated from measurement of ethanolic extracts (absorbance at max. 365 nm, $\varepsilon = 16600$ mol^{-1}·cm^{-1}).

Total quantity of TC was analyzed separately by elution with 0.1 M HCl followed by absorbance reading at max. 356 nm ($\varepsilon = 13900$ mol^{-1}·cm^{-1}). The differences of these values correspond to the portions of covalently bound TC, but with an inferior accuracy. The covalently bounded TC was determined more precisely by using a larger amount of sample. In this experiment, the adsorbed TC was removed at first by extraction with ethanol, and then the remaining (covalently bounded) amount of TC was released due to the incubation with 0.1 M HCl.

Extraction of TC from the nanofibers was done as follows: the sample (5–10 mg) was immersed in 4–10 mL of an eluent and placed for at least 8 hours under gentle shaking in the dark. The extinction coefficients were calculated from the plots of absorbance values of standard TC samples series in concentration range from $1 \cdot 10^{-6}$ to $5 \cdot 10^{-5}$ mol·dm^{-3}. Peaks maxima in ethanolic and hydrochloride acid extracts were found the same as in standard TC solutions.

The reliability of the results from spectrophotometric measurements was confirmed by HPLC analysis of selected samples. The adsorbed quantity of TC was determined by measurements of ethanolic samples extracts (calculated from area of the peak with max. 365 nm). After dissolving of ethanol-washed nanofibers in HF/HCl mixture, a covalently bonded TC was detected (area of the peak with max. at 356 nm was measured).

The HPLC analysis of selected samples were made on Dionex Ultimate 3000 HPLC Systems, equipped with the Diode Array Detector and a reverse-phase column Phenomenex Kinetex PFP 2.6 μm 100 R, 150 mm × 4.6 mm, and using a mobile phase 0.05 M trifluoroacetic acid and 0.01 M ammonium-acetate in water and/or in 20% methanol for gradient elution.

2.8. Antibacterial Activity Tests. For testing of the immobilized tetracycline antibacterial efficacy, modified microbiological quantitative method AATCC 147 was chosen. Onto a Petri dish with blood agar, 1 mL of bacterial inoculum at a concentration of 10^8 CFU/mL was pipetted, and the inoculum was triturated (the excess of inoculum was aspirated). The tested material (size of 18 × 18 mm) was placed in the middle of the Petri dish, the plate was closed, and samples were incubated at 37°C for 24 hours. After incubation time, the size of inhibition zones (IZ) of both samples was evaluated.

As a comparative method, the quantitative method of the disc diffusion test was utilized; this method is commonly used for determining of bacterial strain sensitivity to the tested antibiotic. The antibiotic (TC) diffuses from the disc to the surroundings; bacterial growth is inhibited; and a zone of inhibitions is created (IZ) around the disk. Subsequently, the diameter of the inhibition zone is measured and it must be

Table 1: Analysis results of samples after functionalization by APTES: [a]elemental analysis, [b]calculation from % N, and [c]data from spectrophotometric measurements.

Sample	Content of N[a] (wt%)	APTES captured[b] (μmol/g)	Accessible NH$_2$ groups[c] (μmol/g)
1	0.13	93	4.46
2	0.10	71	3.76
3	0.11	79	9.83
4	0.13	93	4.52

compared with the reference inhibition zone specified by the manufacturer. The result is sensitive or resistant bacterial strain to the antibiotics, according to the inhibition zone diameter in comparison with manufacturer data. For this test, Müeller-Hinton agar was used.

3. Results and Discussion

3.1. Silica Nanofibers Morphology. The silica nanofibers produced by electrospinning by applying a string electrode (Figure 1) have a standard bimodal distribution with diameter about 250 nm and 650 nm. The silica nanofibrous layer includes both nanofibers (diameter of 70–500 nm) and microfibers (diameter of 500–1500 nm). This material shows better mechanical properties for the manipulation required in medical applications compared with nanomaterial without thick silica fibers [7]. Final nanofibrous layer has the specific surface area 8.8 m^2·g^{-1}; it was determined by the krypton adsorption method.

3.2. Results of Amino Groups and Tetracycline Quantification on Silica Nanofibers. Elemental analysis of silica nanofibers after the treatment with APTES showed the nitrogen content in the range 0.10–0.13 wt%. If the silica nanofibers before functionalization did not contain any nitrogen, the calculations based on wt% N gave the amount of APTES entrapped on nanofibers. These values were much higher than the amounts of accessible (reactive) amino groups (assigned with fluorescein isothiocyanate) in consequence of the known multilayer deposition of the reagent. The full utilization of amino groups should give the load of tetracycline from 0.17 to 0.4 wt%. Summarized data for samples 1–4 (taken from four different batches of the silica nanofibers) are in Table 1.

Table 2 summarizes the results of the TC attachment on the functionalized samples 1–4. Elemental analysis results of all samples demonstrated an increased content of nitrogen in comparison with values in Table 1. These differences served for rough calculations of TC content. In most cases, estimations were in accordance with the results of the subsequent spectrophotometric analysis and HPLC analysis. The analysis of the samples in Table 2 showed the content of tetracycline within 0.6% to 3.7%, which is a good range for an intended medical application. The prevailing quantity of tetracycline was bound weakly by physisorption forces, while the minor quantity was covalently bound. As the adsorbed TC quantity went up more rapidly than covalent

TABLE 2: Results of tetracycline analysis: [a]concentration of TC solution in immobilization process, [b]increase of % N after TC immobilization, [c]calculation from rising of N content, [d]not determined, and [e]value from separate analysis of larger sample.

Sample	Concentration of TC (wt%)[a]	N[b] (wt%)	Estimated wt% TC[c]	Spectrophotometric measurements			HPLC Analysis	
				Total TC (wt%)	Adsorbed TC (wt%)	Bound TC (wt%)	Adsorbed TC (wt%)	Bound TC (wt%)
1	1	0.21	2.86	2.88	2.71	0.17	2.61	0.05
2	0.1	0.04	0.63	0.63	0.54	0.09	—[d]	—[d]
2	1	0.20	3.33	3.69	3.52	0.17	—[d]	—[d]
3	1	0.23	3.65	3.69	3.58	0.11	3.59	0.04
4	1	0.26	4.13	3.73	3.68	0.05/0.06[e]	—[d]	—[d]
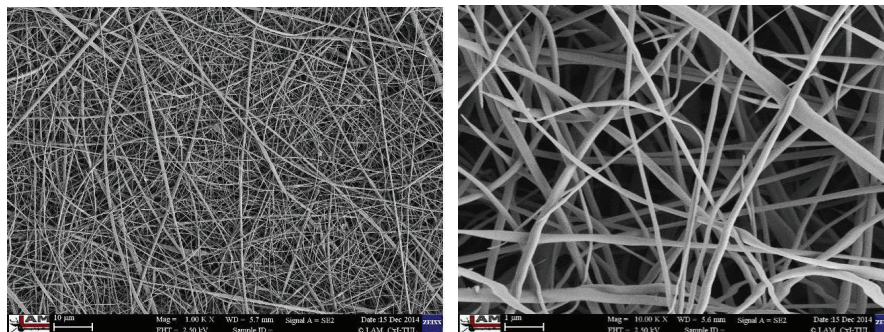
FIGURE 1: SEM pictures of pure silica nanofibers at various magnifications.

bonding with an increased concentration of TC solution, this proportion can be influenced in this way (see sample 2). The content of covalently bound TC is determined 0.04–0.17%. These percentages correspond to 0.9 to 3.83 μmol TC/g. The comparison with data in Table 1 implies that not all accessible amino groups were involved in TC covalent bonding.

By calculation of the number of amino groups per surface area from the elemental analysis results (0.10–0.13 wt% N) and the surface area determined by krypton sorption (8.8 m^{2}g^{-1}), we can determined the range of 4.9–6.4 molecules/nm^2. These values correspond to multilayer binding of APTES.

3.3. Antibacterial Activity of Silica Nanofibers with Tetracycline. Newly developed dressing material—silica nanofibers with tetracycline—shows a large number of advantages which does not provide any other commercial wound dressing of this type. The advantage of this dressing is that it closely adheres to wound bed; the silica nanofibers are gradually dissolved and the gradual release of the immobilized and anchored TC occurs simultaneously. The total content of tetracycline (i.e., covalently and noncovalently bonded) for nanofibers with specific weight of 49.3 g·dm^{-2} was determined to be 17.0 mg·dm^{-2} (on average). The size 10 × 10 cm is standard size of commercial wound dressing. Compared with TC tablets form, where the TC dosage is 400 mg/24 hours (later 200 mg/24 hours), using of this nanofibrous material is dosage decreased to 17 mg/72 hours. The human organism is not overloaded by the drug and no resistance to the antibiotics occurs.

The tests clearly demonstrated the effect of tetracycline on testing bacterial strains. Tests proved that the pure silica nanofibers exhibit no inhibitory effect on the tested bacterial strains; there is no obvious IZ. In contrast, for bacterial strain *E. coli* 14.6 mm is the size of IZ and for the bacterial strain *S. aureus*, the size of IZ is measured 10.6 mm (Figure 2). As a control sample, a TC disc was used. Dual method of TC binding (covalently and noncovalently) can offer an advantage in the longer-term effects of the substance. First, noncovalently bound TC is released, and subsequently depending on the silica nanofibers degradation, covalently bound TC is released. TC thus affects the long term and high intensity in the wound bed, which cannot be achieved with systemic administration of antibiotics.

4. Conclusion

This material represents a new and very convenient application form of wound dressing. The nanofibrous material itself is nontoxic (based on a silica which does not irritate) and after suitable surface treatment, it may be immobilized a wide range of different biomolecules on its surface to cause the same effect of action as tetracycline in this study. Here presented silica nanofibers with determined quantity of tetracycline are a potential novel type of wound dressing. The quantity of tetracycline was determined by two different methods, spectrophotometric analysis and HPLC analysis to compare. Antibacterial tests showed that the specific quantity of tetracycline on the silica nanofibers was sufficient for intended biomedical application. Moreover, tested dosage of the antibiotics is much lower in comparison with commercially used tetracycline drugs, which is highly desirable. The human organism is not overloaded by the drug and resistance to the antibiotics does not occur.

<center>S. aureus   E. coli   S. aureus</center>
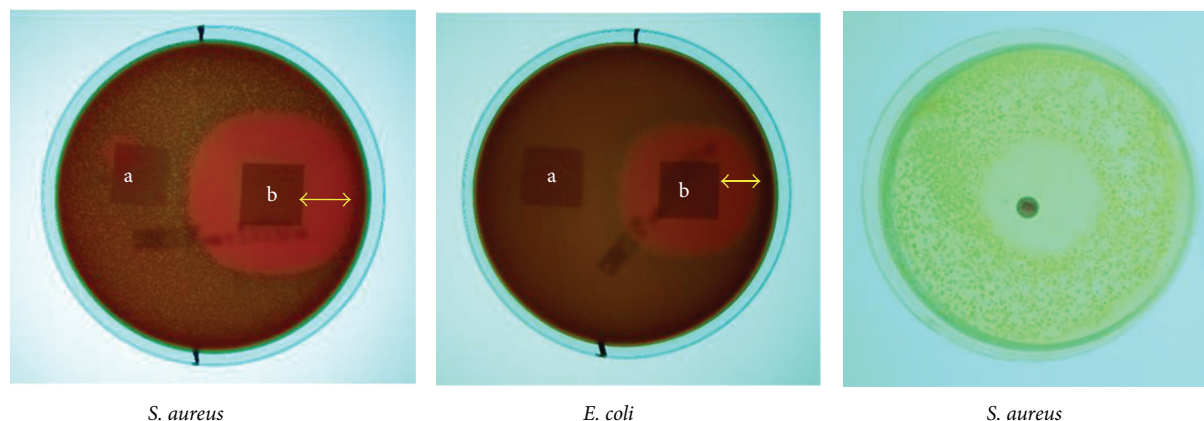
FIGURE 2: Inhibition zones sizes of pure silica nanofibers (a), silica nanofibers with immobilized tetracycline (b), and control disc with 10 μg of tetracycline (right picture).

Competing Interests

The authors declare that there are no competing interests regarding the publication of this paper.

Acknowledgments

References

[1] H. S. Yoo, T. G. Kim, and T. G. Park, "Surface-functionalized electrospun nanofibers for tissue engineering and drug delivery," *Advanced Drug Delivery Reviews*, vol. 61, no. 12, pp. 1033–1042, 2009.

[2] Y. Gao, Y. B. Truong, Y. Zhu, and I. Louis Kyratzis, "Electrospun antibacterial nanofibers: production, activity, and in vivo applications," *Journal of Applied Polymer Science*, vol. 131, no. 18, pp. 9041–9053, 2014.

[3] G. Wang, A. N. Otuonye, E. A. Blair, K. Denton, Z. Tao, and T. Asefa, "Functionalized mesoporous materials for adsorption and release of different drug molecules: a comparative study," *Journal of Solid State Chemistry*, vol. 182, no. 7, pp. 1649–1660, 2009.

[4] S. Hashemikia, N. Hemmatinejad, E. Ahmadi, and M. Montazer, "Optimization of tetracycline hydrochloride adsorption on amino modified SBA-15 using response surface methodology," *Journal of Colloid and Interface Science*, vol. 443, pp. 105–114, 2015.

[5] C. Fu, T. Liu, L. Li, H. Liu, D. Chen, and F. Tang, "The absorption, distribution, excretion and toxicity of mesoporous silica nanoparticles in mice following different exposure routes," *Biomaterials*, vol. 34, no. 10, pp. 2565–2575, 2013.

[6] I. Šlamborová, V. Zajícová, P. Exnar, and J. Studničková, "Nanofiber structure with immobilized organic agens and the

method of its preparation," (Patent), CZ 303 911, 14.8.2012, 9.5.2013; WO 2014026656, 20.2.2014; EP2884968A1, 24.6.2015; US2015240411A1, 27.8.2015.

[7] I. Lovětinská–Šlamborová, P. Exnar, I. Danilová, and I. Veverková, "Medical and biochemical applicability of silica nanofibers," in *Proceedings of the Nanofibers, Applications and Related Technologies (NART '15)*, pp. 263–269, Liberec, Czech Republic, 2015.

[8] S. Saivain and G. Houin, "Clinical pharmacokinetics of doxycykline and minocykline," *Clinical Pharmacokinetics*, vol. 15, no. 6, pp. 355–366, 1988.

[9] H. Lüllmann, K. Mohr, and M. Wehling, *Farmakologie a Toxikologie*, Grada Publishing, Praha, Czech Republic, 2nd edition, 2002.

[10] C. Simon and W. Stille, *Antibiotika v Současné Lékařské Praxi*, Grada Publishing, Praha, Czech Republic, 1st edition, 1998.

[11] J. A. Sowjanya, J. Singh, T. Mohita et al., "Biocomposite scaffolds containing chitosan/alginate/nano-silica for bone tissue engineering," *Colloids and Surfaces B: Biointerfaces*, vol. 109, pp. 294–300, 2013.

[12] Z. Luo, Y. Deng, R. Zhang et al., "Peptide-laden mesoporous silica nanoparticles with promoted bioactivity and osteo-differentiation ability for bone tissue engineering," *Colloids and Surfaces B: Biointerfaces*, vol. 131, pp. 73–82, 2015.

[13] T.-H. Kim, M. Kim, M. Eltohamy, Y.-R. Yun, J.-H. Jang, and H.-W. Kim, "Efficacy of mesoporous silica nanoparticles in delivering BMP-2 plasmid DNA for in vitro osteogenic stimulation of mesenchymal stem cells," *Journal of Biomedical Materials Research Part A*, vol. 101, no. 6, pp. 1651–1660, 2013.

[14] R. K. Sharma, S. Mittal, S. Azami, and A. Adholeya, "Surface modified silica gel for extraction of metal ions: an environment friendly method for waste treatment," *Surface Engineering*, vol. 21, no. 3, pp. 232–237, 2005.

[15] Nanofiber Equipment, http://www.elmarco.com/nanofiber-equipment/nanofiber-equipment/.

[16] H. Ritter and D. Brühwiler, "Accessibility of amino groups in postsynthetically modified mesoporous silica," *The Journal of Physical Chemistry C*, vol. 113, no. 24, pp. 10667–10674, 2009.

Research Article

Polyetherimide Nanofibres as Sorbents for Organochlorinated Pesticides Determination

Antoš Vojtěch, Hrabák Pavel, Komárek Michal, and Stuchlík Martin

Technical University of Liberec, CxI, Studentská 2, 461 17 Liberec, Czech Republic

Correspondence should be addressed to Antoš Vojtěch; vojtech.antos@tul.cz

Electrospun polyetherimide (PEI) nanofibres were fixed on a steel wire solid phase microextraction (SPME) assembly. The basic properties of the prepared nanofibres were determined by thermogravimetry, differential scanning calorimetry, adsorption, and SEM. The analytical performance of prepared PEI SPME fibres was compared with three commercially available SPME fibres, $7\,\mu$m PDMS, $100\,\mu$m PDMS, and DVB/Carboxene/PDMS. As model water pollutants, persistent organochlorinated pesticides hexachlorocyclohexanes (HCH) and chlorobenzene (ClB) were chosen as model water pollutants. The fibres were compared in the headspace- (HS-) SPME mode of GC-MS/MS instrumentation. The comparison omitted other method parameters and focused exclusively on the extraction time variability. Lab-made PEI SPME fibres showed significantly better response for the target compounds than the other tested fibres from industrial production. Based on the results, the extraction time could be shortened from 50 to 10 min, if PEI SPME fibres were used as a modification of existing analytical protocol.

1. Introduction

Headspace solid phase microextraction (HS-SPME) is a modern analytical technique for sample introduction into gas chromatographic systems [1]. The HS-SPME technique combines extractive sorption (enrichment) of targets to be quantified with ongoing thermal desorption and injection to the GC system. All of the above-mentioned steps can be performed by an ordinary autosampler [2]. This fact makes the technique attractive, as it meets the current laboratory demands on high sample throughput, precision, and green analytical approach as solventless operation [3]. With the progress in automation of sample preparation steps, HS-SPME is often involved in wider protocols of coupled techniques such as on-fibre derivatization [4, 5].

SPME fibres are commercially available in various geometries: as polymeric coatings on a stainless steel or on a glass core, as polymeric cylinders with a surface membrane, as needle trap devices, and so forth [6, 7]. The most often routinely employed polymers are polydimethylsiloxane (PDMS), divinylbenzene (DVB), polyacrylate (PA), or polyethylene glycol (PEG) [8]. Polypyrrole [9], cyclodextrin [10], polymeric ionic liquids [11], or graphene-based [12] materials were proposed to become the next generation of SPME sorbents.

A syringe-like SPME fibre geometry appears to be most viable: polymeric coatings, sandwiches, and mixtures are placed at the tip of the plunger, which is either hidden in a needle (during the transport phase) or exposed off the needle (during the extraction and thermal desorption phases of the analysis). The usual length of the plunger tip is 10 mm and its diameter is 0.1 mm. Polymeric layer thickness ranges from 7 to $100\,\mu$m. It should be noted at this point that there is a vast amount of literature and running research on SPME fibres prepared by sol-gel based techniques (see, e.g., the review by Kumar et al. [13]), which are commercially available, for example, from Supelco or CTC Analytics, AG. Our study contributes to the fresh technique of making SPME assemblies from nanofibres. First analytically successful preparations of electrospun SPME assemblies were announced few years earlier: in 2012 for polyamide [14]; in 2014 for polyacrylate-polyethylene glycol copolymer (PA-PEG) [15] and for polyetherimide (PEI) [16]. The latter polymer is also the topic of this research.

Amongst other parameters, the duration of the extractive sorption part of the sample introduction step (enrichment) seems to highly influence the overall time of analysis. This is especially the case if less volatile organic compounds are the target analytes. Various solutions are proposed to avoid the long enrichment times: First of all, the salting out effect is utilized for water samples whereby NaCl addition of up to 10% solution is used [17]. Temperature is another parameter driving the analyte transfer velocity from the water phase towards the sorption fibre. However, water vapour competes with organic analytes vapours for sorption places at higher temperatures [18]; therefore, temperatures exceeding 80°C are rarely used even for organic compounds with a low Henry constant. Last but not least, sorption fibre polymeric material affinity for specific analytes and its surface preconditioning play an important role [19].

Polyetherimide (PEI) nanofibres were chosen as the polymeric surface of the lab-made steel core SPME assemblies to be evaluated in our study. During the production of PEI nanofibres by needle electrospinning, a lab-made SPME plunger was rotated inside a stream of freshly spewed PEI nanofibres in order to obtain a surface covering. Completed SPME assemblies were compared with commercial PDMS and DVB/Carboxene/PDMS fibres with an emphasis on the possible shortening of the duration of the enrichment step. As a matrix for enrichment time tests, water contaminated by hexachlorocyclohexanes (HCH) and chlorobenzene (ClB) was used. These compounds were selected: (a) as they belong to the group of persistent organochlorinated pesticides listed as POPs under the Stockholm Convention on persistent organic pollutants and have therefore priority attention, (b) as there is a need to perform detailed monitoring of the environmental contamination of HCH and ClB due to their former industrial production in the Czech Republic [20], and (c) as organochlorinated pesticides belong to widely studied groups of target analytes with SPME utilization [21–25]. HCH are always accompanied by ClB in groundwater, as ClB are products of HCH natural transformations [20]. Aside from characterization of PEI SPME analytical performance by GC-MS/MS system response, the prepared assemblies were characterized by thermogravimetry (TGA), differential scanning calorimetry, adsorption (BET isotherm), and scanning electron microscopy (SEM).

2. Materials and Methods

2.1. Materials and Reagents.
Lab-made SPME fibres were assembled from a stainless steel capillary and 304H wire supplied by Teseco and RDG810 3D-printer polymer supplied by VeroClear (Figure 2). PEI was obtained from Sigma-Aldrich (CAS: 61128-46-9, melt index 18 g/10 min, 337°C/6.6 kg) and was dissolved overnight in a mixture of dimethylformamide/tetrahydrofuran (Sigma-Aldrich) 80 : 20 into 15% w/w solution (labelled S1) for electrospinning, following the procedure of Bagheri et al. [16].

Chromatographic standards of hexachlorocyclohexanes (HCH), Mix 5 (100 μg·mL^{-1} in acetone), and chlorobenzene (ClB), Mix 12 (1000 μg·mL^{-1} in acetone), were purchased from Neochema; isotopically labelled γ-HCH D6

(100 μg·mL^{-1} in cyclohexane) was obtained from Dr. Ehrenstorfer GmbH (Table 1). SPME commercial fibres were obtained from Supelco (100 μm PDMS and 50/30 μm DVB/ Carboxene/PDMS) and CTC Analytics AG (7 μm PDMS).

Helium of 5.0 purity and argon of 4.8 purity (Linde Gas) were used as a carrier gas and collision gas for GC-MS/MS measurements, respectively. Argon and nitrogen gases of 4.8 purity (Linde Gas) were used for surface area determination. Low purity nitrogen was used for the thermogravimetric and calorimetric measurements.

2.2. Apparatus and Equipment.
Mass loss temperature dependence of 100 μm PDMS and PEI fibres was compared by measurements using TGA Q500 (Thermo). Fibres were tested under nitrogen flow (60 mL per min), which resembles GC injector inert conditions rather than air composition. The temperature program was started at 25°C, graduating by 10°C per minute to 750°C, with a hold for 60 min at 250°C.

The appearance of manufactured PEI and Supelco PDMS fibres was documented using SEM microscope Tescan Vega 3 (Figure 2). The specific surface of electrospun PEI fibres was determined by the absorption method nitrogen/krypton upon liquid nitrogen temperature and was evaluated with a BET adsorption isotherm. Measurement was performed on an Autosorb IQ-MP instrument (Quantachrome Instruments).

The temperature of glass transition was determined by differential scanning calorimetry (Mettler Toledo DSC1). The temperature was program started at 0°C, graduating by 10°C per minute to the final temperature of 250°C. The flow of carrier gas (nitrogen) was adjusted to 50 mL per minute. This program was repeated twice, firstly to remove sample thermal history and secondly to determine the real physical properties of the PEI nanofibres.

Analytical performance of all SPME fibres was tested on a gas chromatograph (Thermo Trace 1310) equipped with a mass spectrometer triple quadrupole detector (Thermo TSQ™ 8000), autosampler (CTC Analytics AG, PAL LHX-xt), and a programmed temperature vapourizing injector (PTV). For the 4.5 min long fibre conditioning step, the PTV was set at 255°C in the case of the commercial fibres and at 205°C for lab-made PEI fibres. The split flow was set at 50 mL per min for the conditioning phase. For the 1 min long desorption and injection step, the PTV was set at 200°C in splitless operation.

A VF-5MS chromatographic column (30 m long, 0.25 mm thick with a stationary phase thickness of 0.25 μm, Agilent) was installed in the gas chromatograph. The temperature program of the chromatographic oven started at 60°C, graduating firstly by 10°C per min to 250°C, followed by a temperature gradient of 35°C per min to 300°C and held on this temperature for 3 min. The carrier gas flow was adjusted to 1 mL per min. All of the SPME fibres were tested for graduating extraction (enrichment) time in the headspace of the measured vials: for 1, 2, 3, 4, 5, 10, 30, and 50 minutes at the same incubation temperature of 70°C and an agitator speed of 250 rpm. For each tested fibre, twenty-four tap water samples spiked with the same concentration of HCH and ClB standard (2.5 μg·L^{-1} of each HCH isomer, 0.3 μg·L^{-1}

TABLE 1: Retention times and SRM transitions of the studied HCH and ClB.

Compound	GC retention time min	Precursor ion m/z	Product ion m/z	Collision energy eV
1,3-Dichlorobenzene	5.88	146	75	20
1,4-Dichlorobenzene	6.01	146	75	20
1,2-Dichlorobenzene	6.30	146	75	20
1,3,5-Trichlorobenzene	7.75	180	109	20
1,2,4-Trichlorobenzene	8.43	180	109	20
1,2,3-Trichlorobenzene	8.93	180	109	20
1,2,4,5 + 1,2,3,5-Trichlorobenzene	10.54	214	108	30
1,2,3,4-Trichlorobenzene	11.24	214	108	30
Pentachlorobenzene	13.04	250	215	18
α-HCH	15.20	181	145	22
Hexachlorobenzene	15.29	284	214	30
β-HCH	15.75	181	145	15
γ-HCH	15.93	181	145	22
γ-HCH D6	15.93	224	150	20
δ-HCH	16.52	181	145	24
ε-HCH	16.73	217	181	8
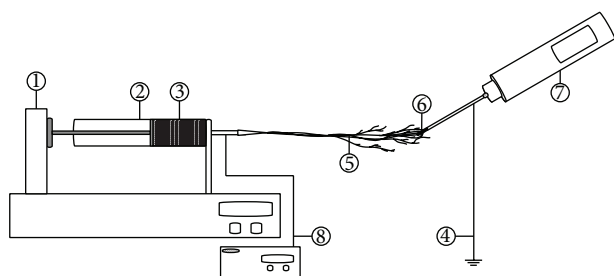
(1) Syringe pump
(2) Syringe
(3) Polymeric solution
(4) Grounded collector
(5) Nanofibres
(6) SPME fibre
(7) Motor
(8) High voltage power supply

FIGURE 1: The scheme of the needle electrospinning apparatus.

FIGURE 2: From left: plastic components, steel capillary and wire for lab-made fibre, 2 pieces of assembled lab-made fibres, and a commercial SPME fibre.

of deuterated γ-HCH, and $0.6\,\mu g \cdot L^{-1}$ of each ClB) were prepared. Lower concentrations of γ-HCH D6 were used as they are established on this level as a GC-MS/MS internal standard for routine HCH determination via HS-SPME in our laboratory.

The retention times of all of the HCH and ClB isomers were determined previously in the full scan mode of MS detector and, subsequently, selected reaction monitoring (SRM) transitions were specified in order to enhance detector selectivity and sensitivity for HCH and ClB (Table 1).

2.3. Methods

2.3.1. Preparation of PEI Nanofibres. Solution S1 was pumped into the electrospinner needle with a flow of $5\,\mu L$ per min, whereby the needle was connected at 16 kV. The grounded SPME plunger collected the freshly produced nanofibres at a speed of 50 rpm at $25°C$ and relative humidity of 38% (Figure 1).

All of the commercial SPME fibres were conditioned according to the manufacturer's instruction before the measurements. Lab-made PEI fibres were conditioned at $200°C$ for 90 minutes in PTV injector with the flow of carrier gas set to 20 mL per min.

The analytical performance of the HS-SPME fibre was tested in 20 mL vials capped with PTFE/silicon septa and a magnetic cap, with 10 mL of the water sample. These method parameters together with chromatographic and MS settings were used as they had been previously validated on a GC-MS/MS instrument for HCH and ClB determination in water with the legally required sensitivity (LOQ $0.01\,\mu g \cdot mL^{-1}$ of γ-HCH and $0.02\,\mu g \cdot mL^{-1}$ of the sum of HCH isomers).

3. Results and Discussion

For the purpose of this study, several pieces of SPME assemblies with plunger tips covered by electrospun PEI were prepared (Figures 2 and 3). Thermogravimetric characterization of both PDMS and PEI SPME fibres shows an insignificant difference in the temperature dependent mass

(a)

(b)
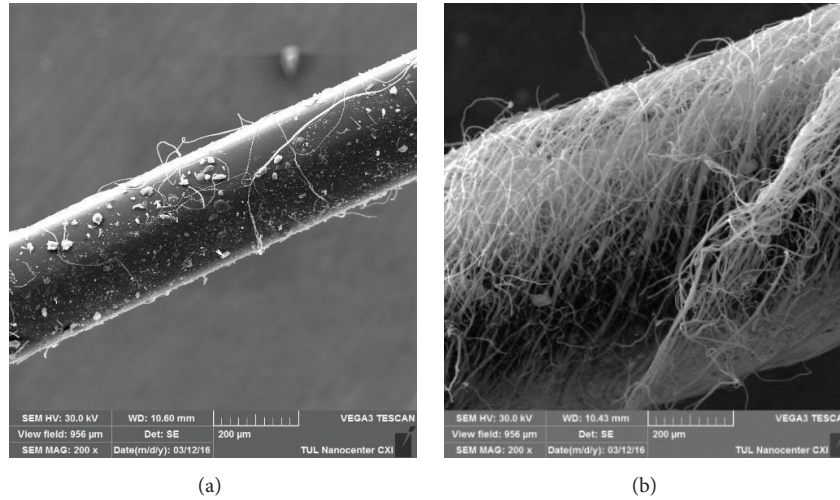
FIGURE 3: A spent 100 μm PDMS fibre from Supelco (a) and a lab-made PEI fibre (b).
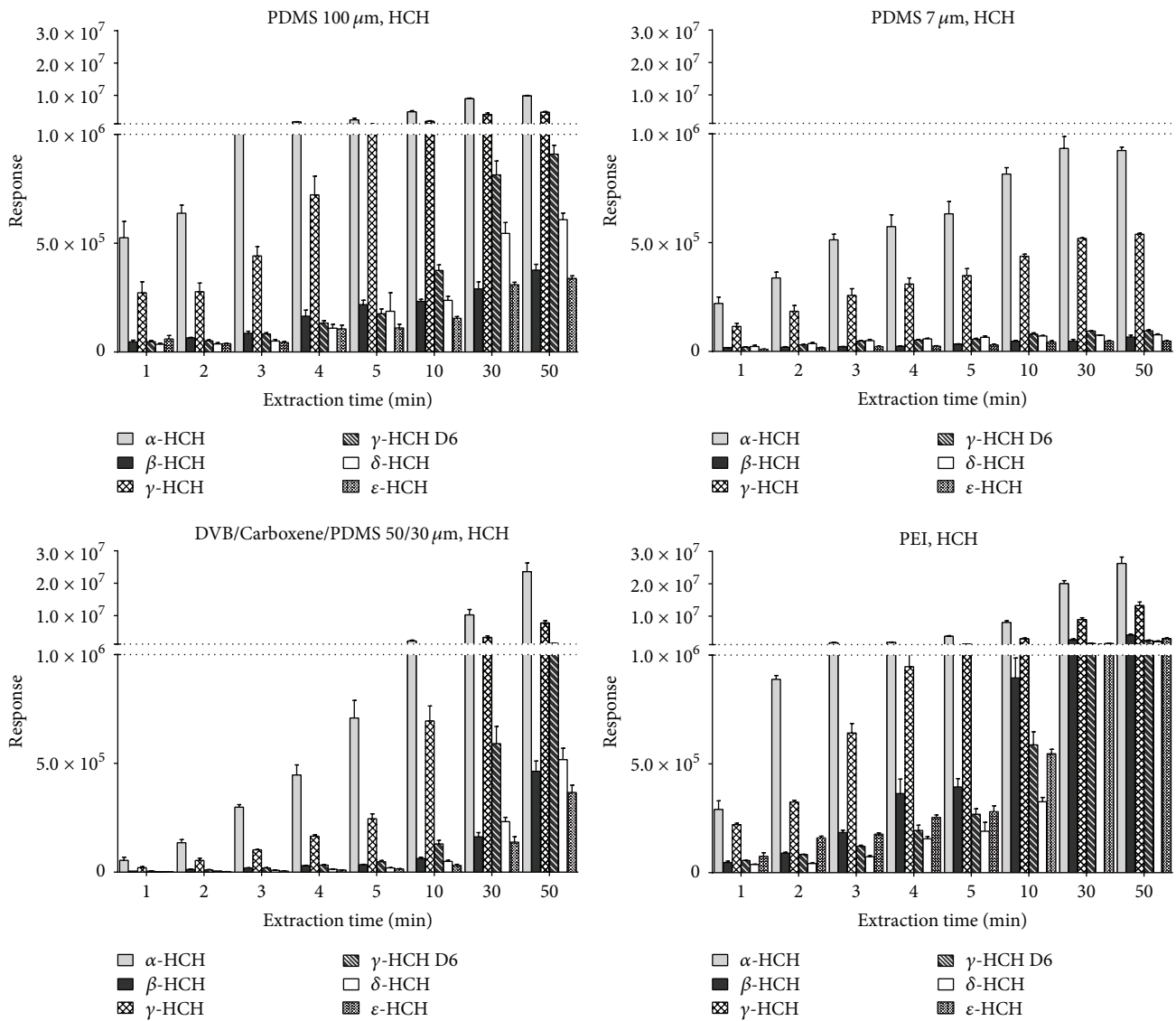
FIGURE 4: HCH response for 3 commercial and PEI fibres (the scale is interrupted at the response value of 1.0×10^6 on all of the graphs, error bars at 1σ, $n = 3$).
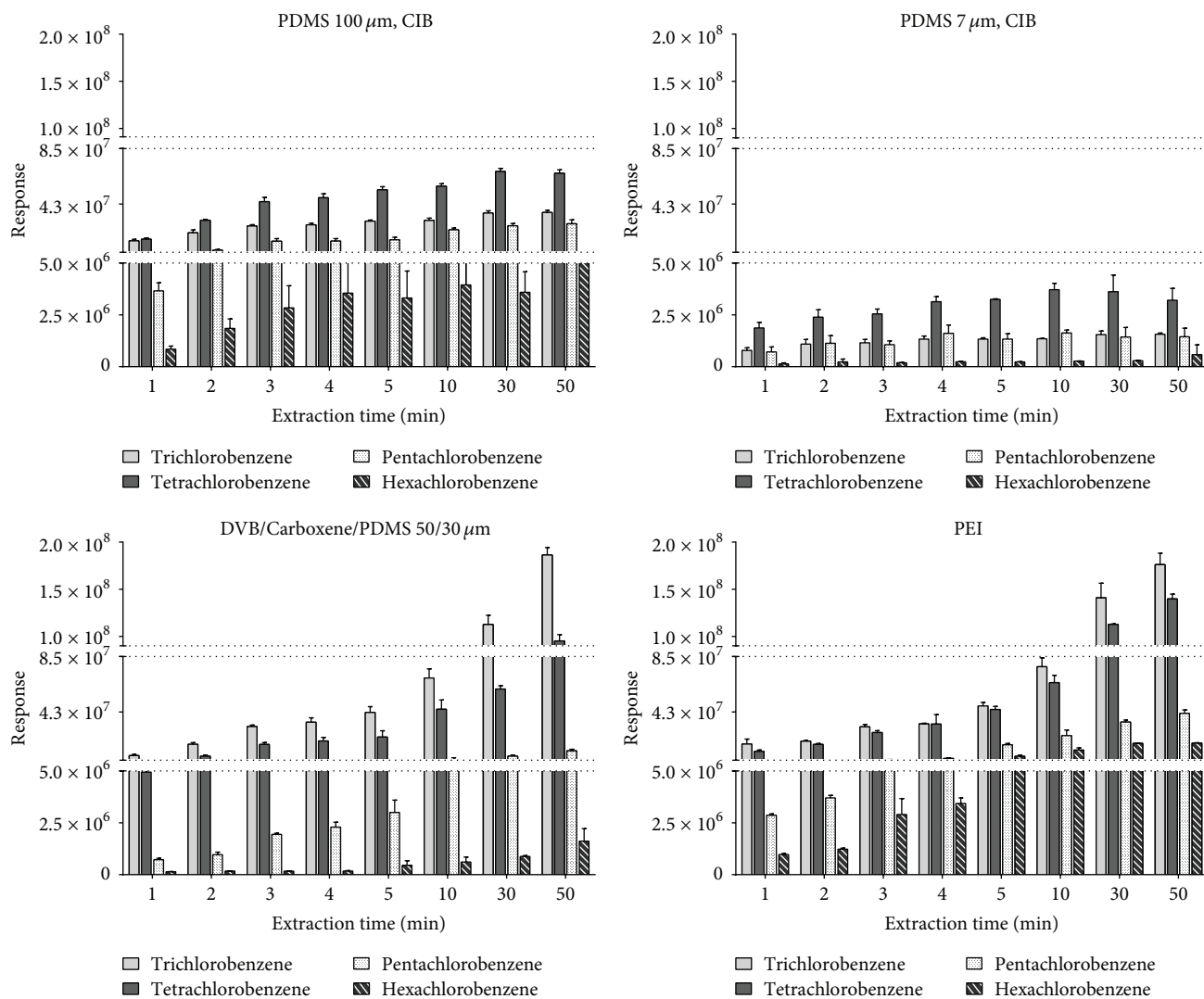
FIGURE 5: ClB response for 3 commercial and PEI fibres (the scale is interrupted at the response values of 5.0×10^6 and 8.5×10^7 on all of the graphs, error bars at 1σ, $n = 3$).

loss. This was a prerequisite for fibre analytical utilization because polymer degradation products are not welcome in a GC-MS/MS system.

Calorimetric testing determined the glass transition temperature of PEI to approximately 210°C. This explains the decrease in the sorption capacity of the PEI fibres, when an injector temperature of 250°C was used (data not shown). The data presented (Figures 4 and 5) were collected at an injector temperature of 200°C.

The surface area was the last measured nonanalytical parameter of the prepared nanofibres. A high value of $58.1\,\mathrm{m}^2\cdot\mathrm{g}^{-1}$ seemed promising in the effort to make the extractive (enrichment) phase the shortest one as possible.

The dependencies of GC-MS/MS peak areas on the extraction time for 6 HCH isomers (including one isotopic labelled isomer) and for four groups of ClB are shown in Figures 4 and 5, respectively. For clarity, ClB data were grouped according to the degree of chlorination (sum of trichlorinated

benzene, sum of tetrachlorinated benzene, pentachlorobenzene, and hexachlorobenzene). The DVB/Carboxene/PDMS fibre appeared to have the absolutely highest response values from commercial fibres. This fibre also did not approach the sorption equilibrium during 50 min of extraction time. Conversely, pure PDMS fibres either reached the sorption equilibrium after 50 min (7 μm fibre) or were close to it (100 μm fibre). The responses at distinct extraction times were noticeably lower for PDMS fibres. In the case of 7 μm PDMS fibre the response was only a few % compared to all other fibres.

The PEI fibre performed similarly to the DVB/Carboxene/PDMS fibre in the meaning of high response. However, there are some differences between the PEI and DVB/Carboxene/PDMS fibres. The response of the PEI fibre only reaches about 95% of the DVB/Carboxene/PDMS fibre response of tri-ClB, 150% of the response of tetra-ClB, about 325% of the response of penta-ClB, and about 1100% of

the response of hexa-ClB (see Figure 5). As for HCH isomers, the PEI fibre performed with noticeably higher responses than DVB/Carboxene/PDMS fibre. For some of the HCH isomers, the difference was several times higher (see Figure 5).

There is a validated procedure in our laboratory for HCH and ClB determination in water based on 100 μm PDMS fibre. This procedure fulfils the required LOQ and LOD and employs a 50 min long extraction time. The PEI fibre reaches the corresponding response of a 100 μm PDMS fibre (1×10^7 of arbitrary units) already within a 10 min extraction time.

These results are very promising in terms of the applicability of PEI fibres in the analysis of organochlorinated pesticides. However, long-term performance tests of PEI fibres are still missing. This could be a weak point in the involvement of nanoscaled sorbents in SPME, as the fibres can quickly lose the flexibility during GC temperature cycles. On the other hand, there was no visible damage to the PEI fibre after the 24 injections conducted in this study.

The other parameter, which remains unclear for the laboratory preparation of SPME PEI fibres for routine analytical purposes, is the fibre-to-fibre reproducibility of sorption properties. This aspect could be solved by using fibre quality control samples at the beginning of the work with a new fibre.

4. Conclusions

The feasibility of lab-scale preparation of several pieces of SPME PEI fibres by electrospinning has been proven. The prepared electrospun PEI nanofibres had better performance than three commercial SPME fibres in terms of the GC-MS/MS system response for representatives of organochlorinated pesticides (HCH, ClB). Therefore, the extraction time could be shortened from 50 to 10 min by switching the PEI fibre for the 100 μm PDMS fibre while maintaining the required sensitivity. This practically means considerable reduction of one-sample analysis time to the GC runtime (slightly over 20 min). Fibre conditioning and another sample extraction can be done by GC-MS/MS autosampler in parallel during the GC runtime of the previous sample. As a result, 50 samples could be measured daily with PEI fibre instead of 20 samples with 100 μm PDMS fibre.

Fast sorption and cheap, fast, and easy production of PEI nanofibres are the most beneficial properties in their application as sorbents in the SPME fibres. Based on obtained data, polyetherimide nanofibres as sorbent used in analytical chemistry deserve more detailed future research. Currently, only very few laboratories care about producing their own lab-made SPME fibres. However, with the global availability of all of the necessary components, the concept of lab-made SPME fibres is becoming a more valid option.

Competing Interests

The authors declare that they have no competing interests.

Acknowledgments

References

[1] G. Ouyang and J. Pawliszyn, "SPME in environmental analysis," *Analytical and Bioanalytical Chemistry*, vol. 386, no. 4, pp. 1059–1073, 2006.

[2] S. Risticevic, Y. Chen, L. Kudlejova et al., "Protocol for the development of automated high-throughput SPME-GC methods for the analysis of volatile and semivolatile constituents in wine samples," *Nature Protocols*, vol. 5, no. 1, pp. 162–176, 2010.

[3] J. Pawliszyn, *Handbook of Solid Phase Microextraction*, Elsevier, 2011.

[4] P. Viñas, N. Campillo, N. Martínez-Castillo, and M. Hernández-Córdoba, "Solid-phase microextraction on-fiber derivatization for the analysis of some polyphenols in wine and grapes using gas chromatography-mass spectrometry," *Journal of Chromatography A*, vol. 1216, no. 9, pp. 1279–1284, 2009.

[5] H.-G. Schmarr, W. Sang, S. Ganß et al., "Analysis of aldehydes via headspace SPME with on-fiber derivatization to their *O*-(2,3,4,5,6-pentafluorobenzyl)oxime derivatives and comprehensive 2D-GC-MS," *Journal of Separation Science*, vol. 31, no. 19, pp. 3458–3465, 2008.

[6] S. Risticevic, V. H. Niri, D. Vuckovic, and J. Pawliszyn, "Recent developments in solid-phase microextraction," *Analytical and Bioanalytical Chemistry*, vol. 393, no. 3, pp. 781–795, 2009.

[7] B. Bojko, E. Cudjoe, G. A. Gómez-Ríos et al., "SPME—Quo vadis?" *Analytica Chimica Acta*, vol. 750, pp. 132–151, 2012.

[8] H. Lord and J. Pawliszyn, "Evolution of solid-phase microextraction technology," *Journal of Chromatography A*, vol. 885, no. 1-2, pp. 153–193, 2000.

[9] M. T. Jafari, M. Saraji, and H. Sherafatmand, "Polypyrrole/montmorillonite nanocomposite as a new solid phase microextraction fiber combined with gas chromatography-corona discharge ion mobility spectrometry for the simultaneous determination of diazinon and fenthion organophosphorus pesticides," *Analytica Chimica Acta*, vol. 814, pp. 69–78, 2014.

[10] X. Hou, L. Wang, X. Tang, C. Xiong, Y. Guo, and X. Liu, "Application of a β-cyclodextrin/graphene oxide-modified fiber for solid-phase microextraction of six fragrance allergens in personal products," *The Analyst*, vol. 140, no. 19, pp. 6727–6735, 2015.

[11] J. López-Darias, V. Pino, Y. Meng, J. L. Anderson, and A. M. Afonso, "Utilization of a benzyl functionalized polymeric ionic liquid for the sensitive determination of polycyclic aromatic hydrocarbons; parabens and alkylphenols in waters using solid-phase microextraction coupled to gas chromatography-flame ionization detection," *Journal of Chromatography A*, vol. 1217, no. 46, pp. 7189–7197, 2010.

[12] X. Wang, B. Liu, Q. Lu, and Q. Qu, "Graphene-based materials: fabrication and application for adsorption in analytical chemistry," *Journal of Chromatography A*, vol. 1362, pp. 1–15, 2014.

[13] A. Kumar, Gaurav, A. K. Malik, D. K. Tewary, and B. Singh, "A review on development of solid phase microextraction fibers by

sol-gel methods and their applications," *Analytica Chimica Acta*, vol. 610, no. 1, pp. 1–14, 2008.

[14] H. Bagheri and A. Aghakhani, "Polyaniline-nylon-6 electrospun nanofibers for headspace adsorptive microextraction," *Analytica Chimica Acta*, vol. 713, pp. 63–69, 2012.

[15] H. Bagheri, H. Najarzadekan, and A. Roostaie, "Electrospun polyamide-polyethylene glycol nanofibers for headspace solid-phase microextration," *Journal of Separation Science*, vol. 37, no. 14, pp. 1880–1886, 2014.

[16] H. Bagheri, A. Akbarinejad, and A. Aghakhani, "A highly thermal-resistant electrospun-based polyetherimide nanofibers coating for solid-phase microextraction," *Analytical and Bioanalytical Chemistry*, vol. 406, no. 8, pp. 2141–2149, 2014.

[17] J. Niu, Z. Li, H. Yang et al., "A water resistant solid-phase microextraction fiber with high selectivity prepared by a metal organic framework with perfluorinated pores," *Journal of Chromatography A*, vol. 1441, pp. 16–23, 2016.

[18] N. P. Brunton, D. A. Cronin, and F. J. Monahan, "The effects of temperature and pressure on the performance of Carboxen/PDMS fibres during solid phase microextraction (SPME) of headspace volatiles from cooked and raw turkey breast," *Flavour and Fragrance Journal*, vol. 16, no. 4, pp. 294–302, 2001.

[19] S. L. Chong, D. Wang, J. D. Hayes, B. W. Wilhite, and A. Malik, "Sol-Gel coating technology for the preparation of solid-phase microextraction fibers of enhanced thermal stability," *Analytical Chemistry*, vol. 69, no. 19, pp. 3889–3898, 1997.

[20] S. Wacławek, V. Antoš, P. Hrabák, M. Černík, and D. Elliott, "Remediation of hexachlorocyclohexanes by electrochemically activated persulfates," *Environmental Science and Pollution Research*, vol. 23, no. 1, pp. 765–773, 2016.

[21] A. A. Boyd-Boland, S. Magdic, and J. B. Pawliszyn, "Simultaneous determination of 60 pesticides in water using solid-phase microextraction and gas chromatography-mass spectrometry," *Analyst*, vol. 121, no. 7, pp. 929–938, 1996.

[22] R. Boussahel, S. Bouland, K. M. Moussaoui, M. Baudu, and A. Montiel, "Determination of chlorinated pesticides in water by SPME/GC," *Water Research*, vol. 36, no. 7, pp. 1909–1911, 2002.

[23] C. Dong, Z. Zeng, and M. Yang, "Determination of organochlorine pesticides and their derivations in water after HS-SPME using polymethylphenylvinylsiloxane-coated fiber by GC-ECD," *Water Research*, vol. 39, no. 17, pp. 4204–4210, 2005.

[24] A. Menezes Filho, F. N. dos Santos, and P. A. de Paula Pereira, "Development, validation and application of a methodology based on solid-phase micro extraction followed by gas chromatography coupled to mass spectrometry (SPME/GC-MS) for the determination of pesticide residues in mangoes," *Talanta*, vol. 81, no. 1-2, pp. 346–354, 2010.

[25] Y. Picó, M. Fernández, M. J. Ruiz, and G. Font, "Current trends in solid-phase-based extraction techniques for the determination of pesticides in food and environment," *Journal of Biochemical and Biophysical Methods*, vol. 70, no. 2, pp. 117–131, 2007.

Review Article

Carbon Nanotube and Graphene Based Polyamide Electrospun Nanocomposites: A Review

Fabiola Navarro-Pardo,[1,2] Ana L. Martinez-Hernandez,[1] and Carlos Velasco-Santos[1]

[1]*División de Estudios de Posgrado e Investigación, Instituto Tecnológico de Querétaro, 76000 Santiago de Querétaro, QRO, Mexico*
[2]*Centre Énergie Matériaux Télécommunications, Institut National de la Recherche Scientifique, Varennes, QC, Canada J3X 1S2*

Correspondence should be addressed to Carlos Velasco-Santos; cylaura@gmail.com

Electrospinning is a unique and versatile technique to produce nanofibres; the facility to incorporate fillers has expanded its range of applications. This review gives a brief description of the process and the different polymers employed for obtaining nanofibres. Owing to the ability of fibrillation of polyamides, these polymers have resulted in a wide variety of interesting results obtained when using this technique; therefore these features are summarised. Additionally, because of the feasibility of incorporating carbon nanotubes and graphene in these nanofibres and the growing interest on these nanomaterials, this review focuses in the most common methods employed for their incorporation in electrospun polyamides. Several equipment setups used for the electrospinning of the nanofibres are explained. The outstanding electrical, optical, crystallinity, and mechanical properties obtained by a number of research groups are discussed. The potential applications of the resulting nanocomposites have also been explored.

1. Introduction

Electrospinning is a unique technique that can effectively produce fibres with diameters ranging from micrometers to several nanometres using a wide variety of materials [1–4]. This approach has been known since its patent was issued in 1924 by Formhals; however it was not until the last couple of decades that there was a revival on the interest of applying such technique in order to produce nanofibres. In this regard, Reneker and Chun promoted the interest of electrospinning and they have also provided a detailed review about the mechanism of electrospinning process including a diversity of polymers that were electrospun in their laboratory [1]. Teo and Ramakrishna have also offered a review on this process about different materials that have been electrospun, such as polymers, composites, ceramics, and metals [3]. Electrospinning of polymers has been very attractive because of the interesting characteristics when the diameters of the fibres are in the nanoscale [1–7].

Luo et al. reviewed the different insights found between the academia and the industry about the nanofibre research,

providing also a comprehensive comparison of the conventional techniques for obtaining fibres [7]. Nanofibres are exceptional when compared to any other fibres due to the very large surface area to volume ratio (which can be as large as 10^3 times compared to a microfibre) which leads superior mechanical performance (e.g., stiffness and tensile strength), high porosity, high gas permeability, and small interfibrous pore size [5–16]. Some authors have reviewed a variety of electrospun nanofibres and highlighted their potential for their use in filtration membranes, [5, 6], solar cells [6, 8], electronic devices [8], and biomedical applications [9, 17, 18].

A number of polymers such as polyacrylonitrile [10], polyvinyl acetate [11], polyvinylidene fluoride/polypyrrole [12], poly-ε-caprolactone [13], polystyrene [14], polyethylene [15], and natural-synthetic hybrids like chitosan/starch/polyethylene terephthalate [16] have been used to obtain electrospun fibres. Huang and coworkers have made an extensive review of the processing parameters, features, modelling, and simulations related to a variety of polymers that have been electrospun into nanofibres [2]. Polyamides are suitable for electrospinning processing due to their polyelectrolytic

behaviour in acid solution [19]. They are among the most used polymers for the successful electrospinning due to their mechanical properties, such as high tensile and impact strength, durability, and chemical and abrasion resistance [5, 19]. The outstanding properties of the nanofibres have attracted a lot of attention from many research groups due to the high production rate and the facility to incorporate reinforcing materials expanding the range of applications that can be obtained through this process.

Nanomaterials can impart remarkable structural and physical properties to the matrix as reinforcement agents [20–22]. Among the fillers used to reinforce nanofibres are metal nanoparticles [23–25], nanoclays [26–28], and carbon nanomaterials [29–38]. CNTs have been studied in the last two decades and since the raising of graphene a lot of research has been focused on these two carbon allotropes in polymer nanocomposites [21, 29, 30]. CNTs are known to possess high aspect ratio, elastic modulus values of ~1 TPa, and tensile strength of 60–150 GPa [21, 29]. They have been observed to have thermal conductivity as high as 6000 W/cmK and electrical conductivity of 5000 S/cm [29]. The tensile strength of graphene is similar or slightly higher than CNTs (130 GPa); although CNTs show comparable mechanical properties to graphene, this 2D carbon filler has superior properties than those of the 1D carbon filler in certain aspects, such as thermal and electrical conductivity [30]. Because of their high strength and high aspect ratio carbon based nanocomposite fibres with extraordinary superior mechanical properties have been obtained [20, 31, 32]. Electrical [33, 34] and physical [35, 36] properties have also been enhanced by the incorporation of these nanomaterials. Yeo and Friend have reviewed several aspects of CNT based electrospun nanofibres [20]. However, there are no reviews on graphene based nanocomposites obtained from electrospinning.

This review focuses on CNT and graphene based polyamide nanofibres because of the above mentioned characteristics that carbon nanofillers can provide and the wide use of this polymer in electrospinning. In addition, it is important to highlight the different properties that can be obtained in the nanofibres taking into account different aspects for the processing of these carbon based nanocomposites. In this regard, we have summarised the different methods and setups used for the nanocomposite preparation and the effects provided in the morphological, optical, electrical, crystallisation, and mechanical properties of nanocomposite electrospun fibres. The prospective applications of these nanofibres are also presented.

2. Nanocomposite Preparation

Electrospun fibres are obtained from a polymer solution; when nanofillers are incorporated, they have to be dispersed in the liquid medium by vigorous stirring and/or sonication followed by the mixing of the dispersion with a polymer solution [29]. Pristine nanometric carbon is extremely difficult to disperse and align in a polymer matrix because it usually forms strong bundles due to van der Waals forces between adjacent carbon nanomaterials [37, 38]. Furthermore, CNTs

and graphene have an atomically smooth nonreactive surface; the lack of interfacial bonding inhibits load transfer from the matrix to nanomaterial across the nanomaterial/polymer interface [64]. Therefore, the main challenges for obtaining carbon based nanocomposites with remarkable properties are the improvement of the dispersion, alignment, and interfacial adhesion of nanometric carbon within the matrix. Many works have been directed to overcome these shortcomings in carbon based nanocomposites [25, 37, 38, 64–69].

Electrospinning is an ideal route for aligning carbon nanomaterials [2, 65]; the different approaches and results obtained by several groups will be discussed in the next section. Functionalisation provides efficient stress transfer from the polymer matrix to the nanometric carbon by preventing aggregation of them, providing a better dispersion of the nanomaterials in the polymer matrix [37, 66, 67]. It also increases the polymer-nanomaterial physical contact and can form chemical bonds between the nanomaterial and the polymer matrix [66]. The functional groups at the surface of nanometric carbon make the strongest type of interfacial bonding with the polar polymer matrices [64]. Selected functional groups can broaden the properties of the carbon nanomaterials through the formation of donor-acceptor complexes with the graphitic structure, affording the tunability of electrical conductivity and optical properties [68]. Moreover, the additional organic moieties on the surface of carbon nanomaterial can improve the solubility of them to suit different solvents [68, 69].

Polyamides consist of methylene segments $(CH_2)_n$ separated by amide units (NH-CO). The presence of the polar groups makes functionalisation of carbon nanofillers a relevant approach for the preparation of electrospun fibres. Table 1 shows the different carbon nanomaterials used in polyamide electrospun fibres. According to the works summarised, the most commonly employed carbon nanofillers are those characterised by having oxygenated groups in their structure. Pristine carbon nanotubes typically contain carbonaceous impurities and metal catalyst particles [21, 29]. Purification of CNTs is typically achieved by oxidation using strong acids [21, 29, 66]. This process originates functional groups such as carbonyl, hydroxyl, and carboxyl on the graphitic surface [21, 69]. An extensively used strategy for obtaining graphene is the modification of graphite through oxidative routes for its subsequent exfoliation to produce GO [38]. The carboxylic acid groups at the sheet edges and epoxy and hydroxyl groups on the basal plane of GO sheets allow them to disperse in polar solvents [64]. Amino functionalised CNTs and graphene have also been incorporated into electrospun nanocomposites [31, 32, 44, 45, 70]. Jeong et al. showed that amino functionalised CNTs have better stability during the same period of time when compared to acid treated nanotubes; see Figure 1 [34, 45]. Our research group studied the influence of the dimensionality of both 1D and 2D carbon fillers on the dispersion of PA66; the capability of the CNTs to bend and the higher amount of NH_2 on their surface when compared to graphene sheets allowed the 1D nanotubes to interact with each other resulting in aggregation of them when incorporated into the polymer matrix [31]. Avila-Vega et al. incorporated nitroxide groups to GO using

TABLE 1: Polyamide electrospun nanofibres reinforced with 1D and 2D carbon.

Nanofiller	Functionalising agents	Polymer matrix	Solvent	Reference
P-MWCNTs	—	PA66	FA	[32]
O-MWCNTs	H_2SO_4/HNO_3	PA66	FA	[32]
A-MWCNTs	EDAC/DMA	PA66	FA	[31]
O-MWCNTs	Not specified	PA66	FA/DCM	[35, 39]
O-SWCNTs	H_2SO_4/HNO_3	PA6	FA	[40]
P-MWCNTs	—	PA6	FA	[41]
P-CNTs	—	PA6	HFIP	[42]
MWCNTs-OH	$KMnO_4$ in the presence of a phase transfer catalyst/dispersed in DMF	PA66	FA	[43]
O-MWCNTs	HNO_3/HCl dispersed in DMF	PA11	FA/DCM	[44]
A-MWCNTs	$SOCl_2/EDA$	PA66	FA	[34, 45]
O-MWCNTs	H_2SO_4/HNO_3	PA6	HFIP	[46]
O-MWCNTs	HNO_3/HCl dispersed in Triton X-100	PA610	HFIP	[47]
O-MWCNTs	HNO_3/HCl dispersed in DMF or Triton X-100 and sodium dodecyl sulfate	PA66	FA	[48]
P-MWCNTs	Dispersed in Triton X-100	PA6	HFIP	[49]
A-MWCNTs	$SOCl_2/EDA$	PA6	FA	[50]
P-MWCNTs	—	PA6	FA	[50]
O-MWCNTs	H_2SO_4/HNO_3	PA6	FA	[51]
Ac-MWCNTs	Friedel-Crafts acylation	PA6	FA	[52]
P-MWCNTs	—	PA6	FA	[52]
O-MWCNTs	Commercially obtained	PA6	HFIP	[53]
O-MWCNTs	Commercially obtained	PA6	Cresol/FA	[54]
RGO	Hydrazine	PA66	FA	[55]
NGO	Oxoammonium salts	PA6	HFIP	[41, 56]
RGO	Hydrazine	PA66	FA/DCM	[33, 57]
RGO	Hydrazine	PA66	FA	[57]
GnPs	Commercially obtained	PA6	HFIP	[58]
GO	Hummers method	PA66	FA	[32]
AGe	EDAC/DMA	PA66	FA	[31]
RGO	Hexamethylentetramine	PA66	FA	[32]
TiO_2 -RGO	Hydrothermal method	PA6	FA/AA	[59]
RGO	Hydrothermal method	PA6	FA/AA	[60]
GO	Hummers and Offeman's method	PA6	FA	[61]
RGO	Hydroiodic acid	PA6	FA	[62]
BSA-GO	Electrostatic self-assembly	PA6	FA	[63]

a new method for functionalising and exfoliating GO sheets in one step [41]. Table 1 also shows that other authors have employed techniques taking advantage of Van der Waals, π-π, CH-π, and other interactions; the adsorbed surfactants, biomolecules, or polymers provide repulsive and attractive forces creating stable dispersions [47–49, 63].

A large number of investigations have employed a nanofiller dispersion followed by mixing with the polyamide solution [31–36, 39, 41, 42, 45, 50, 51, 55, 56, 58–60, 71–73]. Table 1 also shows that PA6 and PA66 are the most studied polymers and the solvents used for the electrospinning of the nanofibres are also included. Kim et al. reported that the ultrasonication of O-MWCNTs in DMF provides a dispersion of individual nanotubes which is stable and can be stored at room temperature for several months without precipitation [48]. According to Lala and coworkers, HFIP is the best solvent for dispersing P-MWCNTs effectively when compared to different solvents [49]. FA has also been used for dispersing CNTs and graphene in polyamides [31, 32, 55]. This organic solvent offers fine dispersion stability of the carbon nanomaterials and good solubility of polyamides [34, 45]. A combination of this solvent with others such as DCM and AA has also been used [33, 35, 39].

Another approach employed for obtaining these nanocomposites is by dip-coating the nanofibres previously obtained by electrospinning in a carbon nanomaterial
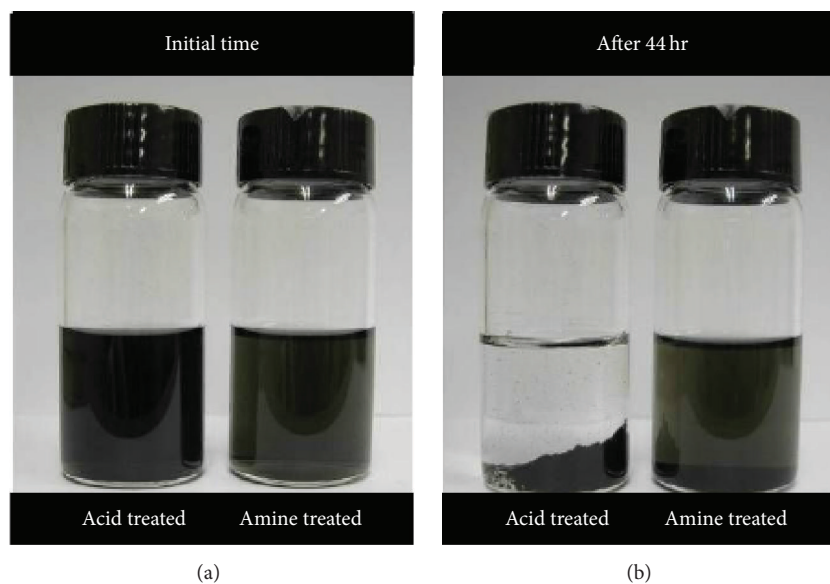
FIGURE 1: Images of the MWCNTs dispersed in a formic acid solution (sonication ~30 min). (a) Initial status and (b) after 44 h. Reprinted from [45], Copyright 2006, with permission from Elsevier.

dispersion [33, 40, 43, 48, 49, 57, 74, 75]. In this method, the nanometric carbon is adsorbed onto the surface of nanofibre mats as shown in Figure 2. Kim et al. studied the effect of two surfactants on the adsorption of O-MWCNTs; the nonionic surfactant resulted in a higher degree of adsorption of the nanotubes on the PA66 nanofibres [48]. This method is useful for obtaining transparent films [40]. Havel et al. adapted a similar method to deposit O-MWCNTs onto nanofibre mats allowing the formation of a thin conductive 2D network [44].

PVP was used to act as a modifier for improving the adsorption of GO sheets onto the nanofibres via strong π-π interactions; the additional sites on the PVP-GO surface provided hydrogen bonding with neighbouring PA66 nanofibres; this route was also used for the reduction of GO by a combination of hydrazine vapour treatment and thermal annealing (350°C) [33]. Pant et al. employed hydrothermal treatment for the reduction of GO in PA6 nanofibres [60]. In addition, another work of these authors showed that these RGO/P6 fibres facilitated the deposition of TiO_2 nanoparticles either on the nanonets or on the graphene sheets present on the main nanofibres [59]. Other authors have adsorbed GO onto the nanofibres followed by the reduction of the graphene sheets [33, 55, 57, 61]. Figure 3 shows a method for fabricating yarns from PA6 electrospun fibres functionalised with BSA molecules (yellow dots, Figure 3(a)). The GO was wrapped via electrostatic self-assembly with BSA (Figure 3(b)), which served as an adhesive for improving the adsorption of GO sheets onto the textile, followed by a low-temperature chemical reduction of GO (Figure 3(c)) [62, 63]. Cruz-Silva et al. developed a new technique for obtaining electrospun PA fibres on top of freestanding GO film [76]. Wang et al. penetrated RGO nanosheets of different sizes onto PA66 nanofibres for constructing smooth conductive paths within polymer nanofibre fabrics [77].

An in situ polymerisation technique has also been used to prepare MWCNT/PA6 nanocomposites with subsequent electrospinning [52], showing better dispersion of the nanotubes when functionalised with amino groups. Kang and Jin also used a similar approach in order to incorporate O-MWCNTs into PA610 [47].

The type of method used for the incorporation of the carbon nanofiller in a matrix will have a repercussion in the application to which they will be destined. A good dispersion of the carbon filler inside the polymer is required for those applications where strength is needed [4, 17, 18, 78–82]. Thin, transparent, conducting films are critical for their use as electrodes in modern electronic devices [8, 22, 40, 57, 77]. For chemical sensors the interactions of the analyte with the carbon nanomaterials have suggested a better performance when they are surface adsorbed using a surfactant [49, 74, 75].

3. Morphology of the Electrospun Fibres

Electrospinning provides electrostatic stretching forces (whipping elongation) for overcoming any entanglement of nanomaterials [70]. A uniform distribution of carbon nanomaterials is critical for preventing nanofiller protrusion, notches, and beads across the fibre body [56, 70]. Polymer solution properties, such as molecular weight, solution viscosity, surface tension, solution conductivity, and dielectric constant, are critical factors that affect the electrospun fibre morphology [68, 83, 84]. Process parameters, such as applied voltage, polymer flow rate, and capillary-collector distance, also have diverse effects on the morphological appearance and average fibre diameter [14, 17, 35, 71, 84].

Different electrospinning setups have been made to control the alignment of the polyamide electrospun fibres [2, 17, 71]; among the different approaches developed are rotating
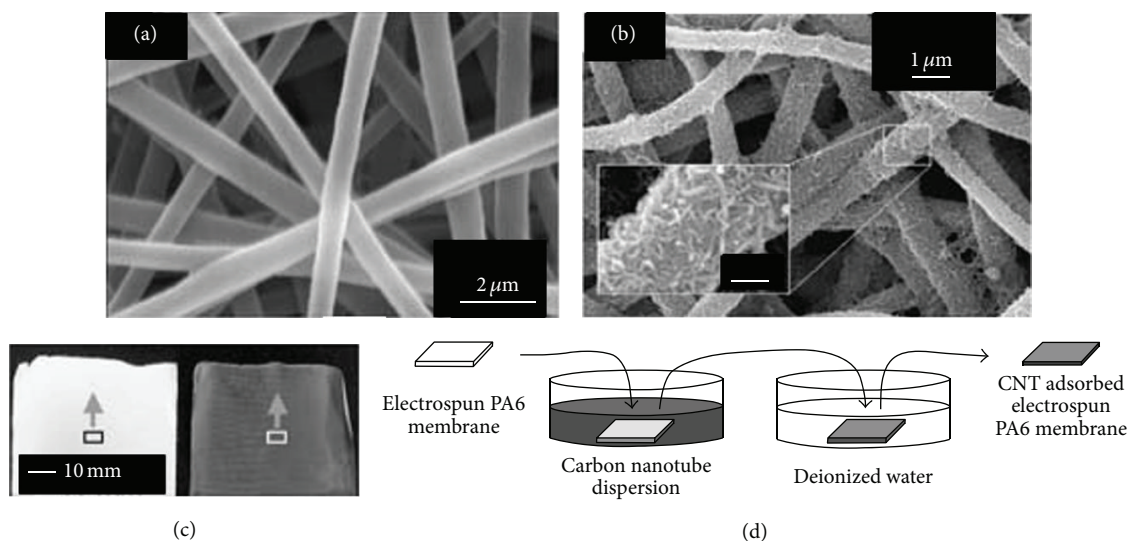
FIGURE 2: High-resolution SEM images of the nonwoven fibrous PA6 membranes (a) before and (b) after dip-coating in a dispersion of O-MWCNTs in water (0.05 wt.%) containing Triton X-100 surfactant (0.3 wt.%). (c) Images of nonwoven fibrous PA6 and the O-MWCNT-adsorbed nonwoven fibrous PA6 and (d) scheme of the simple processing technique used for producing the O-MWCNT-adsorbed nonwoven fibrous PA6 membranes. Reprinted from [48], Copyright 2005, with permission from John Wiley and Sons.
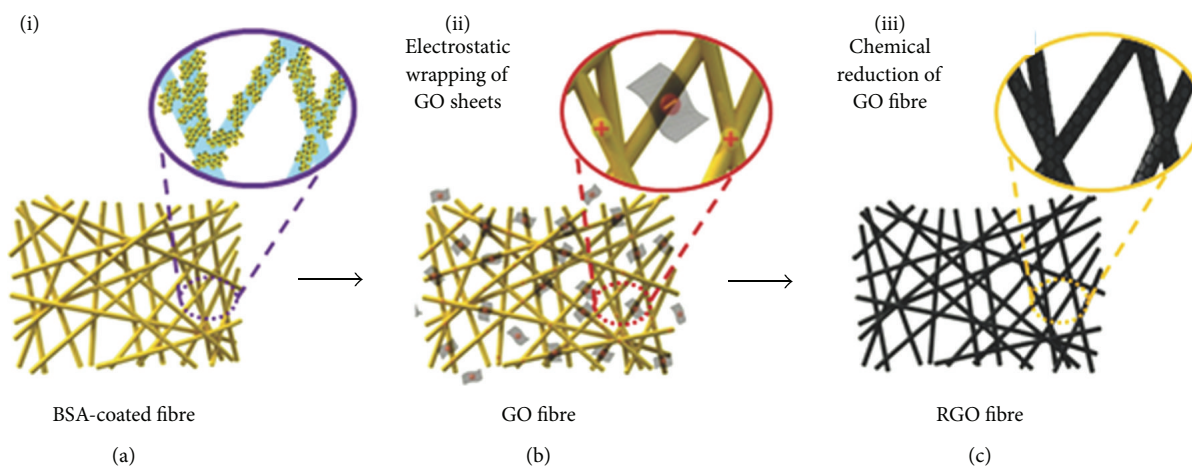
FIGURE 3: Schematic illustration of the three steps used to prepare RGO nanoyarns. Reprinted from [63], Copyright 2005, with permission from John Wiley and Sons.

drums [14, 34, 45], parallel plates [39], rotating discs [70], electrically rotating viscoelastic jets [10], grounded collector plates [31, 32, 55], and self-blending coelectrospinning [58, 85]. Applying other stretching forces can also enhance the alignment of the nanofillers along the fibre axis [70] and this is also a promising way to improve the molecular orientation degree in the fibre [70]. Parallel plates enabled the collection of aligned PA66 fibre arrays [39]. Aligned fibre bundles can also be obtained by a phase-inversion method. In this method the fibres are collected on a water bath; once they are floating on water they are transferred to a rotating drum and aligned in bundles of ~20 μm in diameter [6, 51]. Liu et al. obtained individual fibres of PA6/MWCNTs with diameters ranging from 200 to 300 nm using this technique [51]. This method

has been used to fabricate microfiltration and ultrafiltration membranes [59, 70]. Moreover the manipulation of geometrical stretching of the electrospun nanofibres can favour the alignment of nanomaterials in the polymer matrix [70]. High-speed rotating collectors have also been used to collect and to align CNTs in the polymer matrix. A study showed that the mechanical properties are affected by the alignment of PA6 fibres and the enhanced orientation of MWCNTs by the take-up speed [46]. The alignment of fibres is important for engineering the nanostructure and it also provides the ability to twist the aligned fibre bundles for fabricating nanoyarns [63, 71]. Yarns of twisted electrospun MWCNT/PA6 composite nanofibres, ranging from 5 to 10 μm in diameter, have been produced by a two-disk mechanism where a first disk
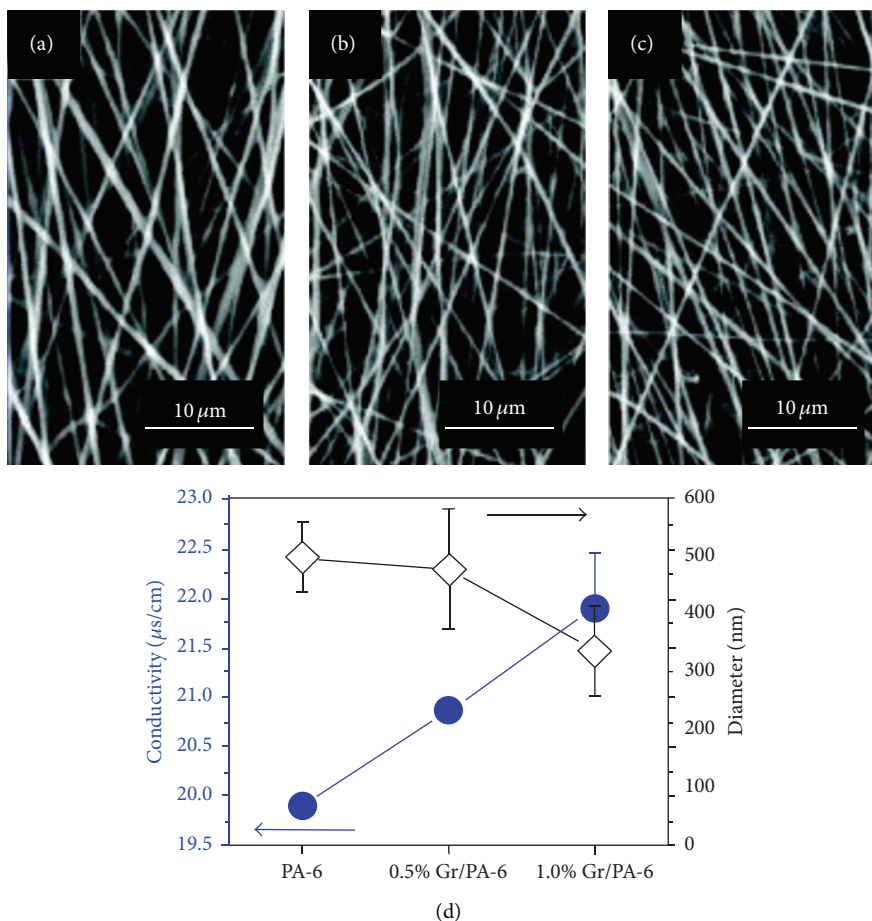
FIGURE 4: SEM images of as-spun (a) PA6 nanofibres, (b) 0.5% GnP/PA6 nanofibres, and (c) 1.0% GnP/PA-6 nanofibres. (d) Plot on the correlations of fibre diameters (black hollow diamond) and electrical conductivity (blue solid circle) versus PA6 solutions containing varied amount of GnP nanosheets. Reprinted from [58], Copyright 2013, with permission from Elsevier.

with controlled rotation imparts twist to a fibre bundle and then this is continuously wound on by a second disk with a constant linear speed [70].

The electrospinning setups have an influence on the morphology of the fibres; however, the content of the nanomaterials also affects the diameter of the nanofibres. These nanofillers produce changes in the physical properties of the solutions such as viscosity and electrical conductivity. Increasing the content of the carbon nanofiller provides a higher viscosity which in turn will produce thicker fibres. On the other hand, the electrical conductivity will also be higher and will favour the stretching of thinner fibres [32]. Due to these opposite behaviours some studies have shown variable fibre diameters as the loading of the nanofiller is increased [32, 46, 50, 51]. Li et al. obtained PA6 nanofibres with decreasing diameter as the loading of GnPs was increased. Figure 4 shows that GnPs gave rise to the electrical conductivity and produced finer nanofibres [58]. There are other works that have shown the reduced diameter of the nanofibres as the nanofiller loading increased [42, 55]. Addition of LA to PA6 for obtaining electrospun fibres produced nanofibres with flat and ribbon-shaped morphologies with wrinkled surfaces when compared to the cylindrical pure PA6 nanofibres.

Furthermore, incorporation of CNTs decreased the fibre diameter, attributed to the increased electrical conductivity of the electrospun solutions [42]. Avila-Vega et al. found that the stability of the solutions also lead to effects on the homogeneity of the diameters of NGO/PA6 nanofibres [41]. The diameter of the nanofibres has been found to be related to the mechanical and thermal properties [35, 39].

Additionally, in the last decade a variant of the commonly known electrospun nanofibres has been developed; this approach known as electrospinning/netting refers to the formation of nanofibres with diameters below 50 nm which connect with each other forming a spider-web-like morphology among the main nanofibres of larger diameter. Wang et al. have made a review on the recent advances when achieving this type of morphology, summarising several properties found in these type of bimodal diameter nanofibres [84]. Interestingly, PA6 was the first polymer to show this type of morphology; therefore there is valuable information about the parameters to obtain this interconnecting nets in electrospun polyamides; however, research regarding this type of morphology in nanofibres reinforced with carbon nanomaterials is limited. Pant et al. have reported that the incorporation of GO into PA6 allowed the formation of a

(a)   (b)   (c)
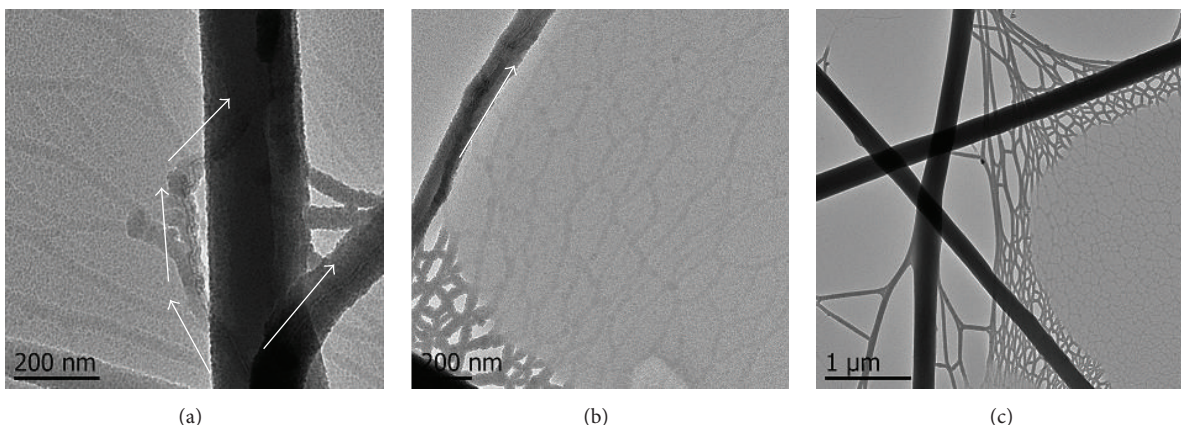
FIGURE 5: TEM images of 1 wt.% O-MWCNT/PA66 nanofibres showing (a) O-MWCNT oriented along the small diameter nanofibre, (b) O-MWCNT oriented in the large diameter nanofibre, and (c) bimodal diameter nanofibres.

(a)   (b)

(c)   (d)
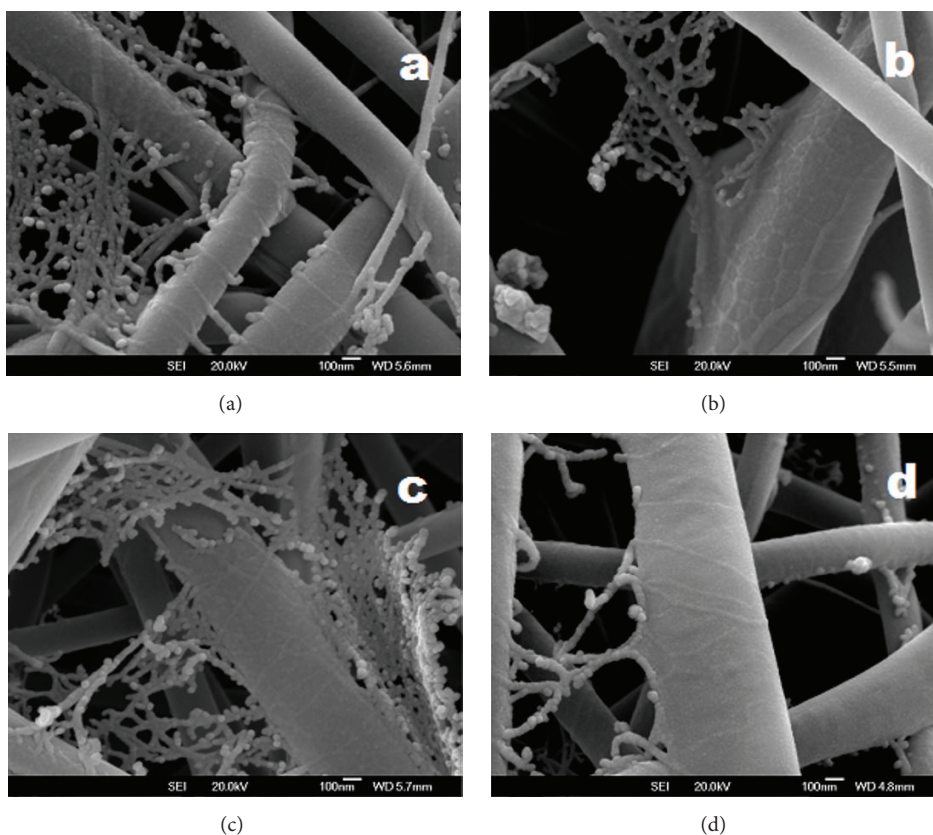
FIGURE 6: SEM images of (a) P-CNT/PA66 nanofibres, (b) A-CNT/PA66, (c) RGO/PA66, and (d) AG/PA66.

large/scale uniform bimodal fibres with distributed thick (~ 200 nm) and thin (~13 nm) fibre diameter in spider-wave-like nanonets [36, 60]. The formation of spider-wave-like nanonets was attributed to the fast solvent degradation of PA6 caused by well dispersed GO sheets through the electrospinning solution [36]. Figure 5 displays TEM images obtained in our research group; the spider-net like structures were also found in PA66 electrospun fibres reinforced with oxidised MWCNTs. Furthermore, Figure 6 shows this type of morphology in PA66 nanofibres containing diverse 1D

and 2D carbon nanomaterials also synthesised in our group, indicating that addition of carbon nanofillers has a favouring effect for the formation of netting among the main PA66 nanofibres. This can be related to the increased conductivity achieved in the solution by the incorporation of nanofillers. Electrospinning conditions can be found in [31, 32].

Pant and coworkers have explained that the increased conductivity of different pure PA6 solutions increased the ionization of polymer and therefore the fibres were characterised by these subnanofibres [86]. Furthermore, several
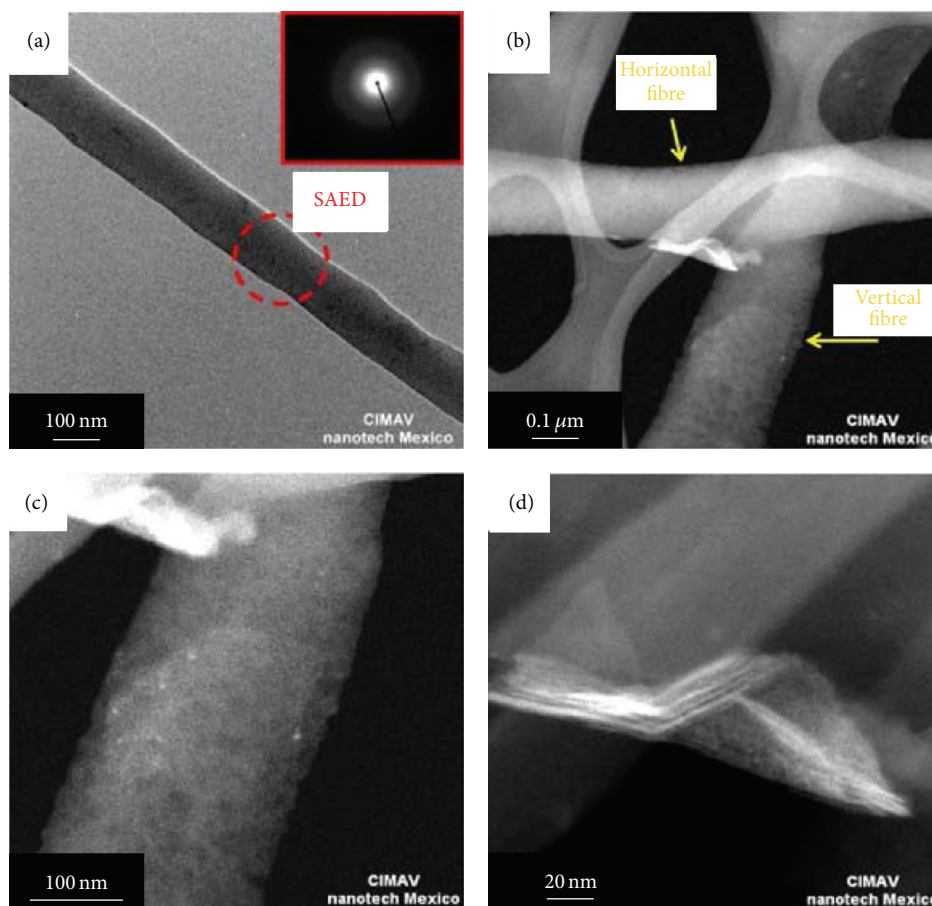
FIGURE 7: (a) TEM bright field image. The inset shows the SAED acquired in the circumscribed region by the red dotted circle. (b) STEM Z-contrast image showing two fibres containing NGO layers. Arrows indicate the horizontal and vertical fibres. Higher magnification Z-contrast images from (c) vertical fibre and (d) horizontal fibre. Reprinted from [56], Copyright 2010, with permission from Elsevier.

authors have found that the electrospinning process usually favours the alignment of CNTs in the nanofibres [31, 32, 53, 70]. This behaviour is due to the converging nanoscale jet reducing the number of available orientations in the flow field [53]. NGO was aligned within the PA6 nanofibres meanwhile agglomerates of the nanofiller could hardly be aligned; therefore the NGO sheets protruded from the fibres; Figure 7 shows the NGO/PA6 nanofibres [56].

Zomer Volpato et al. found that the surface of PA6 electrospun fibres was rough with defects attributed to the fibre stretching and the presence of O-MWCNTs in the nanocomposite fibres resulted in greater surface roughness compared to the control nanofibres [53]. Yun et al. fabricated a RGO/PA6 fabric from randomly oriented nanocomposite fibres with diameters of 150–200 nm; numerous wrinkles were observed by high-resolution SEM, indicating the uniform wrapping of the RGO nanosheets onto PA nanofibres [63]. GnPs/PA6 nanofibres have also been used as reinforcement fillers in simultaneous electrospinning of PMMA [58]. The PMMA fibres were melted in situ to become the matrix, whereas the GnPs/PA6 nanofibres with higher melting point maintained their original morphology within the PMMA

matrix; this method was used for achieving a good dispersion by using the graphene based nanofibres as dispersing carriers in the polymer matrix.

4. Electrical and Optical Properties

Nanometric carbon based films have attracted a lot of interest because of the outstanding electrical and mechanical properties of CNTs and graphene [40, 57, 61]. Using minimal amounts of CNTs or graphene in a polymer makes the resulting nanocomposites electrically conductive. Conductivity of carbon based nanocomposites increases markedly once the nanofiller content becomes high enough to percolate, that is, to form a connected network that acts as a conductive pathway through the nonconductive polymer matrix [33, 34, 43, 49, 69]. In addition, percolation threshold increases significantly when processing methods cause nanofillers to align [69] and also polyamides can offer high transparency depending upon electrospinning parameters [33]. Consequently, electrospinning of polyamides reinforced with carbon nanomaterials offers the possibility to guide the
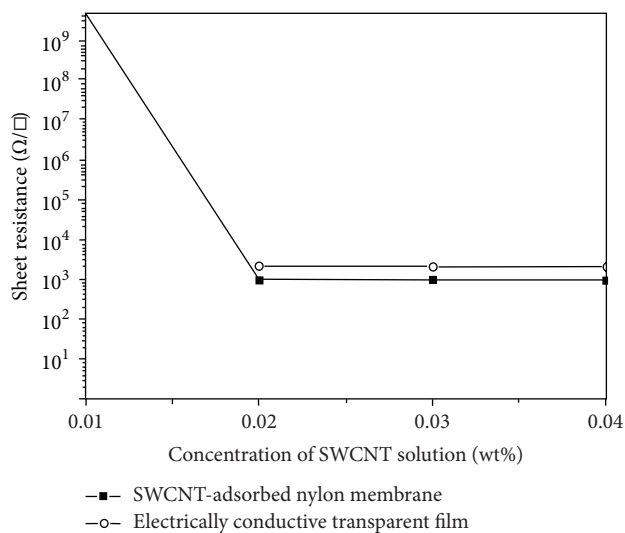
FIGURE 8: Sheet resistances of the O-SWCNT-absorbed PA6 membranes and the electrically conductive transparent films with respect to the O-SWCNT dispersion concentration. Reprinted from [40], Copyright 2013, with permission from Elsevier.

nanofillers adsorbed on the nanofibres in order to obtain thin transparent conducting films [33, 40].

Bak et al. incorporated a transparent epoxy resin into a membrane made from O-SWCNT adsorbed on polyamide nanofibres [40]. Figure 8 shows that a content of 0.02 wt.% was sufficient for the formation of a percolated network of O-SWCNTs with electrical pathways, resulting in sheet resistance of 950 kΩ/sq for the nanofibres and the same behaviour was found in the epoxy resin-impregnated films which achieved higher sheet resistance than the membrane. This film transmitted 77.4% of the light at 550 nm. Another approach for enhancing the electrical conductivity of MWCNT/PA fibres was developed by Blasdel et al., where PPy was used for interconnecting MWCNT in the fibres; the resulting material acted as a reliable resistance temperature detector in the range of 25°C to 45°C [75].

Adsorption of O-MWCNTs on PA11 fibres showed the highest coating of CNTs and thinnest electrospun films resulted in the best combination of electrical and optical properties; the results achieved were a sheet resistance of 440 kΩ/sq and 95% transmittance was achieved after melting the polymer nanofibres [44]. These properties were also studied in RGO/PA66 films as a function of electrospinning time. The surface electrical resistivity gradually decreased with increasing density of PA66 nanofibres and the transmittance decreased as the electrospinning time increased [33]. After annealing a film obtained from 120 s of electrospinning time and immersed in 0.05 wt.% PVP-GO solution exhibited a surface resistance of 8.6 kΩ/sq and 88% light transmittance [33]. Higher loadings of nanofillers have also been used [45, 51]. Liu et al. found that the conductivity of PA6 improved significantly as the loading of MWCNTs was increased up to a 3 wt.% [51]. Jeong et al. conducted I–V measurements of PA66 nanofibres containing different amounts of MWCNTs; they found that the current increased from 0.59 mA to 1.77 mA

when the nanofiller loading was increased from 10 wt.% to 20 wt.% [45]. Nirmala et al. found further increases when adding Ag nanoparticles to MWCNTs/PA6 fibres [87].

Addition of GO or RGO into PA6 nanofibres boosted the electron conduction path. Furthermore the spider-wave structure which was a feature of these nanocomposites allowed the bridging between the PA6 nanofibres and the graphene sheets increasing the amounts of charge carriers and reducing the hopping distance of conduction electrons which favoured the percolation phenomenon [60]. The GO/PA6 nanofibres favoured the electrical conductivity resulting in a three times larger increment on this property than that of the pure PA6 nanofibres; additionally, GO reduction treatment produced an excellent enhancement in this property achieving values 300 times higher than the pure polymer mats [60]. In another work, chemical reduction of GO resulted in an increase of six orders of magnitude in the electrical conductivity when compared to the GO/PA6 nanofibres; this was attributed to the restoration of the conjugated network on the RGO sheets [63]. Wang et al. effectively penetrated RGO into PA66 fibres facilitating the construction of electron pathways within the fabric and promoting electrical conductivity [77].

5. Crystallinity Properties

Semicrystalline polymers are sensitive to shear and deformation producing changes in the polymorphism and crystallite orientation [88]. Polyamides are semicrystalline polymers; their molecular structure, morphology, and crystallinity are determined by hydrogen bonded sheets formed between near-neighbour amide groups; and these sheets are stacked together by Van der Waals forces between methylene chains [5, 89]. Stephens et al. found that electrospinning process modifies the chain conformation of polyamide backbone due to the high stress induced on the jet as the fibres are being formed [90]. Electrospun fibres consist of densely packed aligned lamellae and fibrillar structures. Surrounding the crystalline regions the amorphous phase consists of extended tie molecules [91]. The addition of a second phase is expected to favour crystallisation, reduce crystal size, and therefore impart better mechanical properties to the fibres [26, 31, 32, 35]. However, there is disagreement among diverse studies on carbon nanocomposites as to whether their presence alters the mechanism of crystal growth or the overall degree of crystallinity [69].

Several studies of electrospun CNT/polyamide nanocomposites showed the influence that nanotubes have on crystallisation of the polymer [31, 32, 35, 39, 46, 52, 92]. Jose et al. found that the structure of PA6 transforms from the single γ phase for pure polymer to a mixture of γ and α phases as the nanotube loading increased. This study also showed that the structure of the nanocomposite and the take-up speed of the obtained fibres were independent when comparing similar loadings of O-MWCNTs [46]. Saeed et al. found that electrospinning of P-MWCNTs and Ac-MWCNTs did not affect the crystal structure of PA6 upon functionalisation of nanotubes. On the other hand, this study showed that

the shear force during electrospinning might favour the γ phase [52]. This phase is often associated with the formation of extended chain crystals and is typically obtained from a process involving elongational flow [88]. The addition of a small amount of O-MWCNTs induced crystallisation in PA66 fibres; however no significant difference in enthalpy values was seen when the loading of O-MWCNTs was higher than 1 wt.% [35, 39]. The presence of nanotubes in the fibres leads to smaller but larger number of crystals, explaining the increase of crystallinity in the reinforced fibres [35]. The crystallisation of PA66 electrospun fibres using A-MWCNTs and AGe as filler has also been investigated in our group. CNTs provided decrease in the crystallinity and higher crystal size when compared to graphene based nanofibres [32]. Lee et al. found that P-MWCNTs influenced the crystallinity degree of PA6 nanofibres [50]. In addition, the two crystalline peaks of PA6 downshifted from the theoretical value; this behaviour was attributed to the close-packing during the electrospinning. Cai and coworkers showed that the addition of LA produced a detriment on the crystallisation of PA6 nanofibres. However, the incorporation of P-CNTs could effectively promote the heterogeneous nucleation in the polymer [42]. Jeon et al. also showed the nucleating behaviour of MWCNTs on electrospun fibres, where pristine MWC-NTs started nucleation at higher crystallisation temperatures when compared to O-MWCNTs [92].

The study on the crystallinity properties of graphene based nanofibres obtained from polyamides is limited. Albañil-Sanchez et al. found that increasing the concentration of RGO intensified and narrowed the crystalline reflections of PA66, suggesting the nucleating behaviour of these nanomaterial [55]. Similar results were found in our research group, by adding GO and AGe [31, 32]. Our results showed that an increase in the nanofiller content produced smaller crystal sizes in the nanocomposite fibres. In another experiment, addition of GnPs into PA6 modified the crystalline phase from α to γ, when compared to the pure polymer; this was attributed to high-speed electrospinning process along with the nucleating behaviour of the nanofiller [58]. Figure 9 shows that the crystal structure of PA transforms from γ (Figure 9(a)) to α upon hydrothermal treatment of GO (Figure 9(b)). The diffractogram also shows the presence of the different peaks of the anatase (A) and rutile (R) forms of TiO_2 and also both crystalline phases of PA6 [59].

6. Mechanical Properties

The alignment of carbon nanofillers by electrospinning enhances the axial mechanical and physical properties of the fibres [65]. Several researchers have reported systematic investigations of the effects of electrospinning parameters on fibre diameter, morphology, and the effect on the mechanical properties [33, 36, 39, 46]. A study using different collector speeds showed the influence on mechanical properties at different loadings of O-MWCNTs in PA6 fibres; the high drawing speed provided a fibre rearrangement at testing direction and therefore better load transfer. Combining high
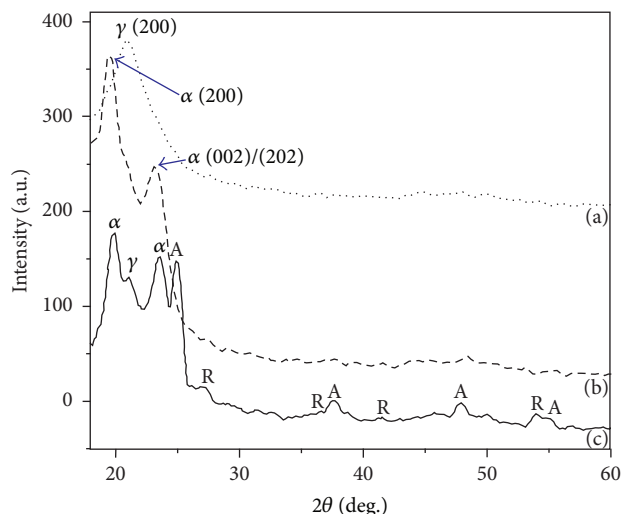
Figure 9: XRD patterns of (a) GO/PA6, (b) RGO/PA6, and (c) TiO_2-RGO/PA6 mats. Reprinted from [59], Copyright 2007, with permission from Elsevier.

take-up speeds and 1 wt.% of O-MWCNTs increased the modulus 797% when compared to pure PA6 fibres, as seen in Figure 10 [46]. Baji et al. studied the influence of diameter on the mechanical properties. The tensile modulus and strength versus O-MWCNT content for each fibre diameter are presented in Figures 11(a) and 11(b), respectively. They concluded that the reinforcement effect of O-MWCNTs is controlled by the fibre diameter. In the fibres with smaller diameter, the size of the surface regions is comparable to the overall fibre diameter, while in the fibres with larger diameter, the surface regions are much smaller compared to the overall fibre diameter. Therefore, fibres of smaller diameter display improved strength and stiffness values [35]. O-MWCNT/PA6 nanofibres showed decreased stiffness when compared to the pure polymer nanofibres; this was attributed to the different architecture of the tested mats [53]. Bazbouz and Stylious found that the tensile test for nonwoven nanofibre mats was not suitable for reflecting the exact mechanical properties of nanofibres. They provided a more accurate characterisation by conducting the tensile tests on single nanofibres or even aligned nanofibre bundles [72].

Functionalisation is also important for the improvement of mechanical properties. Specific tensile strengths of A-MWCNT/PA6 fibres were enhanced from 207 kg_fcm/g for PA6 nanofibres to 389 kg_fcm/g when using 1 wt.% A-MWCNTs. Functionalisation favoured a better dispersion of the nanotubes in the matrix when compared to P-MWCNT/PA6 nanofibres which resulted in 359 kg_fcm/g for the same nanotube content [52]. Breaking strain of A-MWCNT/PA6 nanofibres was improved due to the interfacial bonding between both phases when compared to the P-MWCNT/PA6 nanofibres [50]. Tensile properties of these A-MWCNT/PA6 electrospun fibres, including initial modulus, tensile strength, and breaking strain, were improved after applying a thermal posttreatment [50]. Addition of 1 wt.% O-MWCNTs to PA66 nanofibres increased the tensile modulus
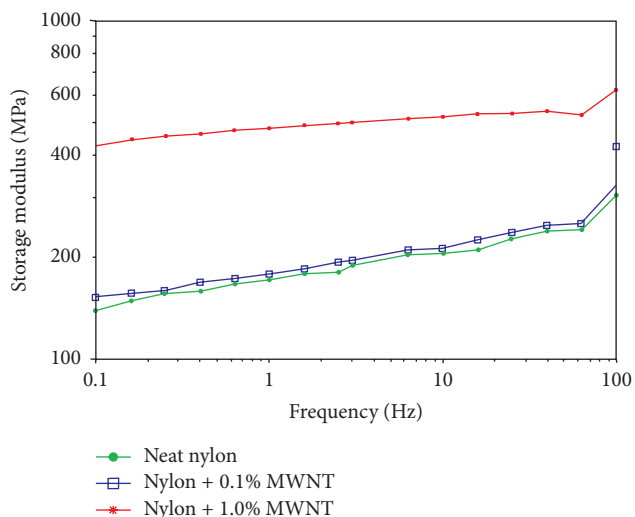
FIGURE 10: Effect of O-MWNT on storage modulus of the nonwoven aligned fibre mat at 6000 rpm. Reprinted from [46], Copyright 2011, with permission from Elsevier.

and strength by ~70% and ~25%, respectively. Dramatic changes on the storage moduli of the electrospun fibres were also observed; at room temperature, the storage modulus of the 7.5 wt.% O-MWCNTs filled fibres was ~250% higher than the pure PA66 fibres [39]. Storage modulus of PA66 electrospun fibres was enhanced by 118% for A-MWCNTs nanofibres and 69% for AGe based nanofibres at 0.1 wt.% content of the nanofiller. However when the A-MWCNT loading was increased this property decreased and the opposite behaviour was found for AGe based nanofibres, as seen in Figure 12 [31]. These results were attributed to the tendency of A-MWCNTs to aggregate at higher loadings due to the interaction of the functional groups at the graphitic surface.

RGO and GO are shown to be better reinforcement agents when compared to P-MWCNTs and O-MWCNTs in electrospun PA66 nanofibres [32]. This was attributed to the 2D nature of graphene which provides a larger surface area compared to the 1D nanotubes, thus favouring the mechanical properties of the nanofibres. GnPs and GO moderately enhanced the mechanical response at low content of these nanofillers; on the other hand, NGO provided increases of 95%, 73%, and 82% in the tensile strength, Young's modulus, and tensile strain, respectively, compared to PA6 nanofibres. The simultaneous increases in these properties were unusual because the usual effect is that one of these properties increases at the expense of another [41]. The strength and stiffness of PA6 nanofibres and nanoyarns were enhanced by the wrapping of RGO onto these structures, showing improvements on the tensile strength of 74% and 41% for the nanofibre and nanoyarn nanocomposites, respectively [63].

7. Applications

The unique characteristics of electrospun fibres make them candidates for a wide variety of applications. They have been studied in order to develop lightweight, ultra-strong structures for miniaturised and load-bearing applications [35]. Moreover tailoring the nonconducting polymeric matrices with conductive fillers like CNTs and graphene could be used to obtain nanocomposites for sensor applications [54, 75]. Cai et al. developed CNT/LA/PA6 nanofibres for obtaining phase change materials to store and retrieve solar energy [42]. The features obtained in GO/PA6 nanofibres of bimodal fibre diameter promise to have great potential in air/water filter applications [36]. The large surface area and porous nature of carbon based nanofibres offer a very large gas absorptive capacity, making possible greater analyte permeability for sensors [43, 49]. Furthermore these composites could have many advantages such as fast response, long-term stability, high sensitivity, and good reproducibility [43]. Choi et al. also fabricated O-MWCNT/PA66 electrospun fibres for sensing low molecular weight alcohol vapours such as methanol, ethanol, 1-propanol, and 1-butanol [43]. O-MWCNT/PA6 nanofibres served as the nanosized backbone for pyrrole electropolymerisation; the obtained nanocomposite was tested for biosensor applications [54]. A similar approach was used by Uzun et al. to electrochemically synthesise a conducting polymer after a graphite electrode was coated with MWCNT/PA6 in order to obtain biosensors for testing glucose containing beverages [93].

Miao et al. have examined a variety of polymers and nanomaterials for their use in electronic devices [8]. These nanofibres have also attracted a lot of attention for fabricating transparent nanocomposites due to the possibility of obtaining fibre diameters smaller than the wavelength of visible light [94]. Furthermore, the incorporation of 1D and 2D carbon structures studied in this review makes the creation of thin, transparent, and electrically conductive materials possible that are required for numerous applications such as liquid crystal displays, light emitting diodes, transistors, actuators, sensors, organic solar cells, and smart textiles [8, 33, 44, 45, 76]. Havel et al. developed thin films of O-MWCNT adsorbed onto PA11 nanofibres in order to obtain a viable candidate to replace ITO, providing sufficient conductivity for most applications, but without the price tag and physical limitations of the current ITO coatings [44]. According to the characteristics found in O-SWCNT/PA6 nanofibres developed by Bak coworkers, these could be applied as transparent electrodes in photoelectronics, such as flexible displays and touch screens, as well as in biological applications, such as actuators [40]. PA66 electrospun fibres were also used as a template to build graphene networks to obtain conductive films while minimising transmittance losses [33]. Ma et al. obtained a patent for producing graphene adsorbed on nanofibres to produce a flexible transparent electrode [57].

Liu and coworkers have provided a review about several electrospun fibres which have found wide applications in biomedical fields [9]. Monty et al. patented a flexible electrode for detecting changes in temperature, humidity, and sodium ion concentration in sweat; this fabric can be made from CNT or graphene adsorbed onto PA electrospun fibres and further functionalised with PPy [74, 75]. CNTs and graphene have been used to reinforce the weak points of existing scaffold materials [13, 18, 62]. Zomer Volpato et al.
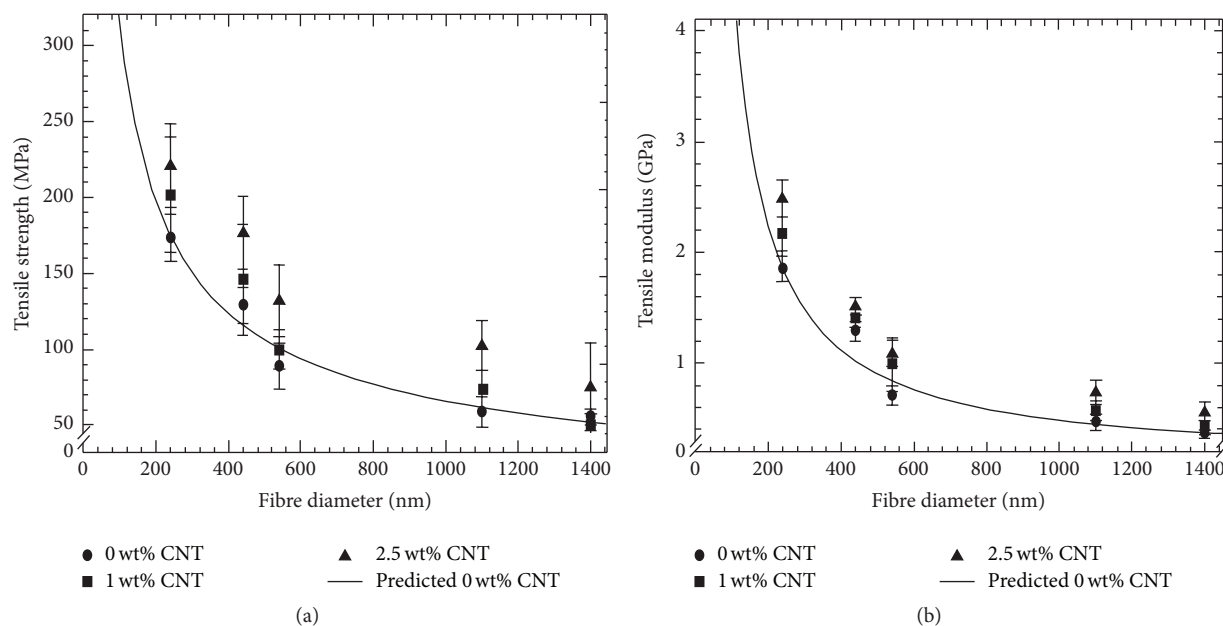
FIGURE 11: (a) Tensile modulus versus fibre diameter and (b) tensile strength versus fibre diameter. Reprinted from [35], Copyright 2014, with permission from Elsevier.
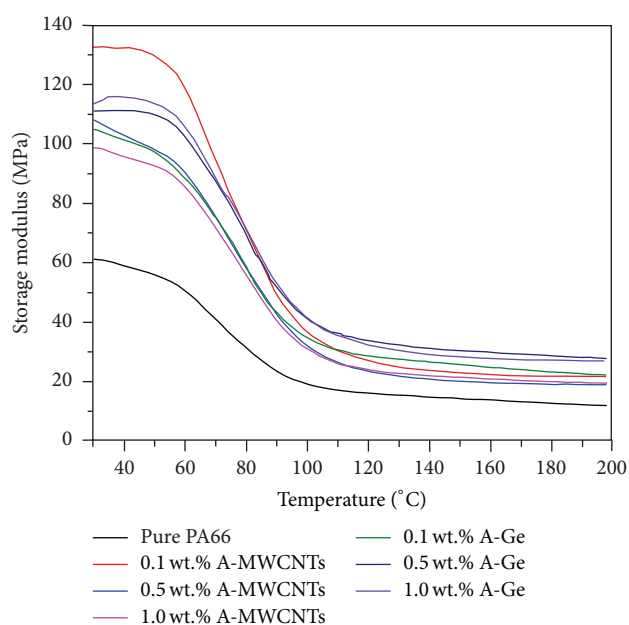
FIGURE 12: Storage modulus of 1D and 2D amino reinforced carbon/PA66 electrospun fibres. Published under licence in *IOP Conference Series: Materials Science and Engineering* by IOP Publishing Ltd.

Nonwoven nanofibres can be useful for limited applications such as filtration, tissue scaffolds, implant coating films, and wound dressings [36, 71, 80, 86]. On the other hand, continuous single nanofibres or uniaxial fibre bundles provide a wider variety of applications and could improve the performance of the nanofibres [49, 71]. Teo and Ramakrishna have reviewed these nanofibres and classified different levels of organisation in order to construct nanocomposites using electrospun fibres [4]. Another potential application of these nanofibres could be in the reinforcement of other polymers using these nanostructured carbon based electrospun fibres [58, 79, 94].

In summary, polyamide nanofibres reinforced with carbon nanomaterials qualify for a number of applications such transparent electrodes [40, 57], electronic devices [61, 87], solar cells [4, 50, 73], drug delivery systems [17, 38], biosensors [54, 62, 93], wearable electronic devices [63, 76, 77], or nanofibrous membranes for filtration [5, 59, 80, 82, 86]. The promising applications of these nanocomposite fibres have resulted in the publication of patents by several research groups [57, 61]. It is clear that the study of carbon based/polyamide electrospun will increase the research of these nanocomposites in future.

8. Conclusion

This review showed the different investigations of polyamide electrospun nanocomposites using CNTs or graphene as fillers. The selection of an appropriate solvent for the dispersion of carbon nanomaterials is an important factor for solving one of the main issues of carbon based nanocomposites, the dispersion. The other main challenge which is the alignment of nanomaterials is a feature provided by

obtained encouraging results for the use of O-MWCNT/PA6 nanofibres in biomedical applications [53]. In addition, the adjustable morphology and mechanical properties of the electrospun nanofibres are very important in order to mimic specific target tissues that need to be replaced or regenerated [53, 78].

electrospinning technique. The diverse studies of polyamide electrospun fibres reinforced with these two novel carbon nanomaterials have showed interesting characteristics for the development of a variety of applications in diverse fields of science and technology. However the potential of this technique in polyamides has not been exploited sufficiently when concerning to the reinforcing of the fibres with CNTs and graphene. More efforts need to be made in understanding the behaviour of these different structures of carbon in polyamide matrices in order to achieve the best dispersion and alignment for obtaining nanocomposites with exceptional properties.

List of Abbreviations

1D:	One-dimensional
2D:	Two-dimensional
AA:	Acetic acid
AGe:	Amino functionalised graphene
A-MWCNTs:	Amino functionalised multiwall carbon nanotubes
Ac-MWCNTs:	Acylated multiwall carbon nanotubes
BSA:	Bovine serum albumin
CNTs:	Carbon nanotubes
DCM:	Dichloromethane
DMA:	Dimethylamine
DMF:	Dimethylformamide
EDA:	Ethylenediamine
EDAC:	1-Ethyl-3-[3-dimethylaminopropyl] carbodiimide hydrochloride
FA:	Formic acid
GnPs:	Graphene nanoplatelets
GO:	Graphene oxide
HFIP:	1,1,1,3,3,3-Hexafluoro-2-propanol
LA:	Lauric acid
MWCNTs-OH:	Hydroxyl functionalised multiwall carbon nanotubes
NGO:	Nitroxide functionalised graphene oxide
O-MWCNTs:	Oxidised multiwall carbon nanotubes
O-SWCNTs:	Oxidised single wall nanotubes
P-CNTs:	Pristine carbon nanotubes
P-MWCNTs:	Pristine multiwall carbon nanotubes
PA6:	Polyamide 6
PA11:	Polyamide 11
PA66:	Polyamide 6,6
PA610:	Polyamide 6,10
PMMA:	Polymethyl methacrylate
PPy:	Polypyrrole
PVP:	Polyvinylpyrrolidone
RGO:	Reduced graphene oxide
$SOCl_2$:	Thionyl chloride.

Competing Interests

The authors declare that they have no competing interests.

References

[1] D. H. Reneker and I. Chun, "Nanometre diameter fibres of polymer, produced by electrospinning," *Nanotechnology*, vol. 7, no. 3, pp. 216–223, 1996.

[2] Z.-M. Huang, Y.-Z. Zhang, M. Kotaki, and S. Ramakrishna, "A review on polymer nanofibers by electrospinning and their applications in nanocomposites," *Composites Science and Technology*, vol. 63, no. 15, pp. 2223–2253, 2003.

[3] W. E. Teo and S. Ramakrishna, "A review on electrospinning design and nanofibre assemblies," *Nanotechnology*, vol. 17, no. 14, pp. R89–R106, 2006.

[4] W.-E. Teo and S. Ramakrishna, "Electrospun nanofibers as a platform for multifunctional, hierarchically organized nanocomposite," *Composites Science and Technology*, vol. 69, no. 11-12, pp. 1804–1817, 2009.

[5] P. Heikkilä, A. Taipale, M. Lehtimäki, and A. Harlin, "Electrospinning of polyamides with different chain compositions for filtration application," *Polymer Engineering and Science*, vol. 48, no. 6, pp. 1168–1176, 2008.

[6] V. Thavasi, G. Singh, and S. Ramakrishna, "Electrospun nanofibers in energy and environmental applications," *Energy and Environmental Science*, vol. 1, no. 2, pp. 205–221, 2008.

[7] C. J. Luo, S. D. Stoyanov, E. Stride, E. Pelan, and M. Edirisinghe, "Electrospinning versus fibre production methods: from specifics to technological convergence," *Chemical Society Reviews*, vol. 41, no. 13, pp. 4708–4735, 2012.

[8] J. Miao, M. Miyauchi, T. J. Simmons, J. S. Dordick, and R. J. Linhardt, "Electrospinning of nanomaterials and applications in electronic components and devices," *Journal of Nanoscience and Nanotechnology*, vol. 10, no. 9, pp. 5507–5519, 2010.

[9] H. Liu, X. Ding, G. Zhou, P. Li, X. Wei, and Y. Fan, "Electrospinning of nanofibers for tissue engineering applications," *Journal of Nanomaterials*, vol. 2013, Article ID 495708, 11 pages, 2013.

[10] C.-C. Liao, C.-C. Wang, C.-Y. Chen, and W.-J. Lai, "Stretching-induced orientation of polyacrylonitrile nanofibers by an electrically rotating viscoelastic jet for improving the mechanical properties," *Polymer*, vol. 52, no. 10, pp. 2263–2275, 2011.

[11] G. Wang, Z. Tan, X. Liu et al., "Conducting MWNT/poly(vinyl acetate) composite nanofibres by electrospinning," *Nanotechnology*, vol. 17, no. 23, pp. 5829–5835, 2006.

[12] K. Ketpang and J. S. Park, "Electrospinning PVDF/PPy/MWCNTs conducting composites," *Synthetic Metals*, vol. 160, no. 15-16, pp. 1603–1608, 2010.

[13] C. Wan and B. Chen, "Poly(ε-caprolactone)/graphene oxide biocomposites: mechanical properties and bioactivity," *Biomedical Materials*, vol. 6, no. 5, Article ID 055010, 2011.

[14] S. Mazinani, A. Ajji, and C. Dubois, "Morphology, structure and properties of conductive PS/CNT nanocomposite electrospun mat," *Polymer*, vol. 50, no. 14, pp. 3329–3342, 2009.

[15] S. R. Givens, K. H. Gardner, J. F. Rabolt, and D. B. Chase, "High-temperature electrospinning of polyethylene microfibers from solution," *Macromolecules*, vol. 40, no. 3, pp. 608–610, 2007.

[16] A. Espíndola-González, A. L. Martínez-Hernández, F. Fernández-Escobar et al., "Natural-synthetic hybrid polymers developed via electrospinning: the effect of PET in chitosan/starch system," *International Journal of Molecular Sciences*, vol. 12, no. 3, pp. 1908–1920, 2011.

[17] T. J. Sill and H. A. von Recum, "Electrospinning: applications in drug delivery and tissue engineering," *Biomaterials*, vol. 29, no. 13, pp. 1989–2006, 2008.

[18] H. Haniu, N. Saito, Y. Matsuda et al., "Basic potential of carbon nanotubes in tissue engineering applications," *Journal of Nanomaterials*, vol. 2012, Article ID 343747, 10 pages, 2012.

[19] R. Nirmala, R. Navamathavan, H.-S. Kang, M. H. El-Newehy, and H. Y. Kim, "Preparation of polyamide-6/chitosan composite nanofibers by a single solvent system via electrospinning for biomedical applications," *Colloids and Surfaces B: Biointerfaces*, vol. 83, no. 1, pp. 173–178, 2011.

[20] L. Yeo and J. R. Friend, "Electrospinning carbon nanotube polymer composite nanofibers," *Journal of Experimental Nanoscience*, vol. 1, pp. 177–209, 2006.

[21] A. L. Martínez-Hernández, C. Velasco-Santos, and V. M. Castaño, "Carbon nanotubes composites: processing, grafting and mechanical and thermal properties," *Current Nanoscience*, vol. 6, no. 1, pp. 12–39, 2010.

[22] R. Verdejo, M. M. Bernal, L. J. Romasanta, and M. A. Lopez-Manchado, "Graphene filled polymer nanocomposites," *Journal of Materials Chemistry*, vol. 21, no. 10, pp. 3301–3310, 2011.

[23] B. Pant, H. R. Pant, D. R. Pandeya et al., "Characterization and antibacterial properties of Ag NPs loaded nylon-6 nanocomposite prepared by one-step electrospinning process," *Colloids and Surfaces A: Physicochemical and Engineering Aspects*, vol. 395, pp. 94–99, 2012.

[24] B. W. Ahn and T. J. Kang, "Preparation and characterization of magnetic nanofibers with iron oxide nanoparticles and poly(ethylene terephthalate)," *Journal of Applied Polymer Science*, vol. 125, no. 2, pp. 1567–1575, 2012.

[25] Y. X. Gan, "Structural assessment of nanocomposites," *Micron*, vol. 43, no. 7, pp. 782–817, 2012.

[26] Y. Lu, Y. Zhang, G. Zhang, M. Yang, S. Yan, and D. Shen, "Influence of thermal processing on the perfection of crystals in polyamide 66 and polyamide 66/clay nanocomposites," *Polymer*, vol. 45, no. 26, pp. 8999–9009, 2004.

[27] G.-M. Kim, G. H. Michler, F. Ania, and F. J. B. Calleja, "Temperature dependence of polymorphism in electrospun nanofibres of PA6 and PA6/clay nanocomposite," *Polymer*, vol. 48, no. 16, pp. 4814–4823, 2007.

[28] G. Nitya, G. T. Nair, U. Mony, K. P. Chennazhi, and S. V. Nair, "In vitro evaluation of electrospun PCL/nanoclay composite scaffold for bone tissue engineering," *Journal of Materials Science: Materials in Medicine*, vol. 23, no. 7, pp. 1749–1761, 2012.

[29] Z. Spitalsky, D. Tasis, K. Papagelis, and C. Galiotis, "Carbon nanotube-polymer composites: chemistry, processing, mechanical and electrical properties," *Progress in Polymer Science*, vol. 35, no. 3, pp. 357–401, 2010.

[30] T. Kuilla, S. Bhadra, D. Yao, N. H. Kim, S. Bose, and J. H. Lee, "Recent advances in graphene based polymer composites," *Progress in Polymer Science*, vol. 35, no. 11, pp. 1350–1375, 2010.

[31] F. Navarro-Pardo, G. Martínez-Barrera, A. L. Martínez-Hernández et al., "Nylon 6,6 electrospun fibres reinforced by amino functionalised 1D and 2D carbon," *IOP Conference Series: Materials Science and Engineering*, vol. 40, Article ID 012023, 2012.

[32] F. Navarro-Pardo, G. Martínez-Barrera, A. L. Martínez-Hernández et al., "Effects on the thermo-mechanical and crystallinity properties of nylon 6,6 electrospun fibres reinforced with one dimensional (1D) and two dimensional (2D) carbon," *Materials*, vol. 6, no. 8, pp. 3494–3513, 2013.

[33] Y.-L. Huang, A. Baji, H.-W. Tien et al., "Self-assembly of graphene onto electrospun polyamide 66 nanofibers as transparent conductive thin films," *Nanotechnology*, vol. 22, no. 47, Article ID 475603, 2011.

[34] J.-S. Jeong, S.-J. Park, Y. H. Shin, Y.-J. Jung, P. S. Alegaonkar, and J.-B. Yoo, "Fabrication of carbon nanotube embedded nylon nanofiber bundles by electrospinning," *Solid State Phenomena*, vol. 124–126, no. 2, pp. 1125–1128, 2007.

[35] A. Baji, Y.-W. Mai, and S.-C. Wong, "Effect of fiber diameter on the deformation behavior of self-assembled carbon nanotube reinforced electrospun polyamide 6,6 fibers," *Materials Science and Engineering A*, vol. 528, no. 21, pp. 6565–6572, 2011.

[36] H. R. Pant, C. H. Park, L. D. Tijing, A. Amarjargal, D.-H. Lee, and C. S. Kim, "Bimodal fiber diameter distributed graphene oxide/nylon-6 composite nanofibrous mats via electrospinning," *Colloids and Surfaces A: Physicochemical and Engineering Aspects*, vol. 407, pp. 121–125, 2012.

[37] N. G. Sahoo, H. K. F. Cheng, L. Li, S. H. Chan, Z. Judeh, and J. Zhao, "Specific functionalization of carbon nanotubes for advanced polymer nanocomposites," *Advanced Functional Materials*, vol. 19, no. 24, pp. 3962–3971, 2009.

[38] T. Kuila, S. Bose, A. K. Mishra, P. Khanra, N. H. Kim, and J. H. Lee, "Chemical functionalization of graphene and its applications," *Progress in Materials Science*, vol. 57, no. 7, pp. 1061–1105, 2012.

[39] A. Baji, Y.-W. Mai, S.-C. Wong, M. Abtahi, and X. Du, "Mechanical behavior of self-assembled carbon nanotube reinforced nylon 6,6 fibers," *Composites Science and Technology*, vol. 70, no. 9, pp. 1401–1409, 2010.

[40] H. Bak, S. Y. Cho, Y. S. Yun, and H.-J. Jin, "Electrically conductive transparent films based on nylon 6 membranes and single-walled carbon nanotubes," *Current Applied Physics*, vol. 10, no. 3, pp. S468–S472, 2010.

[41] Y. I. Avila-Vega, C. C. Leyva-Porras, M. Mireles, M. Quevedo-López, J. Macossay, and J. Bonilla-Cruz, "Nitroxide-functionalized graphene oxide from graphite oxide," *Carbon*, vol. 63, pp. 376–389, 2013.

[42] Y. Cai, X. Xu, C. Gao et al., "Effects of carbon nanotubes on morphological structure, thermal and flammability properties of electrospun composite fibers consisting of lauric acid and polyamide 6 as thermal energy storage materials," *Fibers and Polymers*, vol. 13, no. 7, pp. 837–845, 2012.

[43] J. Choi, E. J. Park, D. W. Park, and S. E. Shim, "MWCNT-OH adsorbed electrospun nylon 6,6 nanofibers chemiresistor and their application in low molecular weight alcohol vapours sensing," *Synthetic Metals*, vol. 160, no. 23-24, pp. 2664–2669, 2010.

[44] M. Havel, K. Behler, G. Korneva, and Y. Gogotsi, "Transparent thin films of multiwalled carbon nanotubes self-assembled on polyamide 11 nanofibers," *Advanced Functional Materials*, vol. 18, no. 16, pp. 2322–2327, 2008.

[45] J. S. Jeong, S. Y. Jeon, T. Y. Lee et al., "Fabrication of MWNTs/nylon conductive composite nanofibers by electrospinning," *Diamond and Related Materials*, vol. 15, no. 11-12, pp. 1839–1843, 2006.

[46] M. V. Jose, B. W. Steinert, V. Thomas et al., "Morphology and mechanical properties of Nylon 6/MWNT nanofibers," *Polymer*, vol. 48, no. 4, pp. 1096–1104, 2007.

[47] M. Kang and H.-J. Jin, "Electrospun nanofiber of nylon 610/multi-walled carbon nanotube composites," *Key Engineering Materials*, vol. 321–323, pp. 934–937, 2006.

[48] H. S. Kim, H.-J. Jin, S. J. Myung, M. Kang, and I.-J. Chin, "Carbon nanotube-adsorbed electrospun nanofibrous membranes of nylon 6," *Macromolecular Rapid Communications*, vol. 27, no. 2, pp. 146–151, 2006.

[49] N. L. Lala, V. Thavasi, and S. Ramakrishna, "Preparation of surface adsorbed and impregnated multi-walled carbon nanotube/nylon-6 nanofiber composites and investigation of their gas sensing ability," *Sensors*, vol. 9, no. 1, pp. 86–101, 2009.

[50] S. Y. Lee, B. Yoo, M. K. Lim, T.-K. Lee, A. R. S. Priya, and K.-J. Kim, "Influence of nylon 6 in I3-/I- redox electrolyte on the photovoltaic performance and stability of dye-sensitized solar cells," *Langmuir*, vol. 26, no. 9, pp. 6638–6642, 2010.

[51] Y. Liu, J. Li, and Z.-J. Pan, "The dispersion of CNT and the conductive property of PA6/MWNTs nanofiber filaments by electrospinning," *Advanced Materials Research*, vol. 295–297, pp. 1993–1997, 2011.

[52] K. Saeed, S.-Y. Park, S. Haider, and J.-B. Baek, "In situ polymerization of multi-walled carbon nanotube/nylon-6 nanocomposites and their electrospun nanofibers," *Nanoscale Research Letters*, vol. 4, no. 1, pp. 39–46, 2009.

[53] F. Zomer Volpato, S. L. Fernandes Ramos, A. Motta, and C. Migliaresi, "Physical and in vitro biological evaluation of a PA 6/MWCNT electrospun composite for biomedical applications," *Journal of Bioactive and Compatible Polymers*, vol. 26, no. 1, pp. 35–47, 2011.

[54] X. Wang, X. Wang, X. Wang et al., "Novel electrochemical biosensor based on functional composite nanofibers for sensitive detection of p53 tumor suppressor gene," *Analytica Chimica Acta*, vol. 765, pp. 63–69, 2013.

[55] L. Albañil-Sanchez, A. Romo-Uribe, A. Flores, and R. Cruz-Silva, "Electrospun nylon-graphene nanocomposites synthesis and microstructure," *MRS Proceedings*, vol. 1453, 8 pages, 2012.

[56] C. Leyva-Porras, C. Ornelas-Gutiérrez, M. Miki-Yoshida, Y. I. Avila-Vega, J. Macossay, and J. Bonilla-Cruz, "EELS analysis of Nylon 6 nanofibers reinforced with nitroxide-functionalized graphene oxide," *Carbon*, vol. 70, pp. 164–172, 2014.

[57] C.-C. M. Ma, Y.-L. Huang, S.-Y. Yang, and H.-W. Tien, "Transparent electrode with flexibility and method for manufacturing the same," US Patent 0295384, 2013.

[58] B. Li, H. Yuan, and Y. Zhang, "Transparent PMMA-based nanocomposite using electrospun graphene-incorporated PA-6 nanofibers as the reinforcement," *Composites Science and Technology*, vol. 89, pp. 134–141, 2013.

[59] H. R. Pant, B. Pant, P. Pokharel et al., "Photocatalytic TiO_2-RGO/nylon-6 spider-wave-like nano-nets via electrospinning and hydrothermal treatment," *Journal of Membrane Science*, vol. 429, pp. 225–234, 2013.

[60] H. R. Pant, B. Pant, C. H. Park et al., "RGO/Nylon-6 composite mat with unique structural features and electrical properties obtained from electrospinning and hydrothermal process," *Fibers and Polymers*, vol. 14, no. 6, pp. 970–975, 2013.

[61] Y. J. Yun and D. Kibong Song, "Graphene electronic device and method of fabricating the same," US Patent 0313523, 2013.

[62] Y. J. Yun, W. G. Hong, N.-J. Choi et al., "A 3D scaffold for ultrasensitive reduced graphene oxide gas sensors," *Nanoscale*, vol. 6, no. 12, pp. 6511–6514, 2014.

[63] Y. J. Yun, W. G. Hong, W.-J. Kim, Y. Jun, and B. H. Kim, "A novel method for applying reduced graphene oxide directly to electronic textiles from yarns to fabrics," *Advanced Materials*, vol. 25, no. 40, pp. 5701–5705, 2013.

[64] J. Shen, M. Shi, B. Yan et al., "Covalent attaching protein to graphene oxide via diimide-activated amidation," *Colloids and Surfaces B: Biointerfaces*, vol. 81, no. 2, pp. 434–438, 2010.

[65] T.-W. Chou, L. Gao, E. T. Thostenson, Z. Zhang, and J.-H. Byun, "An assessment of the science and technology of carbon nanotube-based fibers and composites," *Composites Science and Technology*, vol. 70, no. 1, pp. 1–19, 2010.

[66] K. Yang, M. Gu, Y. Guo, X. Pan, and G. Mu, "Effects of carbon nanotube functionalization on the mechanical and thermal properties of epoxy composites," *Carbon*, vol. 47, no. 7, pp. 1723–1737, 2009.

[67] G. Mago, C. Velasco-Santos, A. L. Martinez-Hernandez, D. M. Kalyon, and F. T. Tisher, "Effect of functionalization on the crystallization behavior of MWNT-PBT nanocomposites," *Materials Research Society Symposium Proceedings*, vol. 1056, pp. 295–300, 2008.

[68] Q. Bao, H. Zhang, J.-X. Yang et al., "Graphene-polymer nanofiber membrane for ultrafast photonics," *Advanced Functional Materials*, vol. 20, no. 5, pp. 782–791, 2010.

[69] M. J. Green, N. Behabtu, M. Pasquali, and W. W. Adams, "Nanotubes as polymers," *Polymer*, vol. 50, no. 21, pp. 4979–4997, 2009.

[70] M. B. Bazbouz and G. K. Stylios, "Novel mechanism for spinning continuous twisted composite nanofiber yarns," *European Polymer Journal*, vol. 44, no. 1, pp. 1–12, 2008.

[71] M. B. Bazbouz and G. K. Stylios, "Alignment and optimization of nylon 6 nanofibers by electrospinning," *Journal of Applied Polymer Science*, vol. 107, no. 5, pp. 3023–3032, 2007.

[72] M. B. Bazbouz and G. K. Stylios, "The tensile properties of electrospun nylon 6 single nanofibers," *Journal of Polymer Science, Part B: Polymer Physics*, vol. 48, no. 15, pp. 1719–1731, 2010.

[73] S. Y. Jan, H. S. Park, S. M. Jo et al., "Graphene composite nanofibre and preparation method thereof," 2013 US Patent 8,519,045, December 2010.

[74] C. N. Monty, E. K. Wujcik, and N. J. Blasdel, "Flexible electrode for detecting changes in temperature, humidity and sodium ion concentration in sweat," US Patent 2013/0197319, August 2013.

[75] N. J. Blasdel, E. K. Wujcik, J. E. Carletta, K.-S. Lee, and C. N. Monty, "Fabric nanocomposite resistance temperature detector," *IEEE Sensors Journal*, vol. 15, no. 1, pp. 300–306, 2015.

[76] R. Cruz-Silva, A. Morelos-Gomez, H.-I. Kim et al., "Super-stretchable graphene oxide macroscopic fibers with outstanding knotability fabricated by dry film scrolling," *ACS Nano*, vol. 8, no. 6, pp. 5959–5967, 2014.

[77] Y.-S. Wang, S.-M. Li, S.-T. Hsiao et al., "Integration of tailored reduced graphene oxide nanosheets and electrospun polyamide-66 nanofabrics for a flexible supercapacitor with high-volume- and high-area-specific capacitance," *Carbon*, vol. 73, pp. 87–98, 2014.

[78] L. Pan, X. Pei, R. He, Q. Wan, and J. Wang, "Multiwall carbon nanotubes/polycaprolactone composites for bone tissue engineering application," *Colloids and Surfaces B: Biointerfaces*, vol. 93, pp. 226–234, 2012.

[79] A. Kausar, "Mechanical, thermal, and electrical properties of epoxy matrix composites reinforced with polyamide-grafted-MWCNT/poly(azo-pyridine-benzophenone-imide)/ polyaniline nanofibers," *International Journal of Polymeric Materials and Polymeric Biomaterials*, vol. 63, no. 16, pp. 831–839, 2014.

[80] N. Vitchuli, Q. Shi, J. Nowak et al., "Multifunctional ZnO/Nylon 6 nanofiber mats by an electrospinning–electrospraying hybrid process for use in protective applications," *Science and Technology of Advanced Materials*, vol. 12, no. 5, Article ID 055004, 2011.

[81] R. Zhang and H. Olin, "Carbon nanomaterials as drug carriers: real time drug release investigation," *Materials Science and Engineering C*, vol. 32, no. 5, pp. 1247–1252, 2012.

[82] S. Zhang, W. S. Shim, and J. Kim, "Design of ultra-fine nonwovens via electrospinning of Nylon 6: spinning parameters and filtration efficiency," *Materials and Design*, vol. 30, no. 9, pp. 3659–3666, 2009.

[83] L. M. Guerrini, M. C. Branciforti, T. Canova, and R. E. S. Bretas, "Electrospinning and characterization of polyamide 66 nanofibers with different molecular weights," *Materials Research*, vol. 12, no. 2, pp. 181–190, 2009.

[84] X. Wang, B. Ding, G. Sun, M. Wang, and J. Yu, "Electrospinning/netting: a strategy for the fabrication of three-dimensional polymer nano-fiber/nets," *Progress in Materials Science*, vol. 58, no. 8, pp. 1173–1243, 2013.

[85] C. Zhang, Y. Li, W. Wang et al., "A novel two-nozzle electrospinning process for preparing microfiber reinforced pH-sensitive nano-membrane with enhanced mechanical property," *European Polymer Journal*, vol. 47, no. 12, pp. 2228–2233, 2011.

[86] H. R. Pant, M. P. Bajgai, C. Yi et al., "Effect of successive electrospinning and the strength of hydrogen bond on the morphology of electrospun nylon-6 nanofibers," *Colloids and Surfaces A: Physicochemical and Engineering Aspects*, vol. 370, no. 1–3, pp. 87–94, 2010.

[87] R. Nirmala, K. S. Jeon, R. Navamathavan, M. Park, H. Y. Kim, and S.-J. Park, "Enhanced electrical properties of electrospun nylon66 nanofibers containing carbon nanotube fillers and Ag nanoparticles," *Fibers and Polymers*, vol. 15, no. 5, pp. 918–923, 2014.

[88] S.-Y. Park, Y.-H. Cho, and R. A. Vaia, "Three-dimensional structure of the zone-drawn film of the nylon-6/ layered silicate nanocomposites," *Macromolecules*, vol. 38, no. 5, pp. 1729–1735, 2005.

[89] N. A. Jones, E. D. T. Atkins, and M. J. Hill, "Investigation of solution-grown, chain-folded lamellar crystals of the even-even nylons: 6 6, 8 6, 8 8, 10 6, 10 8, 10 10, 12 6, 12 8, 12 10, and 12 12," *Journal of Polymer Science, Part B: Polymer Physics*, vol. 38, no. 9, pp. 1209–1221, 2000.

[90] J. S. Stephens, D. B. Chase, and J. F. Rabolt, "Effect of the electrospinning process on polymer crystallization chain conformation in nylon-6 and nylon-12," *Macromolecules*, vol. 37, no. 3, pp. 877–881, 2004.

[91] C. T. Lim, E. P. S. Tan, and S. Y. Ng, "Effects of crystalline morphology on the tensile properties of electrospun polymer nanofibers," *Applied Physics Letters*, vol. 92, no. 14, Article ID 141908, 2008.

[92] K. S. Jeon, R. Nirmala, R. Navamathavan, and H. Y. Kim, "Mechanical behavior of electrospun Nylon66 fibers reinforced with pristine and treated multi-walled carbon nanotube fillers," *Ceramics International*, vol. 39, no. 7, pp. 8199–8206, 2013.

[93] S. D. Uzun, F. Kayaci, T. Uyar, S. Timur, and L. Toppare, "Bioactive surface design based on functional composite electrospun nanofibers for biomolecule immobilization and biosensor applications," *ACS Applied Materials & Interfaces*, vol. 6, no. 7, pp. 5235–5243, 2014.

[94] M. M. Bergshoef and G. J. Vancso, "Transparent nanocomposites with ultrathin, electrospun nylon-4,6 fiber reinforcement," *Advanced Materials*, vol. 11, no. 16, pp. 1362–1365, 1999.

Research Article

Flux Enhancement in Membrane Distillation Using Nanofiber Membranes

T. Jiříček,[1,2] M. Komárek,[2] J. Chaloupek,[2] and T. Lederer[2]

[1]*MemBrain s.r.o, Pod Vinicí 87, 47127 Stráž pod Ralskem, Czech Republic*
[2]*Technical University of Liberec, Studentská 1402/2, 46117 Liberec 1, Czech Republic*

Correspondence should be addressed to T. Jiříček; tomas.jiricek@membrain.cz

Membrane distillation (MD) is an emerging separation technology, whose largest application potential lies in the desalination of highly concentrated solutions, which are out of the scope of reverse osmosis. Despite many attractive features, this technology is still awaiting large industrial application. The main reason is the lack of commercially available membranes with fluxes comparable to reverse osmosis. MD is a thermal separation process driven by a partial vapour pressure difference. Flux, distillate purity, and thermal efficiency are always in conflict, all three being strictly connected with pore size, membrane hydrophobicity, and thickness. The world has not seen the ideal membrane yet, but nanofibers may offer a solution to these contradictory requirements. Membranes of electrospun PVDF were tested under various conditions on a direct contact (DCMD) unit, in order to determine the optimum conditions for maximum flux. In addition, their performance was compared to commonly available PTFE, PE, and PES membranes. It was confirmed that thinner membranes have higher fluxes and a lower distillate purity and also higher energy losses via conduction across the membrane. As both mass and heat transfer are connected, it is best to develop new membranes with a target application in mind, for the specific membrane module and operational conditions.

1. Introduction

As sources of fresh water are becoming scarcer, new possibilities of sea and brackish water desalination are being investigated. Traditional technologies like reverse osmosis still cover most of the demand due to the high capacity, but issues like brine disposal and energy consumption need to be addressed in order to keep the need for desalination sustainable. Investigation of membrane distillation has gained popularity in recent years. Driven by temperature rather than pressure gradient, MD can concentrate feed solutions to their saturation point without a significant flux decline. The process can be driven by low grade waste heat, including solar and geothermal energy [1].

Indeed, membrane distillation is still waiting for its large industrial application, mainly because of the unavailability of proper hydrophobic membranes with high fluxes and low heat losses. MD performance is strongly influenced by the structure of the membrane, such as thickness, porosity, and pore size distribution. Such a membrane is required

to provide an interface for the feed and distillate, while providing a resistance for them to mix. The optimum balance must be found between the conflicting requirements of high fluxes (thin membranes and large pores), low heat losses (thick membranes and small pores), and distillate purity (high liquid entry pressure and high contact angle).

(i) *Membrane thickness* plays a rather complicated role. Some authors state that the effect of membrane thickness is not completely clear [1]; others have found the optimum between 30 and 60 μm [2]. Membranes with low thickness have less resistance to mass transport, while they suffer from poor heat efficiency due to temperature polarization and conduction losses across the membrane [3].

(ii) *Pore size* is critical for MD performance. Porous membranes do not exhibit a single pore size; rather they have a pore size distribution, ideally narrow with a sharp peak. Larger pores cause higher fluxes but also bear a danger of pore wetting. Several large pores

can completely destroy the membrane performance by letting salty feed enter the distillate. The commonly used pore size ranges from 0.1 to 1 μm [4].

(iii) *Hydrophobicity* and optimum membrane pore size are closely connected. Hydrophobic polymers, such as PVDF, PP, and PTFE, are most commonly used. PTFE has the best hydrophobic properties but it is difficult to process; hence most research on membranes has been carried out on PVDF [1].

(iv) In addition, not only pore size but also *membrane porosity* dictates flux and heat efficiency. Air inside the pores has a thermal conductivity smaller by order of magnitude than the polymeric film.

Nanotechnology has a significant potential in desalination by MD by providing a layer with unusual properties. Nanofibers are typically created by an electrostatic field from a polymer solution by electrospinning [5, 6]. Various functional materials can be incorporated into the nanofibers during the electrospinning to enhance desired attributes, such as catalytic [7], biocidal [8, 9], or hydrophobic properties [10].

As recent papers covering electrospun nanofiber membranes [11, 12] declare high porosity and hydrophobicity, highly desirable properties for MD membranes, this paper covers an experimental comparison of nonwoven nanofiber membranes made from PVDF with commonly available film membranes, with the aim to investigate how flux and energy efficiency can be maximized. Previously published data with regard to membrane performance [13] have been confirmed and have been expanded with a comparison between various nanofiber membranes. None of the nanofiber membranes discussed in this paper have been altered by the introduction of hydrophobic additives to the polymer solution or by plasma treatment, as fluoropolymers themselves have excellent hydrophobicity and chemical resistance.

2. Theory

The flux across the membrane in DCMD is driven by a vapour pressure difference and can be represented simply by

$$N = C\Delta p, \tag{1}$$

where C is the membrane permeability and Δp is the difference of partial vapour pressure between the hot feed and cold distillate and for pure water can be calculated using Antoine's equation. In this work it is assumed that the actual Δp corresponds with ΔT between the feed and distillate, neglecting the effect of temperature polarization. At higher salinities, the actual feed vapour pressure is influenced by the activity of water a_w, and negative fluxes can occur at $\Delta T = 0°C$ due to the osmotic gradient [13].

Mass transport has the same direction as the conduction and convection of heat. The energy efficiency is the ratio of the efficient heat flux caused by the vapour flux and the total heat flux across the membrane and is calculated by

$$E = \frac{N\Delta H A}{mC_p \Delta T}, \tag{2}$$

Table 1: List of the tested membranes.

Membrane name	Lamination	Polymer thermal conductivity (W m^{-1} K^{-1})
PTFE	—	0.25
PE	—	0.43
PES	—	0.15
NanoPVDF03	2 sides	0.19
NanoPVDF04	1 side	0.19
NanoPVDF06	1 side	0.19

where N is flux, ΔH is the enthalpy of condensation, A is the effective membrane area, m is the mass flowrate along the membrane, C_p is the heat capacity, and ΔT is the temperature difference at the inlet and outlet of the module. Heat loss through the membrane can be reduced by optimizing membrane thickness, porosity, and thermal conductivity.

3. Materials and Methods

3.1. Membranes. Commercially available membranes are mainly made of PP, PTFE, PVDF, and PE [14]. Two kinds of membranes were tested in this study: commercial polymeric film membranes made from PTFE, PE, and PES and PVDF nanofiber membranes, supported from one or two sides by a bicomponent PP/PE 70/30 spunbond. The properties of the membranes are summarized in Table 1.

The PVDF nanofiber layers were prepared by continuous needleless electrospinning process. PVDF Solef 1015 was purchased from the "Solvay-Specialty Polymers Co." and dissolved in N,N-Dimethylformamide from Sigma-Aldrich. The solution was electrospun using the Nanospider™ (CZ), equipped with a 0.2 mm wire electrode and a moving applicator head. The voltage was set in the range of 50 to 70 kV and the distance between the electrodes was constantly 175 mm. Relative humidity was kept under 40% to minimize the formation of bead defects. Production speed was varied according to the desired nanofiber sheet thickness. The nanofibers were collected on a nonadhesive paper substrate and laminated on a Meyer (DE) flatbed laminator at 1.5 m min^{-1}, using a pressure of 10 N cm^{-2} at 135°C.

3.2. DCMD Setup. The membrane performance was tested on a bench scale DCMD experimental setup, built around a flat sheet membrane module from Aquastill (NL), with a rather large effective membrane area of 0.05 m^2 (Figure 1). The tests of membrane permeability were carried out with demineralised water in both circuits. The retention tests had demineralised water in the distillate circuit, and sodium chloride solution in the feed, ranging from 0 to 100 g kg^{-1}. The circulation was countercurrent with a horizontal position of the MD module, hot feed on the bottom, and cold distillate on top. The recirculation was powered by a peristaltic pump with a two-way rotation head, with a crossflow velocity of between 45 and 85 mm s^{-1}. The effect of feed concentration on flux and membrane retention was measured at 85 mm s^{-1}. In all of the experiments the logarithmic mean temperature
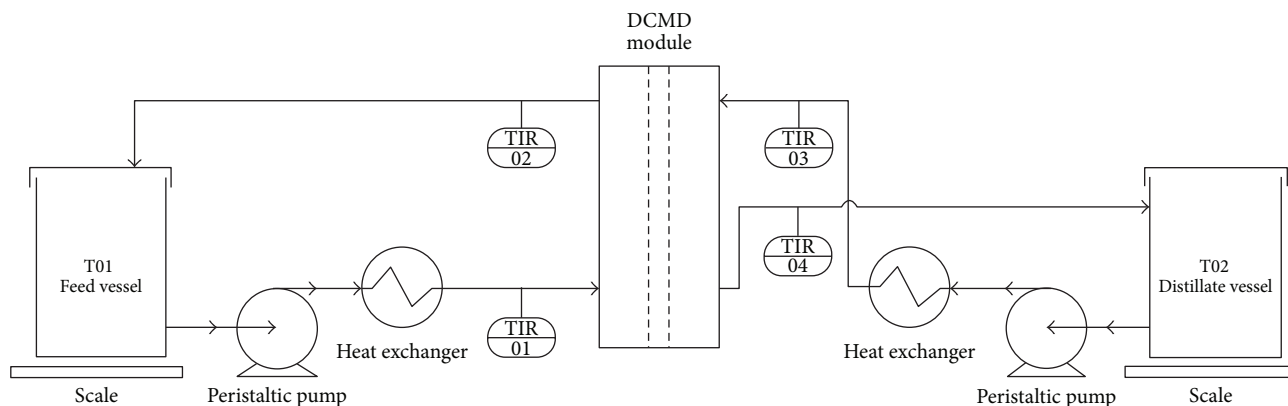
Figure 1: Schematic MD setup.

Table 2: Membrane properties.

Membrane name	Thickness (μm)	Mean pore size (μm)	Maximum pore size (μm)	LEP (bar)	Bubble point pressure (bar)	Contact angle
PTFE	72.1	0.22	0.276	9	2.320	136
PE	82.1	0.34	0.741	3	0.885	120
PES	72.5	0.55	0.620	2.9	1.303	131
NanoPVDF03	13.9	1.77	2.155	<0.64	0.297	123
NanoPVDF04	15.5	1.07	1.364	<0.65	0.469	135
NanoPVDF06	22.6	0.92	1.060	<0.66	0.601	129

difference (LMTD) was kept constant at 10°C, with the feed inlet temperature set to 60°C by a Julabo F12 hot bath and a cooling water circuit. Temperatures were measured by four thermocouples in the inlet and outlet pipes. The flux was calculated from the difference of mass on the feed and distillate A&D EK-12Ki scales. The electrical conductivity was measured by WTW TetraCon probes connected to WTW Mutli9430 and WTW Multi350i. Retention was calculated as $=1 - c_d/c_f$, where c_f is the feed concentration and c_d is the distillate concentration. Data analysis was performed using GraphPad Prism 6 and Microsoft Excel.

3.3. Porometry. POROMETER 3G by Quantachrome was used to measure the bubble point pressure and the maximum and average pore diameter, by using a wet-dry flow method with a wetting liquid Porefil. Water was used as a wetting liquid to estimate the liquid entry pressure (LEP), which is the pressure at which water wets the membrane pores.

3.4. Contact Angle. The contact angle was measured by Optical Tensiometer THETA QC from Attension, using demineralised water. This device automatically carries out the image analysis on the drop and gives the average of the right and left angle.

3.5. Membrane Structure and Thickness. Membrane structure and thickness were studied on a Tescan Vega3SB (CZ) high vacuum scanning electron microscope at an acceleration voltage of 30.0 kV. All of the samples were coated with a 5 nm thick layer of gold/palladium using a sputter coater (Quorum

Technologies, England). The cross section thicknesses of the membranes were obtained by cutting the membranes with a sharp razor, imaging the cut by SEM. Image analysis software from Tescan was used to measure the nanofiber diameters and cross section thickness of the membrane.

4. Results and Discussion

4.1. Membrane Characterisation. The tested membranes were characterised in order to explain the differences in their MD performance. The relevant parameters are summarized below (Table 2). The most obvious difference between the standard film membranes and the nanofiber layers is the membrane thickness, the latter being much thinner. Also, the pore size distribution is quite different, interestingly with the nonwoven membranes seeming to have larger pores. Nonwoven layers do not have pores as such but the porometer assumes unitary tubular pores.

Two parameters characterise membrane hydrophobicity, contact angle, and LEP.

(i) Considering that PTFE membranes are renowned for their superb hydrophobicity, it is a great achievement to find that PVDF layers have their contact angle in the same range.

(ii) However, when it comes to LEP, nanofiber layers cannot sustain a pressure of more than 0.64 bar, whereas water was able to penetrate PTFE pores only after 9 bar was applied. As no posttreatment was used on the laminated layers (e.g., CF$_4$ plasma), it
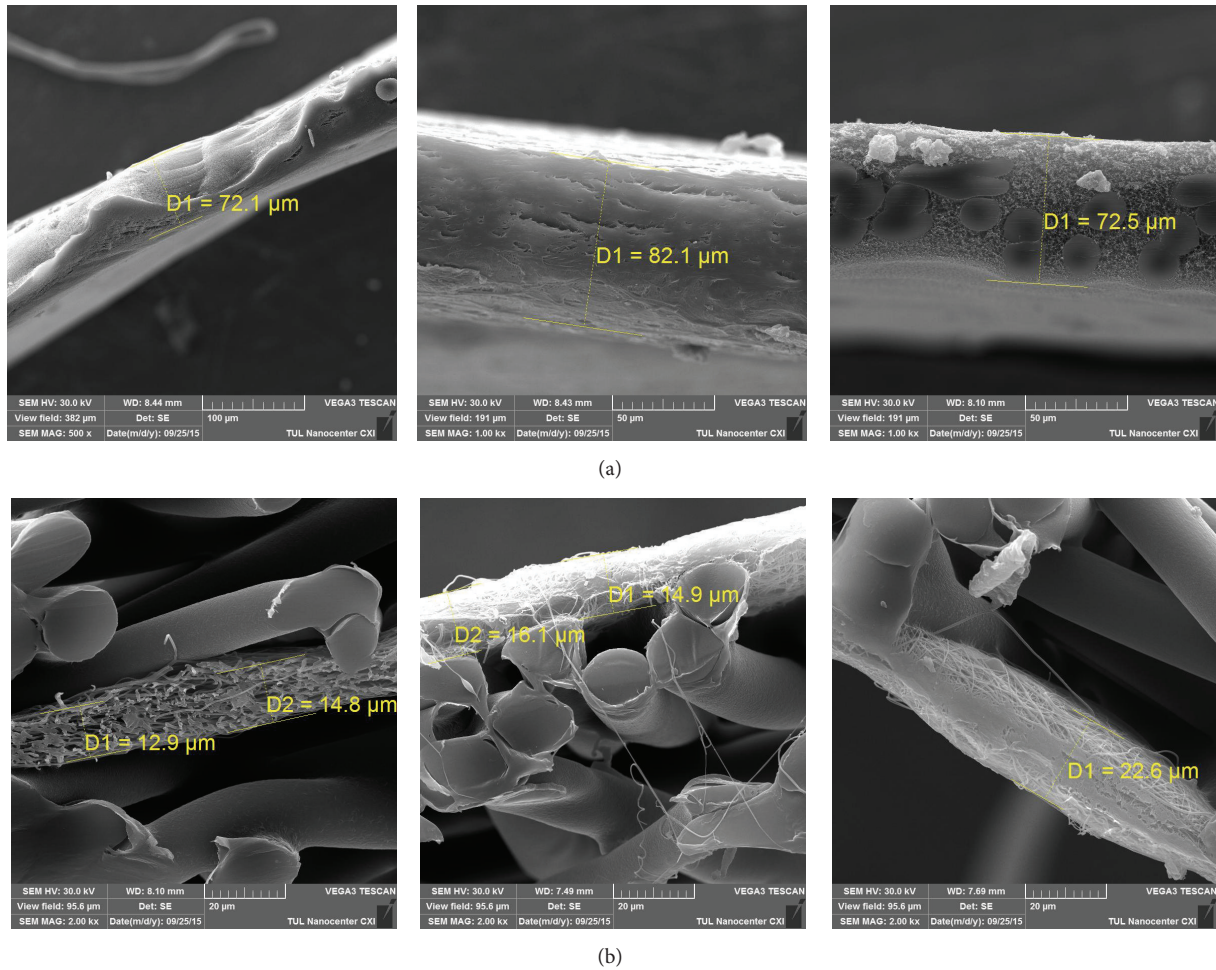
(a)

(b)

FIGURE 2: Cross section of membranes ((a) PTFE 1000x, PE 1000x, and PES 500x and (b) NanoPVDF03 2000x, NanoPVDF04 2000x, and NanoPVDF06 2000x).

is suggested that the lamination step compromised otherwise excellent PVDF hydrophobicity.

A cross section of the membranes with the measurement of their thickness is shown in Figure 2. The film membranes in Figure 2(a) show compression from a razor cut. Figure 2(b) shows the nanofiber membranes. NanoPVDF03 has a supporting spunbond from both sides, whereas NanoPVDF04 and NanoPVDF06 have it only from one side.

The film membranes have different structures from each other (Figure 3). PTFE has the finest structure, PE has rather large shapes, and PES has small circular pores. The nanofibers have a similar look, and in all cases the PVDF fiber diameter was around 200 nm. The structure is not uniform, with occasional polymer drops or fusing caused by nonevaporated solvent.

4.2. Flux. Figure 4 shows the effect of crossflow velocity on demineralised water flux. All of the nanofiber membranes respond better to an increase in crossflow velocity. NanoPVDF04 with one-side lamination shows the highest fluxes thanks to its small thickness, even though thinner

membranes should suffer more from temperature polarization. Larger pores do not contribute to flux increase, as pore size beyond 0.3 μm should not have a significant effect [15].

Two-side lamination spoils the membrane performance. NanoPVDF03 has the same thickness as NanoPVDF04 but the fluxes are significantly smaller at all crossflow velocities. The effect of crossflow velocity is smaller on the film membranes, and at smaller flowrates their fluxes are comparable to the better nanofiber membranes.

4.3. Energy Efficiency. Energy efficiency should increase with higher crossflow velocities (Figure 5), as the effective heat of condensation increases with flux, whereas the lossy heat of conduction remains about the same. This is stated because the driving force was set according to LMTD, which accounts for all four inlet and outlet temperatures and not only for the feed and distillate ΔT. There is a clear difference between the thick film and thin nonwoven membranes, the latter having much worse energy efficiency. The thermal conductivity of PTFE is about the same as PVDF but thanks to the PTFE thickness and superb hydrophobicity, it is assumed that only vapour is present in the membrane pores and heat losses are negligible.
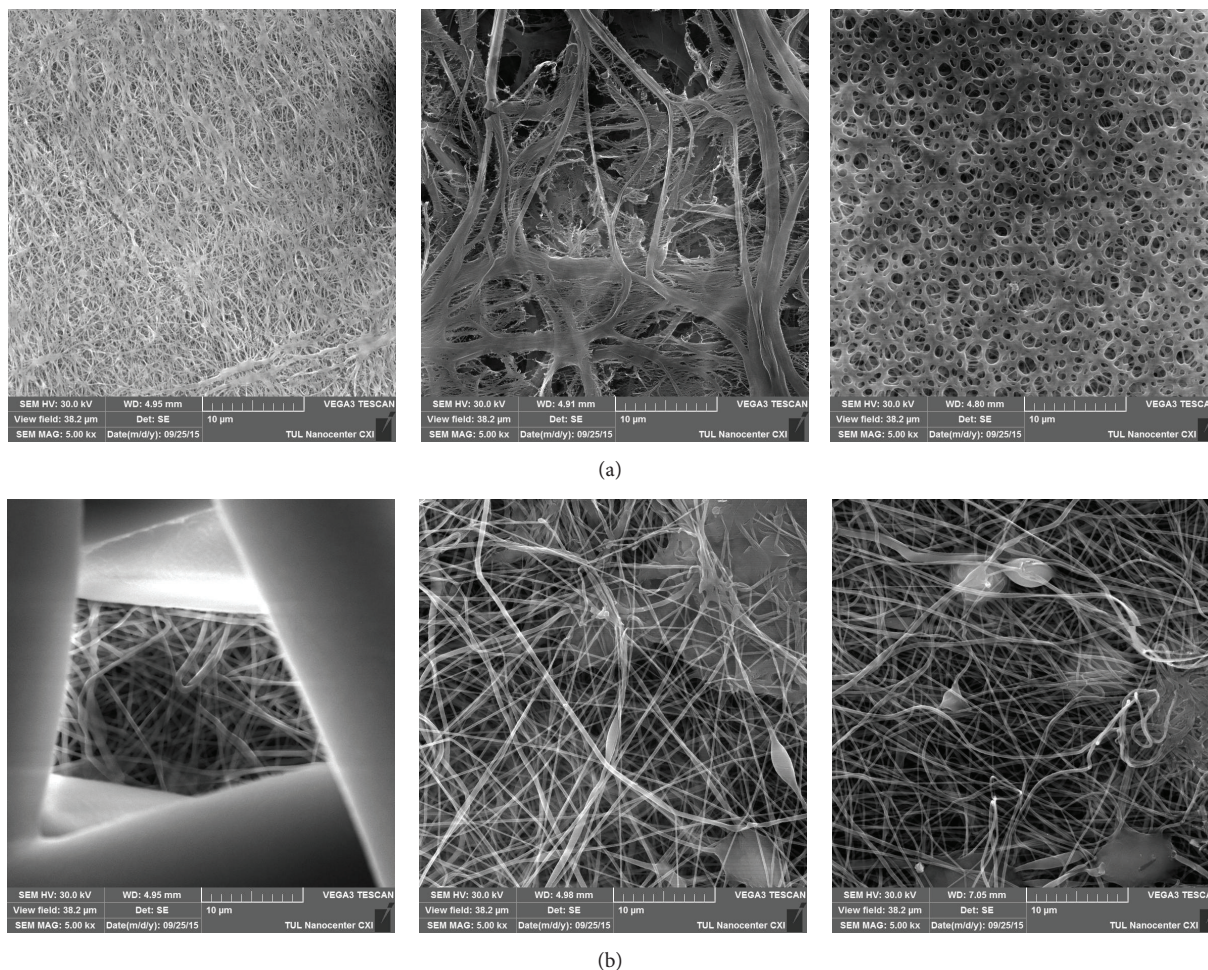
(a)

(b)

Figure 3: Perpendicular SEM micrographs of the membrane structure 1000x ((a) PTFE, PE, and PES and (b) NanoPVDF03, NanoPVDF04, and NanoPVDF06).

Despite its large membrane area, the estimation of energy efficiency on this current experimental setup is not very precise, as reflected in the fact that the PTFE efficiency is larger than 100% but the nanofibers are still behind. With large-scale application in mind, though, this may not be such a drawback because MD is considered to be driven by cheap low grade waste heat, and low fluxes of common membranes are a more significant disadvantage than suboptimal energy efficiency.

4.4. Retention. There are two aspects with regard to membrane retention: whether feed concentration reduces membrane flux and whether it affects distillate purity. In short, all of the tested membranes had excellent retention of above 99.7%. The only exception was NanoPVDF03 which had retention of around 85% at the highest concentration, and it is not displayed in Figure 6 due to axis scale. Compared to film membranes, nanofiber membranes are affected by the feed concentration and even though the retention is excellent the behaviour is different. The structure of the nonwoven layers is different, pore size distribution is wider (see the difference between maximum and mean pore size in Table 2), and an

occasional imperfection may cause salt to penetrate from the feed to the distillate. This was not caused by membrane wetting as the clean water flux before and after the test was unchanged.

To improve readability only four membranes are displayed in Figure 7. NanoPVDF04 again has the highest flux when the feed contains only demineralised water. Increasing the feed salinity decreases the flux through all of the membranes. The PTFE membrane seems to be least affected and shows the highest flux at $100 \, \mathrm{g \, kg^{-1}}$. NanoPVDF03 shows the lowest fluxes in accordance with the previous observations with clean water (Figure 4), although interestingly it is quite comparable to the rest at the maximum concentration.

5. Conclusions

Membrane thickness proved to be a crucial parameter when high fluxes are most important. With crossflow velocities of above $80 \, \mathrm{mm \, s^{-1}}$ nonwoven nanofiber membranes have unrivalled permeability. However, film membranes have their strengths as well and PTFE in particular demonstrates that decades of development have been worth it. It has by far the
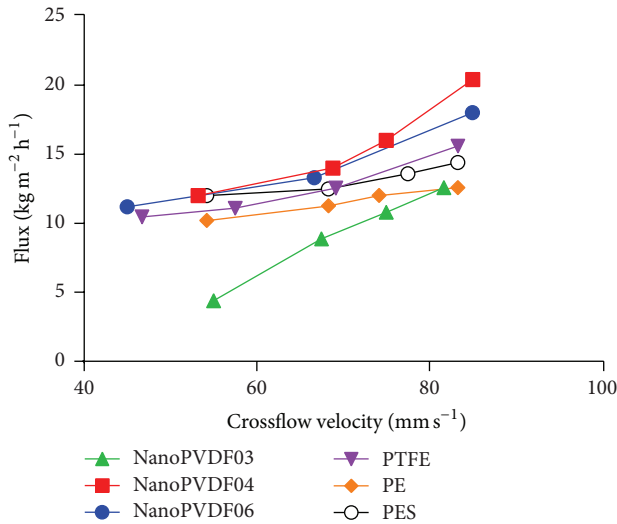
FIGURE 4: The effect of crossflow velocity on clean water flux.

FIGURE 6: Membrane retention varies between nanofiber and film membranes.

FIGURE 5: The effect of crossflow velocity on energy efficiency.
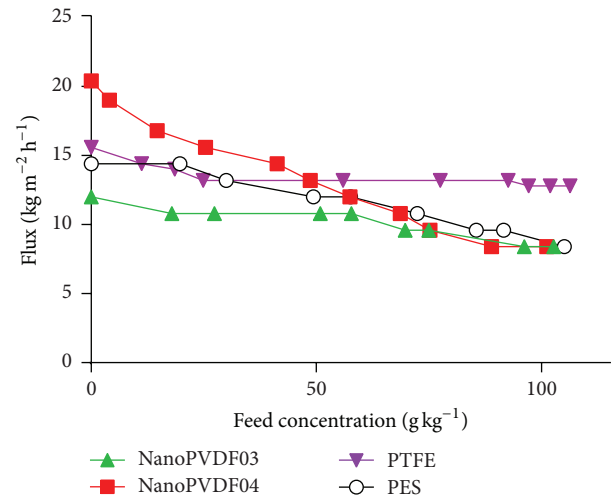
FIGURE 7: The effect of feed concentration on membrane flux.

best energy efficiency and also its fluxes at higher salinities are better than any other membrane tested.

Thus, selection of the right membrane is critical for the MD process, and it is necessary to bear the target application in mind. It has been confirmed that for slightly saline water up to 50 g kg^{-1} thinner membranes have higher permeability, but when feed salinity increases then PTFE has no competition. If the application is for the treatment of solutions that are beyond the range of reverse osmosis due to high osmotic pressure, then PTFE would be the right choice at the moment. On the other hand, when diluted solutions are treated, high fluxes are crucial and overall technological simplicity is required; nanofiber membranes may certainly have their purpose. Typically, any treatment of brackish or very hard groundwater will have its bottleneck in the overall hydraulic performance. Therefore, a very promising application is in power plants—there is enough waste heat

and also a requirement for softened cooling water, which is usually prepared from surface water.

It has been shown that flux, energy efficiency, and distillate purity are closely connected and one cannot be increased without sacrificing the other two. High fluxes are the most desirable progress in MD these days. Nanofiber membranes suggest a solution but further improvement of membrane hydrophobicity in terms of LEP would be required for most future large-scale applications.

Abbreviations and Symbols

N: Flux (kg m^{-2} h^{-1})
C: Permeability (kg m^{-2} h^{-1} bar^{-1})
Δp: Vapour pressure difference (bar)
E: Energy efficiency (%)
ΔH: Enthalpy of condensation (J kg^{-1})
A: Membrane area (m^2)

m: Mass flowrate ($kg\,s^{-1}$)
C_p: Heat capacity at constant pressure ($J\,kg^{-1}\,K^{-1}$)
ΔT: Temperature difference (°C)
LMTD: Logarithmic mean temperature difference (°C)
a_w: Activity of water (1)
R: Retention (%)
C_f: Feed concentration ($g\,kg^{-1}$)
C_d: Distillate concentration ($g\,kg^{-1}$)
LEP: Liquid entry pressure (bar)
DCMD: Direct contact membrane distillation
MD: Membrane distillation
PTFE: Polytetrafluoroethylene
PE: Polyethylene
PES: Polyethersulfone
PP: Polypropylene
PVDF: Polyvinylidene fluoride.

Competing Interests

The authors declare that there is no conflict of interests regarding the publication of this paper.

References

[1] E. Drioli, A. Ali, and F. Macedonio, "Membrane distillation: recent developments and perspectives," *Desalination*, vol. 356, pp. 56–84, 2015.

[2] F. Laganà, G. Barbieri, and E. Drioli, "Direct contact membrane distillation: modelling and concentration experiments," *Journal of Membrane Science*, vol. 166, no. 1, pp. 1–11, 2000.

[3] S. Al-Obaidani, E. Curcio, F. Macedonio, G. Di Profio, H. Al-Hinai, and E. Drioli, "Potential of membrane distillation in seawater desalination: thermal efficiency, sensitivity study and cost estimation," *Journal of Membrane Science*, vol. 323, no. 1, pp. 85–98, 2008.

[4] A. Alkhudhiri, N. Darwish, and N. Hilal, "Membrane distillation: a comprehensive review," *Desalination*, vol. 287, pp. 2–18, 2012.

[5] D. Lukáš, A. Sarkar, L. Martinová et al., "Physical principles of electrospinning (electrospinning as a nano-scale technology of the twenty-first century)," *Textile Progress*, vol. 41, no. 2, pp. 59–140, 2009.

[6] F. Yener and O. Jirsak, "Comparison between the needle and roller electrospinning of polyvinylbutyral," *Journal of Nanomaterials*, vol. 2012, Article ID 839317, 6 pages, 2012.

[7] C. Basheer, "Nanofiber-membrane-supported TiO$_2$ as a catalyst for oxidation of benzene to phenol," *Journal of Chemistry*, vol. 2013, Article ID 562305, 7 pages, 2013.

[8] A. Haider, S. Kwak, K. C. Gupta, and I.-K. Kang, "Antibacterial activity and cytocompatibility of PLGA/CuO hybrid nanofiber scaffolds prepared by electrospinning," *Journal of Nanomaterials*, vol. 2015, Article ID 832762, 10 pages, 2015.

[9] F. Yalcinkaya, M. Komarek, D. Lubasova, F. Sanetrnik, and J. Maryska, "Preparation of antibacterial nanofibre/nanoparticle covered composite yarns," *Journal of Nanomaterials*, vol. 2016, Article ID 7565972, 7 pages, 2016.

[10] N. Nuraje, W. S. Khan, Y. Lei, M. Ceylan, and R. Asmatulu, "Superhydrophobic electrospun nanofibers," *Journal of Materials Chemistry A*, vol. 1, no. 6, pp. 1929–1946, 2013.

[11] A. Razmjou, E. Arifin, G. Dong, J. Mansouri, and V. Chen, "Superhydrophobic modification of TiO$_2$ nanocomposite PVDF membranes for applications in membrane distillation," *Journal of Membrane Science*, vol. 415-416, pp. 850–863, 2012.

[12] C. Yang, X.-M. Li, J. Gilron et al., "CF4 plasma-modified superhydrophobic PVDF membranes for direct contact membrane distillation," *Journal of Membrane Science*, vol. 456, pp. 155–161, 2014.

[13] L. Eykens, I. Hitsov, K. De Sitter et al., "Influence of membrane thickness and process conditions on direct contact membrane distillation at different salinities," *Journal of Membrane Science*, vol. 498, pp. 353–364, 2016.

[14] B. L. Pangarkar, M. G. Sane, and M. Guddad, "Reverse osmosis and membrane distillation for desalination of groundwater: a review," *ISRN Materials Science*, vol. 2011, Article ID 523124, 9 pages, 2011.

[15] M. I. Ali, E. K. Summers, H. A. Arafat, and J. H. Lienhard V, "Effects of membrane properties on water production cost in small scale membrane distillation systems," *Desalination*, vol. 306, pp. 60–71, 2012.

Research Article
Modified Silica Nanofibers with Antibacterial Activity

Ivana Veverková[1] and Irena Lovětinská-Šlamborová[2]

[1]*Faculty of Textile Engineering, Technical University of Liberec, Studentská 1402/2, 46117 Liberec, Czech Republic*
[2]*Institute of Health Studies, Technical University of Liberec, Studentská 1402/2, 46117 Liberec, Czech Republic*

Correspondence should be addressed to Ivana Veverková; ivana.veverkova@tul.cz

This study is focused on development of functionalized inorganic-organic nanofibrous material with antibacterial activity for wound dressing applications. The nanofibers combining poly(vinyl alcohol) and silica were produced by electrospinning from the sol and thermally stabilized. The PVA/silica nanofibers surface was functionalized by silver and copper nanoparticles to ensure antibacterial activity. It was proven that quantity of adsorbed silver and copper nanoparticles depends on process time of adsorption. According to antibacterial tests results, this novel nanofibrous material shows a big potential for wound dressing applications due to its significant antibacterial efficiency.

1. Introduction

In the past decade, the big attention is paid to tissue engineering, the wide field of nanomaterial application, leading to regeneration or replacement of damaged human tissue. One of the key factors in tissue engineering is the development of functional three-dimensional scaffold with suitable degradation rates. The scaffolds for tissue engineering should have high porosity to allow enough space for adhesion and proliferation of a large number of cells, as well as large interconnected pores to facilitate distribution of cells into the bulk of scaffold and the diffusion of oxygen and nutrients. Essential properties of scaffold for tissue engineering are its biocompatibility and biodegradability. The design of the scaffolds is very important; it should restore tissue structure as closely as possible to the native structure of extracellular matrix.

Typically, biodegradable scaffolds are fabricated using electrospinning. Electrospinning is a method that produces polymer fibers using electrically driven jet; starting material is polymer solution or melt. Despite the simplicity of the process, it produces ultrafine fibers (micro- or nanofibers) with high specific surface area with various pore sizes. Regarding the nanofibers composition, there is a possibility of scaffold modifications by metal particles or various type of

biomolecules (enzymes, peptides, and antibiotics) to adjust its properties for specific application [1]. The electrospun nanofibers are widely used for biomedical applications as mentioned tissue engineering involving also wound dressing [2, 3], drug delivery systems [4], cell culture, and others. There are many studies of research organic [5, 6] or inorganic polymers [7, 8] as a scaffold material for biomedical applications and a few studies considering use of inorganic-organic materials combination [9].

Poly(vinyl alcohol) (PVA) is a hydrophilic polymer with specific properties: inherent nontoxicity, noncarcinogenicity, good biocompatibility, and high degree of swelling in aqueous solutions. Due to these properties, PVA is presented in some frequently used technologies such as hydrogels and biomaterials [10] including soft contact lenses [11], implants, and artificial organs [12]. It is an inexpensive biocompatible material and it is easily electrospinnable.

Silica nanomaterials are a good candidate for medical applications because they are able to meet a number of mentioned strict criteria (low toxicity, high porosity, and relatively suitable surface for subsequent functionalization). Thanks to the Si-O bonds on the surface, these materials represent attractive matrix for binding and release of biomolecules. Localized and controlled release of additives is a crucial aspect to increase efficiency and reduce potential side effects

of additives (antibiotics, enzymes, and metal ions). Thanks to these properties, silica nanofibers appear to be the ideal material for tissue engineering as well as wound dressing for the treatment of chronic wounds [13].

As is generally known, silver (Ag) in form of ions or nanoparticles has a broad spectrum of antibacterial activity. This phenomenon is widely used in commercially available products for wound dressing. Presence of Ag ions in wound bed facilitates wound healing and it has a strong antibacterial activity at the site of damage. Silver ions and nanosilver are able to kill a wide range of bacteria including those which are resistant to antibiotics [14]. In recent years, there have been several published researches of possible antimicrobial mechanism of Ag [15], but the complete mechanism of action is not fully understood. According to available researches, Ag ions immobilized onto the surface of organic or inorganic nanofibers show significant antibacterial activity and cyto-compatibility [16, 17].

It was proven that copper (Cu) is an essential component of the angiogenesis in skin layer [18]. It has been reported that copper ions enhance angiogenesis by imitating hypoxia, which plays a critical role in the cells formation and differentiation leading to blood vessel formation. In combination with specific growth factors (vascular endothelial growth factor, VEGF; basic fibroblast growth factor, bFGF), Cu^{2+} ions were shown to enhance the vascularization of an implant or regenerate tissue [19, 20].

In this study, development of combined polymer/silica nanofibers with silver and copper nanoparticles is presented. These hybrid nanofibers are intended to function as antibacterial wound dressing. There are discussed results of antibacterial activity tests of the PVA/silica nanofibers with various amounts of silver and copper nanoparticles.

2. Materials and Methods

2.1. Materials. The main chemical components of PVA/silica nanofibers were tetraethyl orthosilicate (TEOS, ≥99%, Sigma Aldrich), ethanol (Penta chemicals), cetyltrimethyl-ammonium bromide (CTAB, Acros Organics), hydrochloric acid (HCl, min. 35%, Penta chemicals), (3-mercaptopropyl)trimethoxysilane (MPS, 95%, Sigma Aldrich), and poly(vinyl alcohol) (PVA, 16%, Sloviol R). For modification of the nanofibers surface, silver nitrate (AgNO$_3$, p.a., Penta chemicals) and copper nitrate trihydrate (Cu(NO$_3$)$_2$·3H$_2$O, p.a. 99–104%, Sigma Aldrich) were used.

For antibacterial tests, the Gram-negative *Escherichia coli* (*E. coli*, ATCC 9637) and the Gram-positive *Staphylococcus Aureus* (*S. aureus*, ATCC 12600) were purchased from the Czech Collection of Microorganisms, Masaryk University in Brno. The composition of base for antibacterial tests was the blood agar supplied from Biorad s.r.o, Prague, and nutrient agar (Nutrient Agar number 2, Himedia).

2.2. Preparation of Nanofibers. The PVA/silica nanofibers were produced from sol prepared by sol-gel method. The initial sol was prepared from TEOS by controlled hydrolysis and polycondensation in ethanol as solvent and HCl as catalyst. Into the initial sol, MPS and CTAB were added to improve conductivity and thus electrospinning process. The sol was heated to 60°C and mixed for 60 minutes. After that time, PVA solution was slowly dropped into the sol. The viscous mixture of PVA and silica sol was obtained.

The nanofibrous layer was produced by needleless electrospinning. The electrospinning was performed on laboratory instrument. The instrument consisted of an adjustable, regulated, high-voltage power supply (up to 80 kV), a rod electrode, and collector units. The prepared solution was applied on the rod electrode. The electrospinning was performed at room temperature; the applied high voltage was 40–45.7 kV. The electrospun nanofibers were assembled on a conductive plate as a collector, and the collector was placed 10 cm from the top of the rod electrode. The nanofibers were then thermally stabilized (180°C, 2 hours).

2.3. Functionalization of Nanofibers. AgNO$_3$ as well as Cu(NO$_3$)$_2$·3H$_2$O were dissolved in a solution of ethanol and distilled water. The prepared nanofibers samples (cca 0.005 g/1 sample) were immersed into the solution. The functionalization of nanofibers by Ag and Cu nanoparticles was carried out in different process times of 30 min, 45 min, and 60 min. Subsequently, the samples were rinsed in distilled water and dried.

2.4. Characterization of Nanofibers. The morphology of the electrospun nanofibers was observed by field emission scanning electron microscopy (FE-SEM) Zeiss Ultra Plus. Prior to the analysis, the samples were coated with 2 nm of platinum to achieve sustainable surface conductivity. An InLens secondary electron detector operated at accelerating voltage of 2 kV was used for the imaging of topographical contrast. For a local chemical analysis, EDS detector Oxford X-MAX on SEM was used; applied accelerating voltage was 15 kV.

2.5. Antibacterial Activity Test. The antibacterial tests against Gram-negative bacteria *E. coli* and Gram-positive *S. aureus* were carried out by standard test method of spreading on the agar plate (according to ČSN EN ISO 20645, antibacterial activity testing of fabrics). The nutrient agar (final pH = 7.2) was sterilized and inoculated with 1 mL of bacterial inoculum (10^8 CFU/mL). The prepared inoculate agar was mixed thoroughly and 5 mL of the agar was poured into Petri dishes on agar base: standard blood agar. Within each Petri dish, there was placed a sterile sample (2 × 2 cm). The samples were incubated in a thermostat at 37°C for 20 hours. After removal from the thermostat, the inhibitory zone H is measured and evaluated. Pure PVA/silica nanofibers were considered as control sample, where no antibacterial activity was expected.

The size of the inhibition zone H is calculated according to the formula $H = (D-d)/2$, where D is the overall diameter of the sample and inhibition in mm d is diameter of the sample in mm.
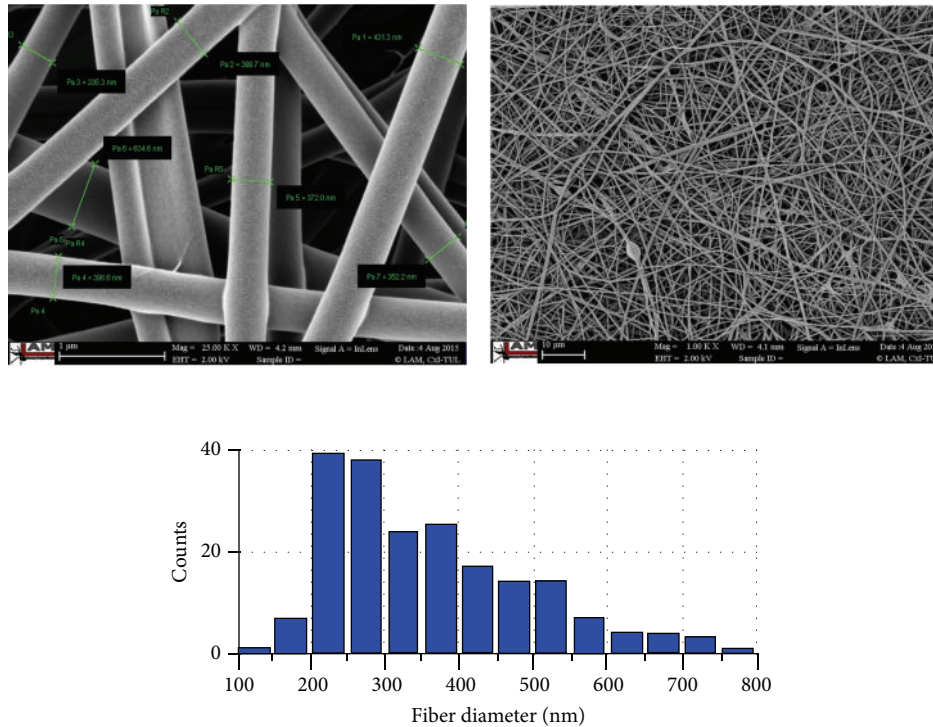
FIGURE 1: SEM images of PVA/silica nanofibers with fiber diameter distribution (magnification 25000x and 1000x).

TABLE 1: Quantitative EDS analysis results for PVA/silica nanofibers with Ag and Cu nanoparticles.

At%	C	O	Si	S	Cu	Ag
Cu-t30	41.54	38.33	15.81	2.95	**1.37**	—
Cu-t45	41.15	38.75	15.79	2.93	**1.38**	—
Cu-t60	38.84	40.44	16.24	2.91	**1.57**	—
Ag-t30	37.90	40.20	15.13	2.84	—	**3.93**
Ag-t45	36.84	40.22	15.57	2.93	—	**4.44**
Ag-t60	37.07	39.86	15.18	2.88	—	**5.01**

3. Results and Discussion

3.1. PVA/Silica Nanofibers Morphology. SEM images of PVA/silica nanofibers after thermal stabilization are depicted in Figure 1. The nanofibers retained their morphology after thermal stabilization; they do not break significantly. The nanofibrous layer was compact and uniform with mean fiber diameter of 362 nm (Figure 1).

3.2. Functionalization of PVA/Silica Nanofibers. The thermally stabilized PVA/silica nanofibers were functionalized by Ag (as presented in [21]) and Cu nanoparticles in different process times: 30, 45, and 60 min (samples labeled Ag/Cu-t30, Ag/Cu-t45, and Ag/Cu-t60).

For PVA/silica nanofibers functionalized by Cu nanoparticles, there were no significant differences between Cu nanoparticles amounts on samples processing for 30 and 45 min (Cu-t30, Cu-t45), as shown in Table 1. Because of that,

samples chosen for antibacterial testing were Cu-t30 and Cu-t60. Figure 2 gives the SEM images of PVA/silica nanofibers with Cu nanoparticles. There are lightened Cu nanoparticles presented in the nanofibrous layer. The presence of Cu nanoparticles was also proved by local quantitative EDS analysis results (Table 1); the quantity of Cu was determined 1.37 At% for sample Cu-t30 and 1.58 At% for sample Cu-t60. According to the researches of Cu ions and nanoparticles function [19, 20], significant antibacterial activity of the samples Cu-t30 and Cu-t60 had not been expected.

In Figure 3, there are displayed SEM images of PVA/silica nanofibers with Ag nanoparticles: samples Ag-t30, Ag-t45, and Ag-t60. As observed, Ag nanoparticles are attached on the nanofibers surface in constant density on the entire surface of single fibers. There are also irregularly presented Ag nanoparticles clusters. Ag nanoparticles are attached not only on the fibers in surface layer of the sample, but also on the fibers inside the bulk of samples. That is a very important factor for long-term antibacterial activity of the samples corresponding with the nanofibers degradation and gradual releasing of Ag.

EDS analysis results for these samples Ag-t30, Ag-t45, and Ag-t60 are given in Table 1. It should be concluded that process time of functionalization by Ag nanoparticles significantly influences the quantity of Ag nanoparticles on the PVA/silica nanofibers. According to Table 1, quantity of Ag nanoparticles for the sample Ag-t30 was 3.93 At%, for the sample Ag-t45 was 4.44 At%, and for the sample Ag-t60 was 5.01 At%. Based on these facts, we can expect intensive antibacterial activity of PVA/silica nanofibers with Ag nanoparticles.
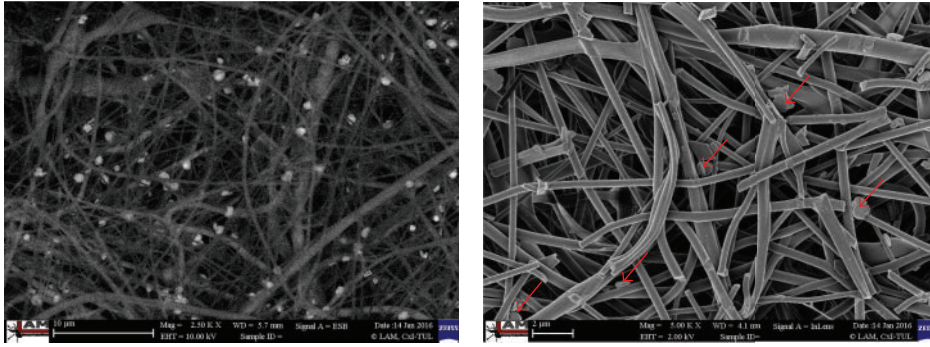
FIGURE 2: SEM images of PVA/silica nanofibers with Cu nanoparticles: sample Cu-t60 (magnification 2500x and 5000x).

(a)

(b)

(c)
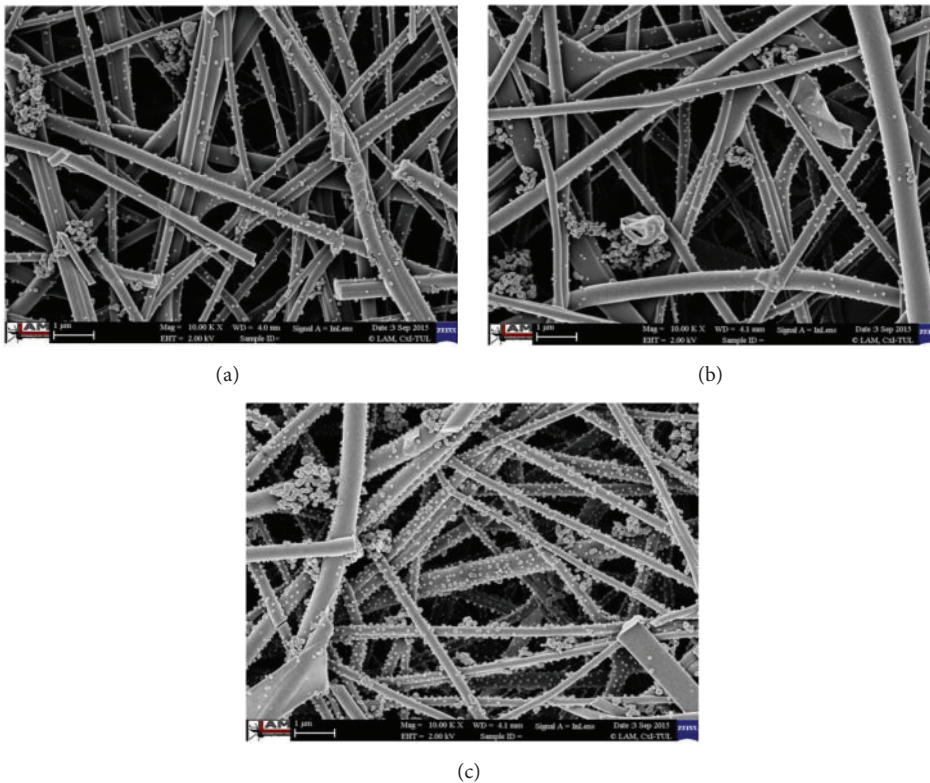
FIGURE 3: SEM images of PVA/silica nanofibers with Ag nanoparticles: samples Ag-t30 (a), Ag-t45 (b), and Ag-t60 (c).

3.3. Antibacterial Activity Test Results. The antibacterial activity of the fiber mats against *E. coli* Gram-negative bacteria and *S. aureus* Gram-positive bacteria, which is commonly found on burn wounds, was tested by using the test method of spreading on the agar plate, where the inhibition zone diameter is measured. The capability of the functionalized nanofibrous mats to inhibit the growth of the tested microorganisms on solid media is shown in Table 2. It was found that the diameter of inhibition zone varied according to the type and quantity of nanoparticles on the nanofibers surface.

Very significant antibacterial activity is presented for PVA/silica nanofibers with Ag nanoparticles. The inhibition zone diameter was 5 mm for Ag-t30 and Ag-t40 samples, 6 mm was measured for Ag-t60 sample (Figure 4).

TABLE 2: Diameters of inhibition zones H (mm) for given samples and the control sample against different test bacteria after 20 h by test method of spreading on the agar plate at 37°C.

Inhibition zone H (mm)	Control PVA/silica NF	Ag-t30	Ag-t45	Ag-t60	Cu-t30	Cu-t60
E. coli	0.5	5	5	6	0	0
S. aureus	1	1	1.5	1	0	0

The inhibition zone diameter of these samples is ≥1 mm; that is evaluated as good antibacterial activity according to the ČSN EN ISO 20645 standard evaluation. In fact, inhibition zone diameters are highly above the limit in
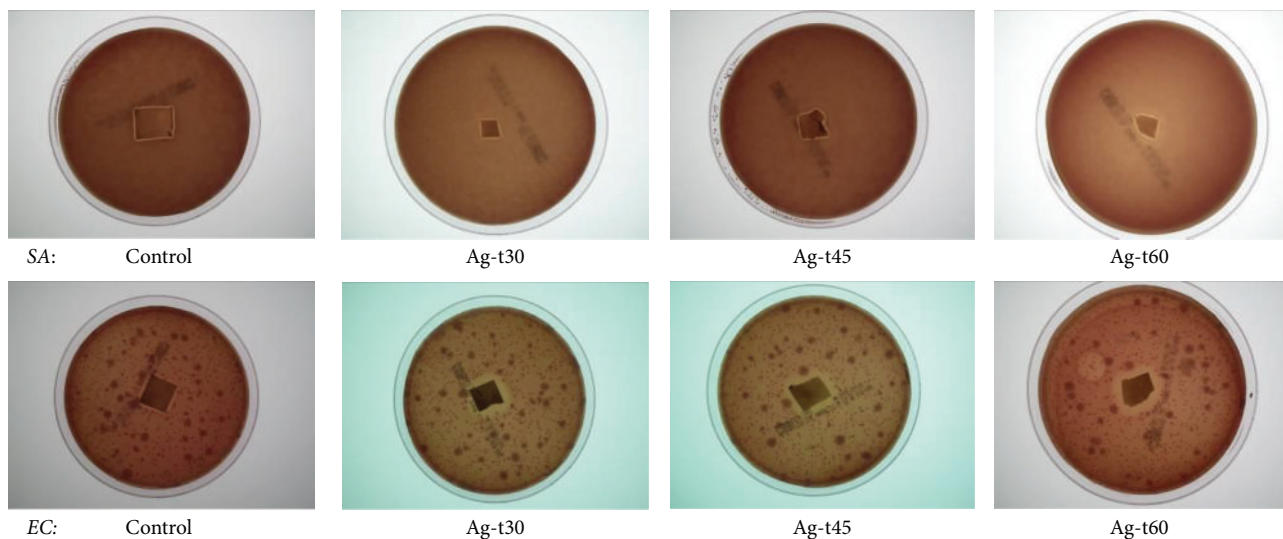
FIGURE 4: The antibacterial activity of the PVA/silica nanofibers with Ag nanoparticles against *S. aureus* (*SA*) and *E. coli* (*EC*).

accordance with the standard for samples Ag-t30, Ag-t40, and Ag-t60. Summarizing the results, it can be noted that PVA/silica nanofibers with Ag ions show significant antibacterial activity. Antibacterial activity is affected by quantity of Ag nanoparticles on the nanofibrous mats. How that was demonstrated, PVA/silica nanofibers with 5.01 At% of Ag nanoparticles (sample Ag-t60) exhibited the most effective antibacterial activity. It is associated with the highest Ag nanoparticles content of all tested samples.

As expected, PVA/silica nanofibers with Cu nanoparticles do not show any significant antibacterial activity. Bacterial colonies both of *E. coli* and *S. aureus* were reproduced after the incubation time; the samples Cu-t30 and Cu-t60 were overgrown by the bacteria. The efficiency of Cu nanoparticles is predicted in support of cell growth (fibroblasts, keratinocytes).

Moderate antibacterial effect is also recognized for control sample: pure PVA/silica nanofibers. It may be caused by presence of CTAB, which itself exhibits an antibacterial effect. The cetrimonium (hexadecyltrimethylammonium) cation is an effective antiseptic agent against bacteria and fungi. It is one of the components of the topical antiseptic cetrimide [22].

4. Conclusion

In the study, preparation of inorganic-organic nanofibers for antibacterial wound dressing is demonstrated. PVA/silica nanofibrous mats were prepared by electrospinning method. This nanofibrous mat is able to adsorb Ag and Cu nanoparticles on the nanofibers surface. Different quantity of Ag and Cu nanoparticles was successfully bonded on the PVA/silica nanofibers. The quantity of adsorbed Ag and Cu nanoparticles depends on the process time. Significant antibacterial activity of the nanofibrous material was proven for the PVA/silica nanofibers with Ag nanoparticles; it was not proven for PVA/silica nanofibers with Cu nanoparticles.

The presence of Ag nanoparticles in PVA/silica nanofibers enhanced the antibacterial ability of the electrospun mats giving the material potential as a good wound dressing material.

Competing Interests

The authors declare that there is no conflict of interests regarding the publication of this paper.

Acknowledgments

References

[1] Y. Ito, H. Hasuda, M. Kamitakahara et al., "A composite of hydroxyapatite with electrospun biodegradable nanofibers as a tissue engineering material," *Journal of Bioscience and Bioengineering*, vol. 100, no. 1, pp. 43–49, 2005.

[2] R. Zhao, X. Li, B. Sun et al., "Electrospun chitosan/sericin composite nanofibers with antibacterial property as potential wound dressings," *International Journal of Biological Macromolecules*, vol. 68, pp. 92–97, 2014.

[3] L. Tan, J. Hu, and H. Zhao, "Design of bilayered nanofibrous mats for wound dressing using an electrospinning technique," *Materials Letters*, vol. 156, pp. 46–49, 2015.

[4] X. Li, M. A. Kanjwal, L. Lin, and I. S. Chronakis, "Electrospun polyvinyl-alcohol nanofibers as oral fast-dissolving delivery system of caffeine and riboflavin," *Colloids and Surfaces B: Biointerfaces*, vol. 103, pp. 182–188, 2013.

[5] P. Karuppuswamy, J. R. Venugopal, B. Navaneethan, A. L. Laiva, S. Sridhar, and S. Ramakrishna, "Functionalized hybrid nanofibers to mimic native ECM for tissue engineering applications," *Applied Surface Science*, vol. 322, pp. 162–168, 2014.

[6] S. Chahal, F. Hussain, and M. Yusoff, "Characterization of modified cellulose (Mc)/poly (Vinyl Alcohol) electrospun nanofibers

for bone tissue engineering," *Procedia Engineering*, vol. 53, pp. 683–688, 2013.

[7] S. P. Adhikari, H. R. Pant, H. M. Mousa et al., "Synthesis of high porous electrospun hollow TiO$_2$ nanofibers for bone tissue engineering application," *Journal of Industrial and Engineering Chemistry*, vol. 35, pp. 75–82, 2016.

[8] L. Ren, R. Ozisik, and S. P. Kotha, "Rapid and efficient fabrication of multilevel structured silica micro-/nanofibers by centrifugal jet spinning," *Journal of Colloid and Interface Science*, vol. 425, pp. 136–142, 2014.

[9] M. Mehrasa, M. A. Asadollahi, K. Ghaedi, H. Salehi, and A. Arpanaei, "Electrospun aligned PLGA and PLGA/gelatin nanofibers embedded with silica nanoparticles for tissue engineering," *International Journal of Biological Macromolecules*, vol. 79, pp. 687–695, 2015.

[10] Y.-L. Liu and Y.-C. Chiu, "Novel approach to the chemical modification of poly(vinyl alcohol): phosphorylation," *Journal of Polymer Science Part A: Polymer Chemistry*, vol. 41, no. 8, pp. 1107–1113, 2003.

[11] S. H. Hyon, W. I. Cha, Y. Ikada, M. Kita, Y. Ogura, and Y. Honda, "Poly(vinyl alcohol) hydrogels as soft contact lens material," *Journal of Biomaterials Science*, vol. 5, no. 5, pp. 397–406, 1994.

[12] J.-H. Juang, S. Bonner-Weir, Y. Ogawa, J. P. Vacanti, and G. C. Weir, "Outcome of subcutaneous islet transplantation improved by polymer device," *Transplantation*, vol. 61, no. 11, pp. 1557–1561, 1996.

[13] I. Lovětinska-Šlamborova, P. Exnar, L. Vatahová et al., "Křemičitá nanovlákna pro léčbu chronických ran," *Zdravotnické Listy*, vol. 2, no. 4, pp. 6–13, 2014.

[14] M. S. Mauter, Y. Wang, K. C. Okemgbo, C. O. Osuji, E. P. Giannelis, and M. Elimelech, "Antifouling ultrafiltration membranes via post-fabrication grafting of biocidal nanomaterials," *ACS Applied Materials & Interfaces*, vol. 3, no. 8, pp. 2861–2868, 2011.

[15] K. Chaloupka, Y. Malam, and A. M. Seifalian, "Nanosilver as a new generation of nanoproduct in biomedical applications," *Trends in Biotechnology*, vol. 28, no. 11, pp. 580–588, 2010.

[16] J. Y. Chun, H. K. Kang, L. Jeong et al., "Epidermal cellular response to poly(vinyl alcohol) nanofibers containing silver nanoparticles," *Colloids and Surfaces B: Biointerfaces*, vol. 78, no. 2, pp. 334–342, 2010.

[17] Z. Ma, H. Ji, D. Tan et al., "Silver nanoparticles decorated, flexible SiO$_2$ nanofibers with long-term antibacterial effect as reusable wound cover," *Colloids and Surfaces A: Physicochemical and Engineering Aspects*, vol. 387, no. 1–3, pp. 57–64, 2011.

[18] R. Barbucci, S. Lamponi, A. Magnani, F. M. Piras, A. Rossi, and E. Weber, "Role of the Hyal–Cu (II) complex on bovine aortic and lymphatic endothelial cells behavior on microstructured surfaces," *Biomacromolecules*, vol. 6, no. 1, pp. 212–219, 2005.

[19] C. Gérard, L.-J. Bordeleau, J. Barralet, and C. J. Doillon, "The stimulation of angiogenesis and collagen deposition by copper," *Biomaterials*, vol. 31, no. 5, pp. 824–831, 2010.

[20] S. Zhao, H. Wang, Y. Zhang et al., "Copper-doped borosilicate bioactive glass scaffolds with improved angiogenic and osteogenic capacity for repairing osseous defects," *Acta Biomaterialia*, vol. 14, pp. 185–196, 2015.

[21] I. Veverková and I. Lovětinská–Šlamborová, "Hybrid silica nanofibers with Ag ions for biomedical applications," in *Proceedings of the 7th International Conference on Nanomaterials—Research & Application (NANOCON '15)*, Brno, Czech Republic, 2015.

[22] U. K. Laemmli, "Cleavage of structural proteins during the assembly of the head of bacteriophage T4," *Nature*, vol. 227, no. 5259, pp. 680–685, 1970.

Review Article

Electrospun Nanofibers Applications in Dentistry

Seog-Jin Seo,[1,2] Hae-Won Kim,[1,2,3] and Jung-Hwan Lee[1]

[1]*Institute of Tissue Regeneration Engineering (ITREN), Dankook University, Cheonan 31115, Republic of Korea*
[2]*Department of Nanobiomedical Science and BK21 PLUS NBM Global Research Center for Regenerative Medicine,
Dankook University, Cheonan 31115, Republic of Korea*
[3]*Department of Biomaterials Science, College of Dentistry, Dankook University, Cheonan 31115, Republic of Korea*

Correspondence should be addressed to Hae-Won Kim; kimhw@dku.edu and Jung-Hwan Lee; ducious@gmail.com

Nanofibrous structures exhibit many interesting features, such as high surface area and surface functionalization and porosity in the range from submicron to nanoscale, which mimics the natural extracellular matrix. In particular, electrospun nanofibers have gained great attention in the field of tissue engineering due to the ease of fabrication and tailorability in pore size, scaffold shape, and fiber alignment. For the reasons, recently, polymeric nanofibers or bioceramic nanoparticle-incorporated nanofibers have been used in dentistry, and their nanostructure and flexibility have contributed to highly promotive cell homing behaviors, resulting in expecting improved dental regeneration. Here, this paper focuses on recently applied electrospun nanofibers in dentistry in the range from the process to the applications.

1. Introduction

In the field of dental tissue engineering, a variety of implanted materials and their fabrication techniques have been introduced and excellent outcomes have been revealed. Particularly, the bioceramics have shown their good biocompatibility with dental tissues and teeth since their physicochemical and biological properties such as osteoconductivity and bioactivity are very similar to those of dental tissues [1]. However, these bioceramics are extremely brittle and poor in flexibility, and therefore their own use has shown a severe limitation in the dental applications [2]. To overcome this hurdle, biodegradable polymers with flexibility have been suggested, resulting in increasing some degree of dental regeneration [3]. Examples of these polymers include poly(ethylene glycol) (PEG) and a series of polyesters, such as poly(lactic acid) (PLA), poly(glycolic acid) (PGA), poly(D,L-lactide-co-glycolide) (PLGA), polycaprolactone (PCL), and their copolymers [4]. Recent works on bioceramic composites based on these polymers have shown significant results in improving regeneration efficiencies [5]. In particular, nanostructured implants have been expected to improve dental restoration due to the structural similarity to that of natural

extracellular matrices (ECMs). Practically, improved cell-favored responses such as cell adhesion, growth, survival, and differentiation have been shown on the nanostructured surface [6], and nanostructured materials have shown increased mechanical stability compared to other typed materials [7].

Among the various types of nanostructured materials, here, we aimed to review the electrospun nanofibrous scaffolds used in dental applications (Figure 1). This paper covers electrospun nanofibrous scaffolds, polymer-based bioceramic composites to enhance their mechanical stability and biological functionality, and their fabrication techniques and processes with the recently studied examples used in the dental applications.

2. Cell Behavior on Nanofibrous Structure

Tissue regeneration is initiated by cellular adhesion to the matrix or neighboring cells [8]. Most tissues and also cells are underlain or surrounded by a natural ECM. These tissues are able to organize cells into the ECM, pave a road for cell migrations, activate signal-transduction pathways, and coordinate their cellular functions [9]. In order to mimic the natural ECM, a lot of biomaterials and fabrication techniques
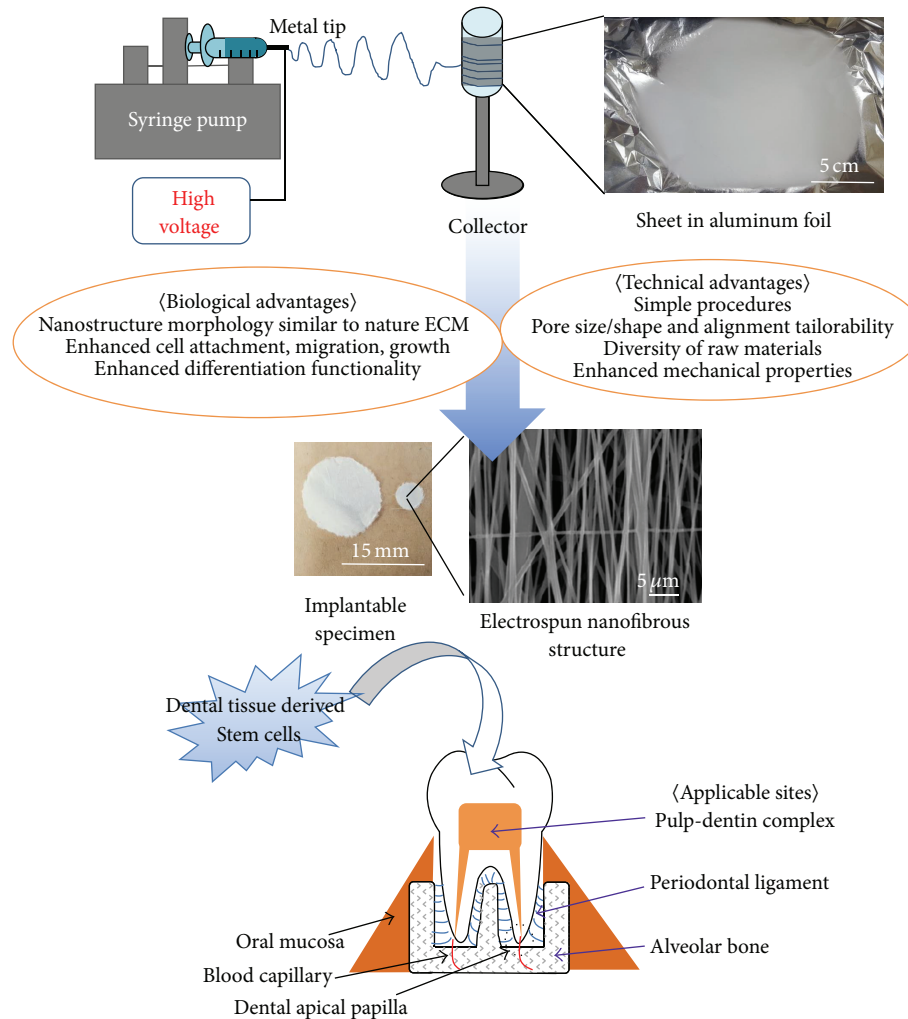
FIGURE 1: Electrospun nanofibrous scaffold which consisted of polycaprolactone was introduced as an exemplar biomaterial for dental tissue regeneration with various biological and technical advantages.

have been explored and optimized. Of these, nanofibrous scaffolds with nanostructure have gained great attention due to their topographical nanostructure similar to that of natural ECM [6], which has shown a great potential to increase cell adhesion, growth, migration rate, and differentiation into somatic cells from stem [6, 10, 11]. Also, nanofibrous scaffolds have been easily fabricated, and their nanostructure has shown cell-favored properties such as high porosity and surface area, control over alignment of fibrous structure for directing regenerative tissue, and controllability in overall shape, diameter, and pore size [12].

The main fabrication of nanofibrous scaffolds is as follows: self-assembly, phase separation, and electrospinning. Self-assembled formation is prepared and consequently can be directly injected for self-assembled nanofibers. In addition, much smaller diameter can be made in fabrication than when electrospinning is used [13]. However, self-assembled nanofibrous scaffolds do not allow for controlling internal pore shape and may have poor mechanical properties due to their intrinsic limitation in the use of raw materials [14]. Phase separation is the first developed

process for the fabrication of nanofibrous scaffolds. In the process of phase separation, nanofibrous structure is made by removing solvent from polymer solutions using thermal treatment, solvent liquefying, porogen leaching, and freeze-drying [15]. PEG, polyesters including PLA, PLGA, and PCL, and other copolymers are the representative materials for the fabrication of nanofibrous scaffolds by phase separation [4]. Despite many advantages such as great reproducibility, low technical sensitivity, and scaffold geometry tailorability, phase separation has been less used than electrospinning due to time consuming complex procedures [16].

Electrospinning predominantly has been used for the fabrication of nanofibrous scaffolds with several advantages such as simple procedure, diameter and alignment tailorability, and raw material diversity [17]. The electrospinning can easily confer nanofibrous structure and control the size of pore and diameter [18, 19] and space between fibers by employing rotating drum collectors [20]. Such control over electrospun fibrous architecture in terms of size and alignment allows cells to migrate on the surface of the scaffold [21]. Representative examples of synthetic polymers for electrospinning include

polydioxanone and a series of polyesters [22]. However, optimization of the electrospinning process depending on the materials for cell growth from their interaction with nanofiber architectures is yet to be fully determined.

In biological applications of electrospun nanofibers, it is advantageous for the growth of cells or tissues since their intrinsic structure such as interconnected pores is able to facilitate input or output of nutrient, waste, and cell signaling molecules [23, 24]. In addition, high porosity of the 3D spun network can promote cell-scaffold interaction in terms of focal adhesion formation for attachment and proliferation [15, 25, 26] and thereby invasion of host tissue [27].

In some examples of the limited interaction between a small size of dental tissue and implant and exposure to large biting force and oral bacteria [28], nanofibrous scaffolds have shown these hurdles. In addition, surface alignment of nanofibrous scaffolds can allow cells to migrate on the right direction. For this reason, electrospun nanofibrous scaffolds can be suggested as dental tissue regenerative biomaterial due to size or alignment tailorability, large interfaces between dental cells and material by high porosity and surface area, and its similarity to nanostructured ECM in nature [29].

3. Basic Principle and Technique

The electrospinning technique involves a strong potential difference between a polymer-based solution flowing through a capillary metal tip and a metallic collector [30]. When the potential voltage difference between them overcomes the solution surface tension, a jet of charged fluid is split into nanofibers that fall into the metallic collection plate and get solidified with solvent evaporation [31]. Typical electrospinning equipment only requires a high voltage power supply, a syringe with pump, a metal tip needle, and a conducting collector (Figure 1) [32]. This basic setup can be modified for various applications such as dual needle syringe (to make blended or core-shell fibers) or rotating mandrel collectors (to make tube like structure) [33, 34].

In electrospinning, several parameters such as processing, physical, systemic, and solution are involved, which affect the fiber morphology and properties of electrospun fibers [35]. A list of key factors affecting electrospun nanofibers is as follows: process parameters (voltage, flow rate, distance of collector, needle diameter, and motion), systemic parameters (polymer type, molecular weight, polymer architecture, and solvent), solution parameter (viscosity, concentration, conductivity, surface tension, charge of jet, and dielectric constant), and physical parameters (humidity, temperature, and air velocity). Among them, most critically considered process parameters for controlling fiber dimension (voltage, flow rate, distance of collector, and needle diameter) are briefly described.

Inputting voltage, distance of collector, flow rate, needle gauge, and type of collector may affect the electrospinning process as a parameter of processing conditions. Higher voltage induces charges on the solution to cause the jet to emerge from the needle with stronger repulsion [36]. As a result, a decrease in fiber diameter as well as increase of

diameter distribution make the control of the process further difficult. Therefore, an optimal voltage is required to inject the solution from the needle.

On the other hand, higher voltage leads to a higher flow rate of solution and faster electrospinning, which may make diameter of fibers higher due to more stretched polymer solution [37]. An increase in flow rate may build up solution at the needle tip because reduced residence time of ions in contact with the needle makes the charge rate into the solution decreased. The flow rate of the solution tailors various features of nanofibers such as diameter, geometry, and porosity [37]. A constant and stable flow rate is essential to minimize the bead formation, which induces large diameter of fibers, nonuniform distribution of fibers, or improper porosity [38]. Generally, slower flow rate results in smaller diameter and a less number of beads compared to faster flow rate [39]. Increased flow rate may also make fibers fused due to improper evaporation of solvent before the fiber collection. Therefore, in order to fabricate nanofiber constantly, the flow rate needs to be optimized.

The reduction of the distance causes flight time for the jet to be shorter, which may not have enough time to evaporate solvent with consequent improper solidification and result in an increase in fibers dimension. It follows a negative power relationship between elongated fibers/decreased fiber diameter and distance from needle to collector because an increase in the distance induces whipping action and bending instabilities [40]. In addition, an increase in gap distance decreases the surface charge density due to diminished magnitude of the electric field [41].

Diameter of the needle orifice also has an effect on fiber dimension. Smaller internal diameter reduces the solution clogging further due to less exposure time of the jet to the environment and an increase in shear stress depending on the flow rate [42]. A decrease in the internal needle diameter increases in the surface tension of the solution resulting in smaller droplet, which induces the jet speed decreased. Therefore, the jet spends more flight time before deposition into collector and is more stretched and elongated, which results in smaller diameter fibers.

4. Pulp-Dentin Complex Regeneration

Dental caries and trauma would result in the loss of pulp-dentin complex (the mineralized layer and fibrous tissue below enamel). Therefore, various forms of pulp-regenerative dental materials such as calcium hydroxide, ferric sulphate, and mineral trioxide aggregate are aimed at regenerating pulp-dentin complex [43]. For the pulp therapy, electrospun nanofibrous scaffolds have been attempted and resulted in excellent regeneration using dental pulp stem cells (DPSCs), which are an established cell source for the formation of dentin-pulp complex. Odontogenic differentiation of human DPSCs on PLA nanofibrous scaffolds was demonstrated by increased alkaline phosphatase (ALP) activity, dentin related marker gene expression, and mineralization [44]. Mineralized PCL nanofibrous scaffolds have shown promoted odontogenic differentiation and growth of human DPSCs through

collagen type I and the integrin-mediated signaling pathway but they still lack mechanical and biofunctional properties for clinical applications [45]. To increase mechanical and biological properties of electrospun nanofibers, nanoparticles such as bioactive glass nanoparticle, magnetic nanoparticle, and hydroxyapatite nanoparticle were incorporated to polymer matrices before electrospinning. Electrospinning techniques is possible to produce bioactive nanoparticle-polymer composite [46]. For instance, Bottino et al. produced electrospun scaffolds of bioactive nanoparticle-incorporated polydioxanone where antibiotics (i.e., metronidazole and ciprofloxacin) were able to be loaded [47]. It was observed that these scaffolds were able to deliver the antibiotics more effectively than pastes. Kim et al. produced electrospun nanofibrous scaffolds consisting of polyvinyl alcohol and hydroxyapatite nanoparticles, which showed dentin regenerative properties [48]. Collagen or PCL-gelatin-based nanofibrous scaffolds incorporating bioactive glass nanoparticles were developed for dentin-pulp regeneration and showed enhanced growth and odontogenic differentiation from human DPSCs compared to collagen nanofibrous scaffold via integrin-mediated process [5, 49]. Magnetite nanoparticles were incorporated to PCL due to its intriguing physical cues that can tailor the behaviors of DPSCs [50]. The effects of these nanocomposite nanofibers on the adhesion, growth, migration, and odontogenic differentiation of human DPSCs were significantly remarkable compared to those of polymeric nanofibers.

Taken together, the major advantage of electrospinning might be its ability to produce complex geometry of nanofibrous scaffolds for dentin-pulp complex regeneration. The ultimate goal of regenerating dentin-pulp complex is to restore both mechanical and physical attributes of the tooth structure. Therefore, electrospun nanofibers are used for carrying dental derived stem cells for optimum regeneration in the next decade.

5. Periodontium Regeneration

Untreated periodontal disease can lead to periodontal tissue destruction and eventual loss of teeth [51]. Regeneration of destructed periodontal tissues has always been a challenge for clinicians. Therefore, periodontal tissue engineering has been of recent interest for the repair of defects in periodontal tissues such as alveolar bone, periodontal ligament (PDL), and cementum. Traditionally, nonresorbable materials such as expanded polytetrafluoroethylene were used as guide tissue regeneration (GTR) membranes but they had the disadvantage of requiring a secondary surgery to remove the membrane. Instead, biodegradable synthetic or natural materials such as collagen, PLGA, PLA, and PCL have been researched but they still lack biological functionality as well as physical properties such as poor control over porosity and surface alignment. Electrospinning has emerged to increase the functionality of these membranes, therefore leading to expecting periodontal regeneration. As a consequence, biodegradable nanofibrous GTR membranes through electrospinning have improved the functionality, such as porosity

to attach cells and fiber alignment for orientation of collagen fibers in PDL regeneration, as investigated on the attachment, proliferation, and differentiation of human PDL cells [52, 53].

Electrospun collagen membranes first gained attention in the GTR application due to their intrinsic biological properties such as differentiating potential into osteoblast-like cells [54]. However, since most of the collagen sources are originated from animals, the use of the collagen in human dental applications could be concerned and have conflicted with ethical issues and concerns of cross-infection. As an alternative, synthetic biodegradable polyester membranes are suggested for PDL regeneration.

Recent studies have shown good attachment and proliferation of PCL cells as well as tissue formation on electrospun PLGA [55], hydroxyapatite-coated electrospun PCL [56], and silk membranes as confirmed by promoted deposition of the main PDL ECM components such as collagen type I and type III [57, 58]. Silk membranes after incorporating graphene oxide [59] or hydroxyapatite nanoparticles [60] have shown human PDL cell attachment and proliferation and tissue formation into cementum and bone tissue.

Although electrospinning has added exciting new prospects to the field of periodontal tissue regeneration, much work is still required to validate the use of electrospun nanofibrous scaffolds in the clinical stage in terms of mechanical properties and *in vivo*/clinical biological properties as well as the underlying mechanisms.

6. Bone Tissue Regeneration

While tissue-engineered bone grafts have been investigated for years, challenges still lie in achieving *in vivo* mechanical/biological properties and vascularization for the treatment of patients who suffer from degeneration or diseases such as periodontitis, trauma, oral cancer, and anatomical abnormality in nature. Electrospun nanofibers may be one of the ideal solutions due to their ECM similarity, since they provide control over nanopores similar to the small blood vessel for the cell survival. Electrospun nanofibers have been studied in a variety of the *in vitro* and *in vivo* tests, such as mesenchymal stem cell- (MSC-) seeded implantation into a rat calvarial defect model [61, 62].

For bone regeneration, Kim's group has shown various electrospun nanofibrous scaffolds made of synthetic and natural polymers with or without mineral deposition such as gelatin-PCL [63], silk-fibroin-PCL [64, 65], PLA [66], gelatin-apatite-poly(lactide-co-caprolactone) [67], mesoporous bioactive glass-incorporated PCL-gelatin [68], mesoporous silica-shelled PCL [69], and magnetic nanoparticle-incorporated PCL nanofibrous scaffolds [70]. In addition, a number of polymeric nanofibers have been revealed and used for a cellular platform for bone, but they lack bioactivity and other biofunctionalities to accelerate bone tissue regeneration. For this, artificial mineralization after fabrication or loading additives (i.e., bioactive nanoparticles and growth factors) to scaffolds during electrospinning process was introduced and resulted in the induction of osteogenesis by accelerating natural mineralization or vascularization [68, 69, 71–73].

These nanofibrous scaffolds would be employed as a carrier for bone-associated growth factors due to their 3D networked pores to facilitate control over drug release [71–73]. Recently, electrospun nanofibrous scaffolds were designed to hold a capacity by loading and releasing dual growth factors for the target of bone regeneration. For example, a core-shell structure of a biopolymer fiber made of polyethylene oxide/PCL was shown to facilitate loading and control releasing properties of these growth factors [33].

To increase cell attachment, biofunnctional materials have been used for electrospinning. Silk nanofibers having the Arg-Gly-Asp (RGD) sequence which act as receptors for cell adhesion [64] were shown to accelerate MSC attachment, proliferation, and differentiation into osteoblastic lineage [65].

7. Concluding Remarks

In the field of dental tissue engineering, a number of dental materials have been advanced to create a suitable microenvironment for dental regeneration. Of these, electrospun nanofibrous scaffolds could be one approach suitable to dental applications due to the ease of fabrication, control over scaffold size, and fiber alignment. Electrospun nanofibers have provided mechanical properties and functionalities biologically favored to biological aspects in dental applications. In addition, electrospun nanofibers have played a versatile role in controlled release of biomolecule therapeutics (i.e., growth factors) or modification with adhesive biomolecules (i.e., fibronectin and RGD sequence) and contributed to further improved dental regeneration. Although a number of experiments on nanofibrous scaffolds in the *in vitro* and *in vivo* study have been conducted, clinically, customization to each patient's defect is still difficult. For the reason, the clinical practice of nanofibrous scaffolds is still scarce. In addition, since dental tissue degeneration may come from biological disorders, further studies of biological interplay between electrospun nanofiber and compromised dental tissue derived cells are essential. These studies will be expected to help to understand the biological effect of nanofibers. Conclusively, further elaborated techniques to customize nanofiber scaffolds are imperative, and clinical defects must be categorized into several groups for their customization.

Competing Interests

The authors declare that there are no competing interests regarding the publication of this paper.

Acknowledgments

References

[1] T. Thamaraiselvi and S. Rajeswari, "Biological evaluation of bioceramic materials—a review," *Trends in Biomaterials and Artificial Organs*, vol. 18, no. 1, pp. 9–17, 2004.

[2] Y. Zhou, C. Wu, and Y. Xiao, "Silicate-based bioceramics for periodontal regeneration," *Journal of Materials Chemistry B*, vol. 2, no. 25, pp. 3907–3910, 2014.

[3] Y. Ikada, "Biodegradable polymers as scaffolds for tissue engineering," in *Handbook of Biodegradable Polymers: Isolation, Synthesis, Characterization and Applications*, pp. 341–362, 2013.

[4] R. Nayak, R. Padhye, I. L. Kyratzis, Y. B. Truong, and L. Arnold, "Recent advances in nanofibre fabrication techniques," *Textile Research Journal*, vol. 82, no. 2, pp. 129–147, 2012.

[5] G.-H. Kim, Y.-D. Park, S.-Y. Lee et al., "Odontogenic stimulation of human dental pulp cells with bioactive nanocomposite fiber," *Journal of Biomaterials Applications*, vol. 29, no. 6, pp. 854–866, 2015.

[6] G. Wei and P. X. Ma, "Nanostructured biomaterials for regeneration," *Advanced Functional Materials*, vol. 18, no. 22, pp. 3568–3582, 2008.

[7] B. Ji and H. Gao, "Mechanical properties of nanostructure of biological materials," *Journal of the Mechanics and Physics of Solids*, vol. 52, no. 9, pp. 1963–1990, 2004.

[8] P. Lu, K. Takai, V. M. Weaver, and Z. Werb, "Extracellular matrix degradation and remodeling in development and disease," *Cold Spring Harbor Perspectives in Biology*, vol. 3, no. 12, 2011.

[9] J. D. Hood and D. A. Cheresh, "Role of integrins in cell invasion and migration," *Nature Reviews Cancer*, vol. 2, no. 2, pp. 91–100, 2002.

[10] V. Hasirci, E. Vrana, P. Zorlutuna et al., "Nanobiomaterials: a review of the existing science and technology, and new approaches," *Journal of Biomaterials Science, Polymer Edition*, vol. 17, no. 11, pp. 1241–1268, 2006.

[11] Y. Tabata, "Nanomaterials of drug delivery systems for tissue regeneration," *Methods in Molecular Biology*, vol. 300, pp. 81–100, 2005.

[12] E. A. Abou Neel, W. Chrzanowski, V. M. Salih, H.-W. Kim, and J. C. Knowles, "Tissue engineering in dentistry," *Journal of Dentistry*, vol. 42, no. 8, pp. 915–928, 2014.

[13] J. D. Hartgerink, E. Beniash, and S. I. Stupp, "Self-assembly and mineralization of peptide-amphiphile nanofibers," *Science*, vol. 294, no. 5547, pp. 1684–1688, 2001.

[14] H. Morita, "Applicable simulation methods for directed self-assembly—advantages and disadvantages of these methods," *Journal of Photopolymer Science and Technology*, vol. 26, no. 6, pp. 801–807, 2013.

[15] P. X. Ma and R. Zhang, "Synthetic nano-scale fibrous extracellular matrix," *Journal of Biomedical Materials Research*, vol. 46, no. 1, pp. 60–72, 1999.

[16] R. Vasita and D. S. Katti, "Nanofibers and their applications in tissue engineering," *International Journal of Nanomedicine*, vol. 1, no. 1, pp. 15–30, 2006.

[17] S.-H. Shin, O. Purevdorj, O. Castano, J. A. Planell, and H.-W. Kim, "A short review: Recent advances in electrospinning for bone tissue regeneration," *Journal of Tissue Engineering*, vol. 3, no. 1, pp. 1–11, 2012.

[18] D. Li and Y. Xia, "Electrospinning of nanofibers: reinventing the wheel?" *Advanced Materials*, vol. 16, no. 14, pp. 1151–1170, 2004.

[19] X. Hu, S. Liu, G. Zhou, Y. Huang, Z. Xie, and X. Jing, "Electrospinning of polymeric nanofibers for drug delivery

applications," *Journal of Controlled Release*, vol. 185, no. 1, pp. 12–21, 2014.

[20] W. Cui, Y. Zhou, and J. Chang, "Electrospun nanofibrous materials for tissue engineering and drug delivery," *Science and Technology of Advanced Materials*, vol. 11, no. 1, Article ID 014108, 2010.

[21] N. Amiraliyan, M. Nouri, and M. H. Kish, "Electrospinning of silk nanofibers. I. An investigation of nanofiber morphology and process optimization using response surface methodology," *Fibers and Polymers*, vol. 10, no. 2, pp. 167–176, 2009.

[22] M. Zafar, S. Najeeb, Z. Khurshid et al., "Potential of electrospun nanofibers for biomedical and dental applications," *Materials*, vol. 9, no. 2, p. 73, 2016.

[23] B. B. Lakshmi, C. J. Patrissi, and C. R. Martin, "Sol-gel template synthesis of semiconductor oxide micro- and nanostructures," *Chemistry of Materials*, vol. 9, no. 11, pp. 2544–2550, 1997.

[24] P. X. Ma, "Biomimetic materials for tissue engineering," *Advanced Drug Delivery Reviews*, vol. 60, no. 2, pp. 184–198, 2008.

[25] X. Zhang, W. J. Goux, and S. K. Manohar, "Synthesis of polyaniline nanofibers by 'nanofiber seeding'," *Journal of the American Chemical Society*, vol. 126, no. 14, pp. 4502–4503, 2004.

[26] L. A. Smith and P. X. Ma, "Nano-fibrous scaffolds for tissue engineering," *Colloids and Surfaces B: Biointerfaces*, vol. 39, no. 3, pp. 125–131, 2004.

[27] C. R. Martin, "Template synthesis of electronically conductive polymer nanostructures," *Accounts of Chemical Research*, vol. 28, no. 2, pp. 61–66, 1995.

[28] M. Hannig and C. Hannig, "Nanomaterials in preventive dentistry," *Nature Nanotechnology*, vol. 5, no. 8, pp. 565–569, 2010.

[29] F. Yang, R. Murugan, S. Ramakrishna, X. Wang, Y.-X. Ma, and S. Wang, "Fabrication of nano-structured porous PLLA scaffold intended for nerve tissue engineering," *Biomaterials*, vol. 25, no. 10, pp. 1891–1900, 2004.

[30] W.-E. Teo, R. Inai, and S. Ramakrishna, "Technological advances in electrospinning of nanofibers," *Science and Technology of Advanced Materials*, vol. 12, no. 1, Article ID 013002, 2011.

[31] T. Subbiah, G. S. Bhat, R. W. Tock, S. Parameswaran, and S. S. Ramkumar, "Electrospinning of nanofibers," *Journal of Applied Polymer Science*, vol. 96, no. 2, pp. 557–569, 2005.

[32] S. Cavaliere, *Electrospinning for Advanced Energy and Environmental Applications*, CRC Press, New York, NY, USA, 2015.

[33] R. A. Perez and H.-W. Kim, "Core-shell designed scaffolds for drug delivery and tissue engineering," *Acta Biomaterialia*, vol. 21, pp. 2–19, 2015.

[34] I.-K. Yoon, J.-Y. Hwang, J.-W. Seo, W.-C. Jang, H.-W. Kim, and U. S. Shin, "Carbon nanotube-gelatin-hydroxyapatite nanohybrids with multilayer core–shell structure for mimicking natural bone," *Carbon*, vol. 77, pp. 379–389, 2014.

[35] S. Ramakrishna, K. Fujihara, W. Teo, T. Lim, and Z. Ma, *An Introduction to Electrospinning and Nanofibers*, World Scientific, River Edge, NJ, US, 2005.

[36] G. Taylor, "Electrically driven jets," *Proceedings of the Royal Society of London A: Mathematical, Physical and Engineering Sciences*, vol. 313, no. 1515, pp. 453–475, 1969.

[37] J. M. Deitzel, J. Kleinmeyer, D. Harris, and N. C. Beck Tan, "The effect of processing variables on the morphology of electrospun nanofibers and textiles," *Polymer*, vol. 42, no. 1, pp. 261–272, 2001.

[38] K. Garg and G. L. Bowlin, "Electrospinning jets and nanofibrous structures," *Biomicrofluidics*, vol. 5, no. 1, Article ID 013403, 2011.

[39] S. Megelski, J. S. Stephens, D. Bruce Chase, and J. F. Rabolt, "Micro- and nanostructured surface morphology on electrospun polymer fibers," *Macromolecules*, vol. 35, no. 22, pp. 8456–8466, 2002.

[40] A. L. Yarin, S. Koombhongse, and D. H. Reneker, "Bending instability in electrospinning of nanofibers," *Journal of Applied Physics*, vol. 89, no. 5, pp. 3018–3026, 2001.

[41] K. S. Rho, L. Jeong, G. Lee et al., "Electrospinning of collagen nanofibers: effects on the behavior of normal human keratinocytes and early-stage wound healing," *Biomaterials*, vol. 27, no. 8, pp. 1452–1461, 2006.

[42] S. Usami, H.-H. Chen, Y. Zhao, S. Chien, and R. Skalak, "Design and construction of a linear shear stress flow chamber," *Annals of Biomedical Engineering*, vol. 21, no. 1, pp. 77–83, 1993.

[43] N. Salako, B. Joseph, P. Ritwik, J. Salonen, P. John, and T. A. Junaid, "Comparison of bioactive glass, mineral trioxide aggregate, ferric sulfate, and formocresol as pulpotomy agents in rat molar," *Dental Traumatology*, vol. 19, no. 6, pp. 314–320, 2003.

[44] J. Wang, H. Ma, X. Jin et al., "The effect of scaffold architecture on odontogenic differentiation of human dental pulp stem cells," *Biomaterials*, vol. 32, no. 31, pp. 7822–7830, 2011.

[45] J.-J. Kim, W.-J. Bae, J.-M. Kim et al., "Mineralized polycaprolactone nanofibrous matrix for odontogenesis of human dental pulp cells," *Journal of Biomaterials Applications*, vol. 28, no. 7, pp. 1069–1078, 2014.

[46] M. C. Bottino, G. H. Yassen, J. A. Platt et al., "A novel three-dimensional scaffold for regenerative endodontics: materials and biological characterizations," *Journal of Tissue Engineering and Regenerative Medicine*, vol. 9, no. 11, pp. E116–E123, 2015.

[47] M. C. Bottino, K. Kamocki, G. H. Yassen et al., "Bioactive nanofibrous scaffolds for regenerative endodontics," *Journal of Dental Research*, vol. 92, no. 11, pp. 963–969, 2013.

[48] G.-M. Kim, A. S. Asran, G. H. Michler, P. Simon, and J.-S. Kim, "Electrospun PVA/HAp nanocomposite nanofibers: biomimetics of mineralized hard tissues at a lower level of complexity," *Bioinspiration and Biomimetics*, vol. 3, no. 4, Article ID 046003, 2008.

[49] W.-J. Bae, K.-S. Min, J.-J. Kim, J.-J. Kim, H.-W. Kim, and E.-C. Kim, "Odontogenic responses of human dental pulp cells to collagen/nanobioactive glass nanocomposites," *Dental Materials*, vol. 28, no. 12, pp. 1271–1279, 2012.

[50] H.-M. Yun, E.-S. Lee, M.-J. Kim et al., "Magnetic nanocomposite scaffold-induced stimulation of migration and odontogenesis of human dental pulp cells through integrin signaling pathways," *PLoS ONE*, vol. 10, no. 9, Article ID e0138614, 2015.

[51] M. Feres, L. C. Figueiredo, G. M. S. Soares, and M. Faveri, "Systemic antibiotics in the treatment of periodontitis," *Periodontology 2000*, vol. 67, no. 1, pp. 131–186, 2015.

[52] S. Shang, F. Yang, X. Cheng, X. F. Walboomers, and J. A. Jansen, "The effect of electrospun fibre alignment on the behaviour of rat periodontal ligament cells," *European Cells and Materials*, vol. 19, pp. 180–192, 2010.

[53] W. Jiang, L. Li, D. Zhang et al., "Incorporation of aligned PCL-PEG nanofibers into porous chitosan scaffolds improved the orientation of collagen fibers in regenerated periodontium," *Acta Biomaterialia*, vol. 25, pp. 240–252, 2015.

[54] J. A. Matthews, G. E. Wnek, D. G. Simpson, and G. L. Bowlin, "Electrospinning of collagen nanofibers," *Biomacromolecules*, vol. 3, no. 2, pp. 232–238, 2002.

[55] B. Inanç, Y. E. Arslan, S. Seker, A. E. Elçin, and Y. M. Elçin, "Periodontal ligament cellular structures engineered with electrospun poly(DL-lactide-co-glycolide) nanofibrous membrane scaffolds," *Journal of Biomedical Materials Research Part A*, vol. 90, no. 1, pp. 186–195, 2009.

[56] S.-H. Park, T.-I. Kim, Y. Ku et al., "Effect of hydroxyapatite-coated nanofibrous membrane on the responses of human periodontal ligament fibroblast," *Journal of the Ceramic Society of Japan*, vol. 116, no. 1349, pp. 31–35, 2008.

[57] Y. Kumada and S. Zhang, "Significant type I and type III collagen production from human periodontal ligament fibroblasts in 3D peptide scaffolds without extra growth factors," *PLoS ONE*, vol. 5, no. 4, Article ID e10305, 2010.

[58] C. S. Ki, J. W. Kim, J. H. Hyun et al., "Electrospun three-dimensional silk fibroin nanofibrous scaffold," *Journal of Applied Polymer Science*, vol. 106, no. 6, pp. 3922–3928, 2007.

[59] F. J. Rodríguez-Lozano, D. García-Bernal, S. Aznar-Cervantes et al., "Effects of composite films of silk fibroin and graphene oxide on the proliferation, cell viability and mesenchymal phenotype of periodontal ligament stem cells," *Journal of Materials Science: Materials in Medicine*, vol. 25, no. 12, pp. 2731–2741, 2014.

[60] S. Suganya, J. Venugopal, S. Ramakrishna, B. S. Lakshmi, and V. R. G. Dev, "Aloe vera/silk fibroin/hydroxyapatite incorporated electrospun nanofibrous scaffold for enhanced osteogenesis," *Journal of Biomaterials and Tissue Engineering*, vol. 4, no. 1, pp. 9–19, 2014.

[61] K. M. Woo, V. J. Chen, H.-M. Jung et al., "Comparative evaluation of nanofibrous scaffolding for bone regeneration in critical-size calvarial defects," *Tissue Engineering Part A*, vol. 15, no. 8, pp. 2155–2162, 2009.

[62] J.-H. Kim, H.-J. Moon, T.-H. Kim et al., "A novel in vivo platform for studying alveolar bone regeneration in rat," *Journal of Tissue Engineering*, vol. 4, 2013.

[63] J. H. Lee, J.-H. Park, A. El-Fiqi et al., "Biointerface control of electrospun fiber scaffolds for bone regeneration: engineered protein link to mineralized surface," *Acta Biomaterialia*, vol. 10, no. 6, pp. 2750–2761, 2014.

[64] P. Bhattacharjee, B. Kundu, D. Naskar et al., "Potential of inherent RGD containing silk fibroin-poly (ϵ-caprolactone) nanofibrous matrix for bone tissue engineering," *Cell and Tissue Research*, vol. 363, no. 2, pp. 525–540, 2016.

[65] P. Bhattacharjee, D. Naskar, H.-W. Kim, T. K. Maiti, D. Bhattacharya, and S. C. Kundu, "Non-mulberry silk fibroin grafted PCL nanofibrous scaffold: promising ECM for bone tissue engineering," *European Polymer Journal*, vol. 71, pp. 490–509, 2015.

[66] H.-W. Kim, H.-H. Lee, and G.-S. Chun, "Bioactivity and osteoblast responses of novel biomedical nanocomposites of bioactive glass nanofiber filled poly(lactic acid)," *Journal of Biomedical Materials Research Part A*, vol. 85, no. 3, pp. 651–663, 2008.

[67] S.-H. Jegal, J.-H. Park, J.-H. Kim et al., "Functional composite nanofibers of poly(lactide-co-caprolactone) containing gelatin-apatite bone mimetic precipitate for bone regeneration," *Acta Biomaterialia*, vol. 7, no. 4, pp. 1609–1617, 2011.

[68] A. El-Fiqi, J.-H. Kim, and H.-W. Kim, "Osteoinductive fibrous scaffolds of biopolymer/mesoporous bioactive glass nanocarriers with excellent bioactivity and long-term delivery of osteogenic drug," *ACS Applied Materials and Interfaces*, vol. 7, no. 2, pp. 1140–1152, 2015.

[69] R. K. Singh, G.-Z. Jin, C. Mahapatra, K. D. Patel, W. Chrzanowski, and H.-W. Kim, "Mesoporous silica-layered biopolymer hybrid nanofibrous scaffold: a novel nanobiomatrix platform for therapeutics delivery and bone regeneration," *ACS Applied Materials and Interfaces*, vol. 7, no. 15, pp. 8088–8098, 2015.

[70] R. K. Singh, K. D. Patel, J. H. Lee et al., "Potential of magnetic nanofiber scaffolds with mechanical and biological properties applicable for bone regeneration," *PLoS ONE*, vol. 9, no. 4, Article ID e91584, 2014.

[71] M. S. Kang, J.-H. Kim, R. K. Singh, J.-H. Jang, and H.-W. Kim, "Therapeutic-designed electrospun bone scaffolds: mesoporous bioactive nanocarriers in hollow fiber composites to sequentially deliver dual growth factors," *Acta Biomaterialia*, vol. 16, no. 1, pp. 103–116, 2015.

[72] H.-S. Yu, S.-J. Hong, and H.-W. Kim, "Surface-mineralized polymeric nanofiber for the population and osteogenic stimulation of rat bone-marrow stromal cells," *Materials Chemistry and Physics*, vol. 113, no. 2-3, pp. 873–877, 2009.

[73] T.-H. Kim, J.-J. Kim, and H.-W. Kim, "Basic fibroblast growth factor-loaded, mineralized biopolymer-nanofiber scaffold improves adhesion and proliferation of rat mesenchymal stem cells," *Biotechnology Letters*, vol. 36, no. 2, pp. 383–390, 2014.

Research Article

Medicated Nanofibers Fabricated Using NaCl Solutions as Shell Fluids in Modified Coaxial Electrospinning

Yong-Hui Wu,[1] Chen Yang,[2] Xiao-Yan Li,[2] Jia-Ying Zhu,[2] and Deng-Guang Yu[2]

[1]*Department of Mechanical Engineering, Guangxi Technological College of Machinery and Electricity, Nanning 530007, China*
[2]*School of Material Science and Engineering, University of Shanghai for Science and Technology, Shanghai 200093, China*

Correspondence should be addressed to Deng-Guang Yu; ydg017@usst.edu.cn

The present study reports the fabrication of medicated nanofibers for potential colon-targeted drug delivery using modified coaxial electrospinning, in which salt (NaCl) solutions were exploited as shell fluids to facilitate the preparation processes. A homemade concentric spinneret with an indented core capillary was developed to conduct the coaxial processes. Optical observations and scanning electron microscopic results demonstrated that the shell-to-core fluid flow rate ratio was a key parameter, which exerted a significant influence on the electrospinning processes and could be exploited to control the fibers' morphology and diameters. A scaling law of $D = 0.173F^{-0.531}$ ($R^2 = 0.9976$) was built, by which the nanofibers' sizes can be predicted and manipulated easily. X-ray diffraction and attenuated total reflected FTIR tests verified that the medicated nanofibers were essentially a polymeric nanocomposite and the guest drug diclofenac sodium (DS) had fine compatibility with the host polymer. All the drug was encapsulated in the filament-forming carrier. *In vitro* dissolution experiments demonstrated that the medicated nanofibers could free the drug in a neutral condition, suggesting potential colon-targeted drug delivery applications. *Ex vivo* tests demonstrated that the medicated fiber mats could enhance the transmembrane of DS. Based on coaxial electrospinning, a new strategy is successfully developed for creating medicated nanomaterials.

1. Introduction

During the past several decades, more and more nano-drug delivery systems (DDS) have become commercial products. These products include polymeric nanoparticles, nanoliposomes, solid lipid nanoparticles, and microemulsions, which are partially fabricated using top-down methods based on the exploitation of mechanical forces, such as milling, high-pressure homogenization, and spray [1–3]. Most recently, the usage of electrostatic energy is drawing increasing attention for creating nanoproducts, such as electrospinning, electrospraying, and e-jet printing, which is termed electrohydrodynamic atomization (EHDA) in total. Because liquids can easily interact with electric fields, thus these methods are frequently exploited to remove solvents directly from the solutions to dry and solidify the micro-fluid jets, meanwhile generating micro/nanosize fibers or particles [4, 5].

Although EHDA methods are widely investigated for developing functional nanomaterials, their mechanisms are still unclear. Often a series of different factors would play their roles in influencing the process and in turn the created nanoproducts. These factors are clear to researchers and can be divided into three categories: (i) operative parameters such as applied voltages, tip-to-collector distance, and fluid flow rate; (ii) environmental conditions such as temperature, humidity, and vacuum; and (iii) the physicochemical properties of working fluids such as surface tension, conductivity, and viscosity. In the traditional single-fluid electrospinning, nanofiber fabrication and dimension control by these parameters have been well investigated for various polymers depending on their categories and the desired applications [6–9]. Although the reported methods are useful to a certain polymer, the size-reducing effect is limited and the implementation conditions are strict. For example, when a polymer concentration is utilized to decrease fiber's diameter, its narrow electrospinnable window would limit the effect; when an additive (such as a surfactant or a salt) is doped into

a polymer solution for downsizing, it may be infeasible due to lacking codissolving solvent or enough solubility.

During the past several years, double-fluid electrospinning (such as coaxial and side-by-side processes) and even multiple-fluid electrospinning (such as triaxial processes) have been reported in literature [10–13]. In these processes, an unspinnable fluid can be treated simultaneously with the electrospinnable polymeric fluids for carrying out double-fluid or multiple-fluid processes and creating nanostructures. Based on this new conception, Yu et al. developed the modified coaxial and triaxial electrospinning processes, which are characterized by the unspinnable outer fluids [9, 14, 15]. These modified processes have been utilized to coat nanofibers with Ag nanoparticles for antibacteria applications [14], to retard initial burst release of drug from medicated nanofibers [15]. With the usage of an unspinnable sheath liquid to conduct a coaxial process, the electrospun nanofibers' diameter can be manipulated in a controlled manner because the sheath fluid often has little influence on the properties of core spinnable polymeric solution. This simple relationship makes the diameter of nanofiber from core polymeric solution able to be adjusted by only one of the parameters of sheath fluid under a certain electrospinning condition. For example, it is reported that polyacrylonitrile nanofibers' diameters were able to be manipulated by the concentrations of LiCl in the sheath solution through a power equation [9]. However, frequent change of sheath fluids is not convenient but time-consuming. Provided the flow rate of sheath fluid can be taken as a key factor for manipulating nanofibers' size, it should be more facile because all need is to press the syringe pump for driving the sheath fluid.

The commencement of an electrospinning process is regarded as the balance of electrical forces and surface tensions. According to the following equation, the increase of conductivity and decrease of surface tension of working fluid should provide new protocols for carrying out an electrospinning process more stably and robustly [16]:

$$V_c \sim \sqrt{\frac{\gamma d^2}{\varepsilon R}}, \tag{1}$$

where V_c is the critical voltage for a jet emanating from the meniscus tip, d is the nozzle-to-collector distance, ε is the permittivity, γ is the surface tension, and R is the principal curvature of the liquid meniscus. Electrons are easy to aggregate on the surface of working fluid [17]. Thus in the coaxial electrospinning, it is often the physical and chemical properties of the shell fluid that determine an electrospinning process. According to the equation, an increase of conductivity (ε) and a decrease of surface tensions (γ) would mean that only a small applied voltage (V_c) was needed to initiate a coaxial electrospinning process.

Here, a salt solution is exploited as a shell working fluid, and the influence of its flow rate on both the electrospinning process and the quality of final nanofiber product is investigated in detail. Different from traditional coaxial electrospinning, in which the shell fluid must be electrospinnable, the modified coaxial processes can exploit a wide series of liquids as the shell working fluids regardless of their electrospinnability (solvent, solutions of little molecules, dilute polymer solutions, and even suspensions and emulsions) [14, 15]. Thus this new modified coaxial process can even expand the capability of electrospinning to create nanomaterials and nanostructures for realizing a series of new possibilities in the field of functional nanomaterials.

In the area of nanomedicine, the polymeric nano-DDS are mainly in the form of nanoparticles (NPs). However, for oral administration, the major and the most favorite way for the patients, electrospun nanofiber-mat-based DDS should have some special advantages over NPs besides the facile, simple, and straightforward fabrication processes using electrospinning [18, 19], such as easy aftertreatment and easy formation transitions from the randomly assembled or aligned fiber mats. Their unique characteristics (diameter in the nanoscale but length in the macroscopic scale) would endow them having the merits possessed by both the NPs DDS at nanoscale in altering the biopharmaceutical and pharmacokinetic properties of the drug molecule for favorable clinical outcomes and also those possessed by the conventional solid dosage forms such as easy processing, good drug stability, and ease of packaging and shipping [20–22].

Based on the above-mentioned knowledge, we developed modified coaxial electrospinning to produce drug-loaded Eudragit® L100 (EL100) nanofibers for potential colon-targeted delivery of diclofenac sodium (DS). A salt (NaCl) solution was exploited as the shell working liquid and its flow rate was exploited as a regulatory factor. EL100, a pH-sensitive methacrylate-based copolymer developed by Röhm Company in Germany, has been widely used for the colon-targeted formulation development in pharmaceutical industry and laboratory, such as tablet coating, tablet matrix, microspheres, and nanoparticles [23].

2. Materials and Methods

2.1. Materials. Eudragit L100 (EL100, average molecular weight approximately 135,000 Da) was purchased from Röhm GmbH & Co. KG (Darmstadt, Germany). Analytical grade N,N-dimethylacetamide (DMAc) and ethanol were provided by the Sinopharm Chemical Reagent Co., Ltd. (Shanghai, China). Sodium chloride was of analytical grade and obtained from Shanghai Shiyi Chemical Reagent Co., Ltd. (Shanghai, China). All other chemicals are of analytical grade and used as received. Water was double distilled just before use.

2.2. Coaxial Electrospinning. The spinning solutions of EL100 were prepared by dissolving 14.0 g EL100 and 2.0 g DS in 100 mL ethanol. The shell solution consisted of 0.1 g NaCl in a 100 mL mixture of DMAc and ethanol (20 : 80, v : v). Two syringe pumps (KDS200, KDS100, Cole-Parmer, USA) and a high-voltage power supply (ZGF 60 kV/2 mA, Shanghai Sute Corp., China) were used. The applied voltage was fixed at 14 kV. The fibers produced were collected on an aluminum foil at a distance of 20 cm. A homemade concentric spinneret was

exploited in both the single-fluid and the modified coaxial processes.

The flow rate of core EL100 fluid was kept at 1.0 mL/h. When the shell fluid was switched off, it was single-fluid electrospinning with the inner capillary as a spinneret. When the pump loaded with the syringe containing the salt solution was switched on to push the shell fluid, it was a modified coaxial electrospinning process. The flow rate of shell solution was exploited as a controlled factor. Experiments were recorded using a digital camera (PowerShot A640, Canon, Japan) under 11x magnifications.

2.3. Morphology.

The surface morphology of electrospun fibers and raw DS powders were assessed using a JSM-5600LV scanning electron microscope (SEM, Japan Electron Optics Laboratory Co. Ltd.). Prior to the examination, the samples were gold sputter-coated under nitrogen atmosphere to render them electrically conductive. The average fiber diameter was determined by measuring diameters of fibers at over 100 times over some different fibers in the FESEM images using ImageJ software (National Institute of Heath, Bethesda, MD, USA).

2.4. Physical Forms of the Components and Their Compatibility.

X-ray diffraction (XRD) analyses were performed using a D/Max-BR instrument with a diffractometer (RigaKu, Tokyo, Japan). The measurements were conducted under CuKα (λ = 1.541 Å), 40 kV, and 30 mA as X-ray source with Kb 142 (Ni) filter. The raw materials (EL100 and DS), their physical mixture (consisting of EL100 and DS in a weight ratio of 7 : 1), and the electrospun nanofibers were measured for angles 2θ between 5° and 60°.

Attenuated reflectance Fourier transform infrared (ATR-FTIR) tests were carried out using a Perkin-Elmer Precisely Spectrum One FTIR Spectrometer with Universal ATR Sampling Accessory (Perkin 135 Elmer, USA). 10 mg of sample (raw DS and EL100 powders, their physical mixture, and the medicated nanofibers) was placed on the diamond surface plate to be scanned. The scanning range was 500–4000 cm^{-1} at an average of 8 scans and the resolution of 2 cm^{-1}.

2.5. Functional Performance.

A standard equation was built for measuring the content of DS in the unknown samples with phosphate buffered saline (PBS, 0.1 N, pH = 7.0) as the solvent of pure drug using a UV spectrophotometer (UV-2102PC, Unico Instrument Co. Ltd., Shanghai, China). To determine drug loading efficiency (LE), 100 mg of electrospun nanofibers was added to 10 mL of 10% ethanol aqueous solution to extract all the loaded DS. Then the solutions were diluted using PBS to a suitable concentration for UV measurement. The LE was calculated using the following equation:

$$
\begin{aligned}
&\mathrm{LE}\,(\%) \\
&= \frac{(\mathrm{DS\ weight\ measured})}{(\mathrm{DS\ weight\ calculated\ from\ the\ preparation})} \\
&\quad \times 100\%.
\end{aligned}
\tag{2}
$$

The *in vitro* dissolution experiments were performed according to the *Chinese Pharmacopoeia* (2015 Ed.) Method II. This paddle method was executed on a RCZ-8A dissolution apparatus (Tianjin University Radio Factory, Tianjin, China). Samples (0.2 g of electrospun nanofibers and the physical mixture) equivalent to 25 mg of DS were added directly in the dissolution vessel containing 900 mL dissolution liquid (in the first two hours, 0.01 N HCl was used; later, 0.36 g NaOH was added to the dissolution media to neutralize them). The temperature was maintained at 37 ± 1°C and it was stirred at 50 rpm. At predetermined time points, samples of 5.0 mL were withdrawn from the dissolution medium and replaced with 5.0 mL fresh PBS to maintain a constant volume. After filtration using a 0.22 μm membrane (Millipore, Billerica, MA, USA) and appropriate dilution with PBS, samples were analyzed by UV spectroscopy at $\lambda_{\max}$ = 276 nm. All measurements were repeated six times. Percentage of dissolution was readily calculated according to the calibration standard equation of DS.

The *ex vivo* permeation studies were performed using a RYJ-6A diffusion test apparatus (Shanghai Huanghai Drug Control Instrument Co., Ltd.), in which materials were mounted in six Keshary-Chien glass diffusion cells and a water bath system maintained a constant temperature of 37 ± 0.2°C. Each cell had a diffusion area of 2.60 cm^2, and the receptor compartment had a capacity of 7.2 mL PBS. Each donor compartment was filled with 1 mL PBS and the hydrodynamics in the receptor compartment were maintained by stirring with a Teflon coated magnetic bead at 50 rpm. Large intestines were obtained from pigs after slaughtering (Baoshan Jiangwan slaughterhouse, Shanghai, China). The intestine was washed carefully with physiological saline solution (NaCl 0.9% w/v) to remove nondigested food. The biomembranes peeled off from the intestines were fixed on the diffusion cells with the mucosal walls upward. They were equilibrated for 30 min before permeation tests.

Physical mixture of EL100 and DS and nanofibers F2 and F4 (100 mg) were placed on the biomembrane surface. Samples (1 mL) were withdrawn from the receptor compartment at timed intervals and 1 mL fresh PBS was compensated. The samples were filtered through a 0.22 μm membrane (Millipore, USA). The absorption of filtrate was measured at 276 nm to determine DS presented in the water phase. All the measurements were carried out in triplicate.

3. Results and Discussion

3.1. Modified Coaxial Electrospinning.

A schematic diagram of the modified coaxial electrospinning is shown in Figure 1(a). Just as a traditional coaxial electrospinning system and also a single-fluid electrospinning system, the modified coaxial electrospinning system consists of four components to exploit the electrostatic force: a power supply, one or two syringe pumps, a fiber collector, and a spinneret. The spinneret is the most important part in a system. It not only provides a template for creating structural nanofibers (such as core-shell and side-by-side), but also determines how many working fluids are needed during the process and correspondingly the needed syringe pumps.

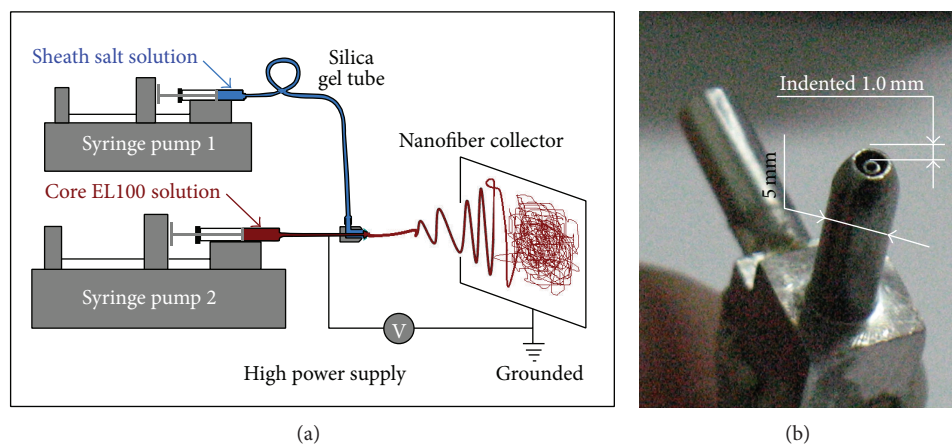(a)   (b)

FIGURE 1: Modified coaxial electrospinning with a salt solution as shell fluid: (a) a schematic diagram shows the components of a modified coaxial electrospinning system; (b) a digital picture of the homemade concentric spinneret.

TABLE 1: Parameters of the electrospinning processes and their products.

Number	Process[a]	Shell-to-core fluid flow rate ratio	Morphology[b]	Diameter[c] (μm)
F1	Single	0	Linear	1.43 ± 0.56
F2		0.05	Linear	0.91 ± 0.23
F3		0.1	Linear	0.75 ± 0.10
F4	Coaxial	0.2	Linear	0.46 ± 0.12
F5		0.3	Linear with a few spindles	0.28 ± 0.14
F6		0.5	Mixed	—

[a]A fixed core fluid flow rate of 1.0 mL/h was exploited.
[b]"Linear" morphology refers to fibers with few beads or spindles and "mixed" morphology refers to nanofibers with beads, spindles, and clumps.
[c]Expressed as the mean ± SD of over 100 fiber diameter measurements.

A digital picture of the homemade concentric spinneret exploited in the present study is shown in Figure 1(b). According to reports in literature, in a concentric spinneret, the reasonable design should be a one in which the inner capillary often projected slightly out the outer capillary. These characteristics help to prevent diffusion and mixture of the core and shell liquids during the electrospinning process. However, here the upper surface of the nozzle of inner capillary was designed to be indented 1.0 mm from the tip of the outer capillary. This should facilitate easier envelopment of the core working fluid by the shell salt solution.

At all the experiments, the core fluid flow rate was fixed at 1.0 mL/h. The shell-to-core fluid flow rate ratio was exploited as a controlled factor to manipulate the electrospinning processes. Six types of fibers were fabricated with the flow rate of shell NaCl solutions increased from 0 to 0.05, 0.1, 0.2, 0.3, and 0.5 mL/h, and they were denoted as F1, F2, F3, F4, F5, and F6, respectively (Table 1).

3.2. The Influence of the Shell Salt Solutions on the Modified Coaxial Processes. Observations of the electrospinning processes for preparing F1 and F3 to F6 and the arrangement of the apparatuses are shown in Figure 2. The spinneret was horizontally placed and connected with the syringe pump driving the core EL100 solution. The shell salt solution driven by another pump was connected with the spinneret

through high elastic silica tubing. The collector, a cardboard wrapped with an aluminum foil, was vertical and kept a 20 cm distance from the nozzle of the spinneret. Both the connections between the high power supply and the spinneret and the grounded line and fiber collector were alligator clips (Figure 2(a) and its inset).

Regardless of one fluid or double fluids, the single-fluid and coaxial electrospinning would experience the three steps similarly, that is, the formation of Taylor cone, the emission of a straight fluid jet from the Taylor cone, and the bending and whipping instable region. However, the single-fluid electrospinning of core EL100 solution was very easy to be clogged due to the formation of semisolid substance around the spinneret (Figure 2(b)). Thus manual removal of the substance was needed now and then to ensure a continuous preparation of fibers F1. This phenomenon should have a close relationship with the easy evaporation of ethanol and the strong interactions between EL100 molecules and the metal spinneret. When there was shell fluid, despite only a small shell-to-core fluid flow rate ration of 0.05 for the preparation of fiber F2, the clogging phenomena were greatly decreased and the straight fluid jets had a variable length. When the flow rate of shell fluid was increased to 0.1 mL/h for producing fibers F3, the modified coaxial electrospinning could run continuously and stably with an embedded Taylor cone and a long straight fluid jet of 35 mm (Figure 2(c) and its
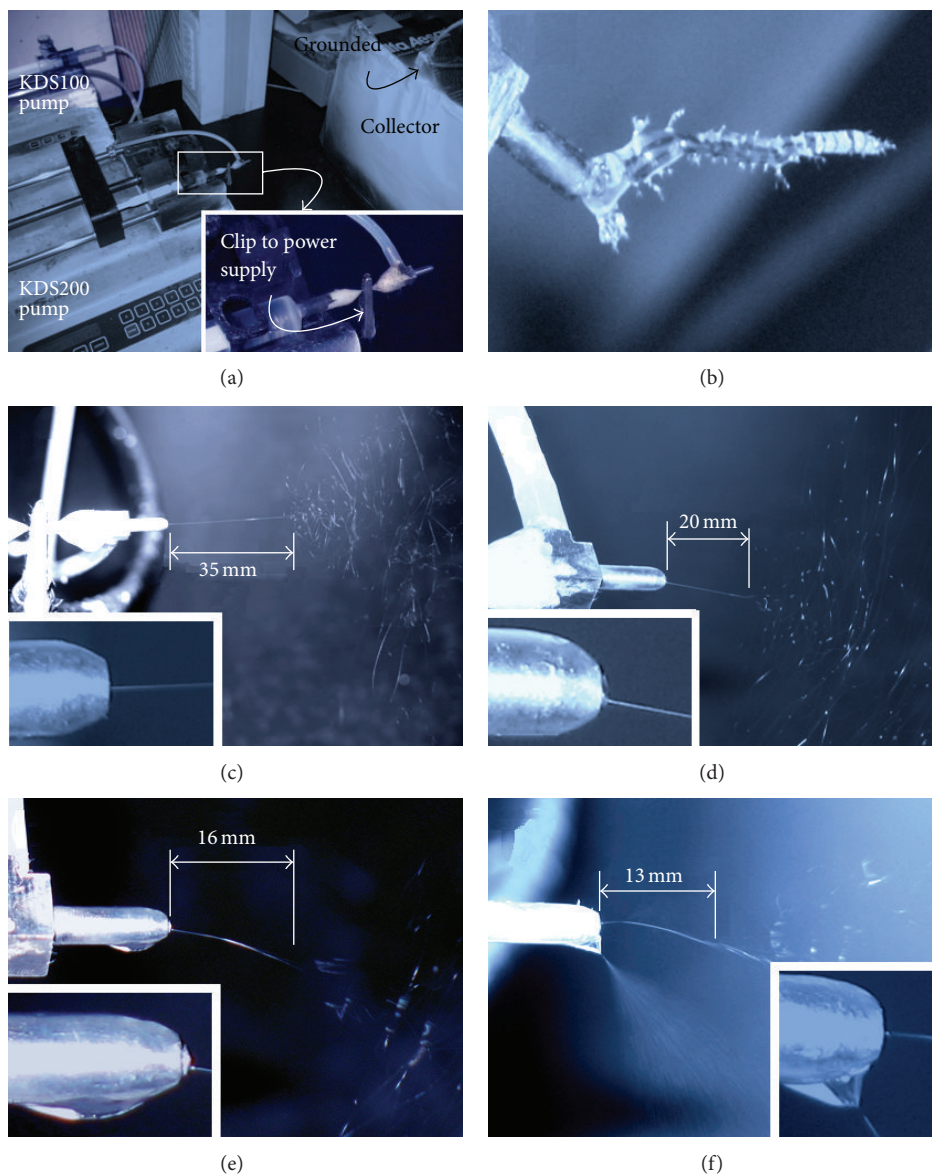
(a)

(b)

(c)

(d)

(e)

(f)

Figure 2: Observations of the electrospinning processes: (a) a digital picture showing the arrangement of apparatuses of the modified coaxial electrospinning system, the bottom-right inset showing the connection of the spinneret with power supply using an alligator clip; (b) a digital picture showing the clogging phenomenon during the single-fluid electrospinning of core EL100 solution; ((c)–(f)) digital pictures showing the production of F3 to F6 using the modified coaxial electrospinning under a shell-to-core fluid flow rate ratio of 0.1 to 0.2, to 0.3, and to 0.5, respectively. The applied voltage was fixed at 14 kV. The left-bottom insets show an enlarged view of the Taylor cone corresponding to the modified coaxial processes.

inset, Table 2). The increase of shell fluid flow rate to 0.2 mL/h and 0.3 mL/h resulted in a similar process, but with a shorter straight fluid jet of 20 mm and 16 mm (Figures 2(d) and 2(e), Table 2) and a discerned Taylor cone (the inset of Figures 2(d) and 2(e)).

With further increase of the shell fluid flow rate to 0.5 mL/h, there were often two separate EHDA processes that happened at the nozzle spinneret (Figure 2(f) and its inset, Table 2). One was still an electrospinning process with a straight fluid of 13 mm, and the other was a typical electrospraying process. The shell solution had a better conductivity but a smaller viscosity than the core fluid and maybe also some action of the gravity of the shell fluid; the division of the core EL solution and shell NaCl solution was inevitable when an excessive shell fluid was driven out. Thus for a stable and robust modified coaxial electrospinning process, a reasonable selection of shell fluid flow rate is very important.

3.3. Morphology of Fibers and Their Size Distribution.

Just as anticipated, fibers F1 fabricated using single-fluid electrospinning of the core EL100 solution show a complicated
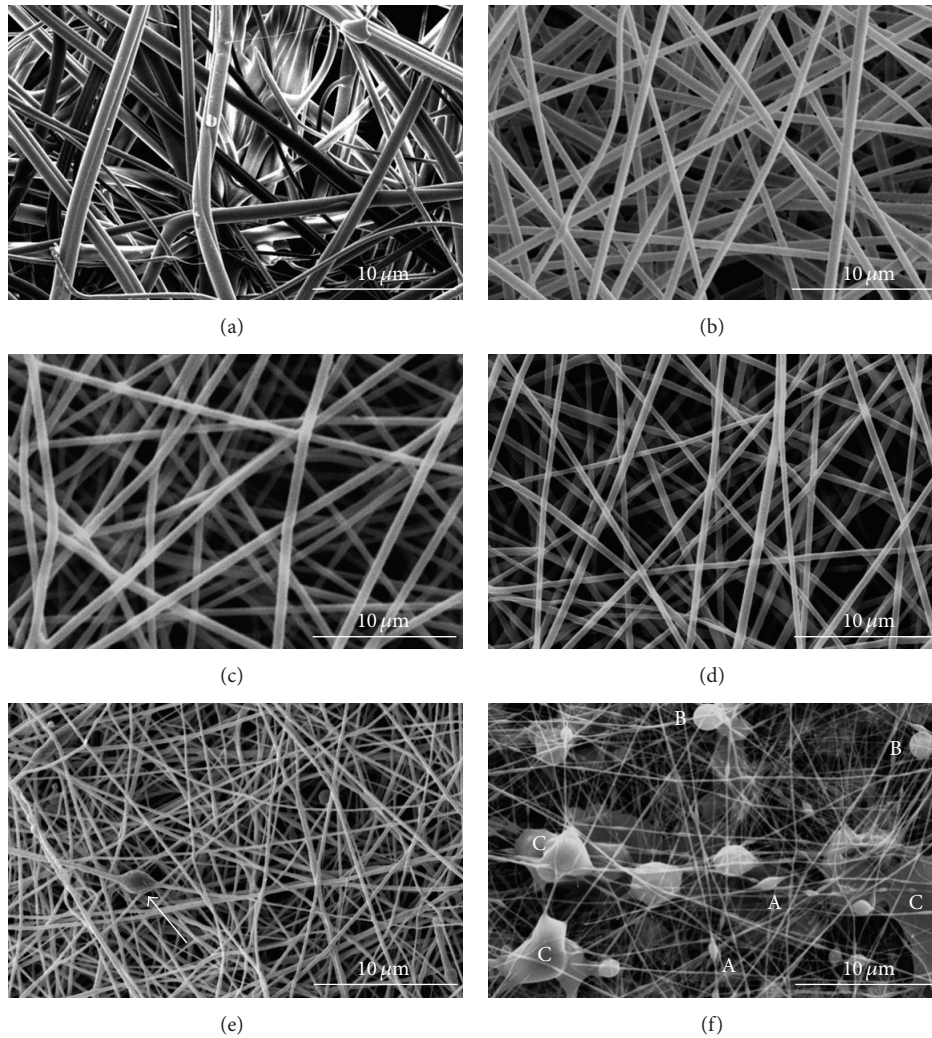
(a)

(b)

(c)

(d)

(e)

(f)

FIGURE 3: FESEM images of the medicated nanofibers: (a) F1, (b) F2, (c) F3, (d) F4, (e) F5, and (f) F6.

TABLE 2: The different behaviors of working fluids under different shell fluid flow rate.

Number	Process	F^{a}	Taylor cone	Straight fluid jet[b]	Instable region
F1	Single	0	Clogging	Varied	Discontinuous bending and whipping
F2	Coaxial	0.1	Indented	35 mm	Continuous and stable bending and whipping
F3		0.2	Smaller	20 mm	Continuous and stable bending and whipping
F4		0.5	Double	13 mm	A combination of spraying and spinning

[a]F refers to sheath-to-core fluid flow rate ratio.
[b]The values are estimated according to the size of spinneret shown in Figure 1(b).

morphology (Figure 3(a)). Some large fibers showed a "side-by-side" topography. The quick evaporation of solvent from the surface of fluid jets generated solid skin on the fibers firstly; later the escape of trapped solvent in the inner part of fibers and the barometric pressure deformed the fibers to form a concave on their surface. The randomly collected fibers distributed ununiformly and some fibers are several times larger than others, reflecting a poor size distribution. In sharp contrast, fibers F2, F3, and F4 show a uniform distribution with all of them exhibiting a linear morphology. No beads-on-a-string or spindles-on-a-line morphology occurs. Also no particles can be discerned on the surface of fibers, suggesting no solid phase separation during the electrospinning processes (Figures 3(b), 3(c), and 3(d)). However, when an abundant shell fluid was pumped during the coaxial processes, nanofibers F5 have some spindles on them (as indicated by the arrow in Figure 3(e)). When excessive shell fluid was provided, nanofibers F6 exhibited a mixed

morphology (Figure 3(f)). Not only do many beads-on-a-string/spindles-on-a-line morphologies occur (as indicated by "A" in Figure 3(f)), but also round particles (as indicated by "B" in Figure 3(f)) and even large clumps (as indicated by "C" in Figure 3(f)) can be found in the fiber mat. During the division of shell and core fluids (Figure 2(f)), the shell solutions should "rob" some EL100 and DS from the core liquid. Thus the core solution with a lower concentration than the original value experienced an electrospinning process to form the spindles-on-a-line morphology, whereas the shell fluids were subjected to an electrospraying process with varied concentrations of the solutes, which in turn resulted in the particles and clumps on the fiber mats.

The diameters' distributions of fibers F1 to F5 are shown in Figures 4(a) to 4(e). Obviously, fibers from the coaxial processes have a finer diameter value and a more homogeneous size distribution ($0.91 \pm 0.23\,\mu$m in Figure 4(b) for fibers F2, $0.75 \pm 0.10\,\mu$m in Figure 4(c) for fibers F3, $0.46 \pm 0.12\,\mu$m in Figure 4(d) for fibers F4, and $0.28 \pm 0.14\,\mu$m in Figure 4(e) for fibers F5) than fibers F1 from the single-fluid electrospinning ($1.43 \pm 0.56\,\mu$m in Figure 4(a)). The single-fluid electrospinning can be regarded also as a modified coaxial process, in which the shell fluid flow rate was 0 mL/h. The relationships between the fibers' diameter and the shell-to-core fluid flow rate ratio are exhibited in Figure 4(f). Regressed using power function, a scaling law of $D = 0.174F^{-0.579}$ ($R^2 = 0.9877$) can be built, which shows better relativity than a regressed linear equation $D = 1.017 - 2.571F$ ($R^2 = 0.9241$) within an F range of 0 to 0.3. Thus the power function equation can be used to predict the diameters of nanofibers fabricated using the coaxial processes within a suitable range of shell solutions' flow rates.

Right after the reviving of electrospinning around 1995, researchers are always looking for new ways for generating nanofibers with tunable diameters. Based on the single-fluid electrospinning, operative parameters, environmental conditions, additives, and also the physical and chemical properties of working fluids have been exploited to exert active influence on the reduction of the nanofibers [24–26]. However, the results were far from satisfactory. The aim of obtaining ultra-thin nanofibers is often compromised by the detriment of nanofiber quality when a single-fluid process is exploited. This is due to the complicated electro-fluid-mechanical property of the electrospinning process and often the filament-forming polymer only having a narrow electrospinnable window. Here, with salt solutions as shell fluids, the coaxial process can be used to fabricate nanofibers in a controllable approach.

A diagram of the mechanism about the sheath fluid flow rate on the formation of polymeric nanofibers is shown in Figure 5. Compared with the electrical force (E) applied on the working fluids, the gravity (G) is often very small and can be neglected [9]. The sheath fluid exerts its influence mainly in the regions of "A" Taylor cone and "B" bending and whipping and in turn the final products in region "C." When there is no sheath fluid, a standard single-fluid electrospinning process can create fibers from the electrospinnable polymeric solutions. When evaporative solvent is utilized to prepare the solution, clogging easily occurs. When a sheath fluid is exploited, it can lubricate the spinneret and provide a liquid protection to prevent the formation of semisolid substance on the surface of fluid jets. Within a suitable range of sheath-to-core fluid flow rate ratio, the increase of sheath fluid flow rate would keep the bending and whipping jets in a fluid state for a longer time to be subjected to the drawing from the electrical forces. Thus fibers with smaller diameter can be achieved. This mechanism is obviously different from a previous publication in which LiCl solution was used as sheath fluid to fabricate polyacrylonitrile nanofibers, where the strategy is to increase LiCl concentrations and thus elevate the electrical drawing forces [9]. Certainly, excessive sheath fluid flow rate would result in the division of Taylor cone and the formation of products with mixed morphology.

3.4. Physical Form and the Compatibility between Components.

As shown in Figure 6(a), the XRD patterns of DS have many sharp peaks, reflecting that the drug is essentially a crystalline material. The XRD pattern of EL100 shows a hump, indicating that it is an amorphous polymeric matrix. Just as anticipated, the physical mixture of drug and polymer has sharp peaks in its XRD patterns. In contrast, there are not any drug peaks occurring in the patterns of fibers F2 and F4. Thus it can be concluded that the coaxial process had altered the drug physical status from crystalline form to an amorphous form with the polymeric matrix.

The ATR-FTIR spectra of raw materials, their physical mixture, and nanofibers F2 and F4 are shown in Figure 6(b). DS has a characteristic peak at $1577\,cm^{-1}$, which should be attributed to the C=C stretch vibration of phenyl groups. EL100 has a characteristic band at $1734\,cm^{-1}$ due to C=O stretch vibration of carbonyl groups. Both of these two above-mentioned characteristic peaks occur in the spectra of physical mixture, reflecting that few interactions happen between the double components in the mixture. However, the characteristic bands of both DS and EL100 disappear in the spectra of nanofibers F3, but a new band of $1691\,cm^{-1}$ occurs. According to the molecular structure of DS and EL100, this change should be attributed to the formation of hydrogen bonds between them.

The solidification from fluid jets to solid nanofibers during the electrospinning process is very quick, often on a time scale of 10^{-2} s. Thus it is thought that the physical forms of the components in the solutions are able to be propagated into the medicated nanofibers after electrospinning [27]. Provided favorable secondary interactions exist between them, the drug and carrier can coexist or mix in a molecular way, which can effectively retard the recrystallization of DS. Thus the medicated nanofibers from the coaxial process are essentially solid dispersions or nanocomposites.

3.5. Functional Performance.

A UV scan of the DS solution containing $20\,\mu$g/mL is shown in the inset of Figure 7(a). DS has a maximum absorbance at 276 nm. Thus this wavelength was exploited to build the standard equation, which is expressed as $A = 0.0082 + 0.0323C$ ($R = 0.9991$) within
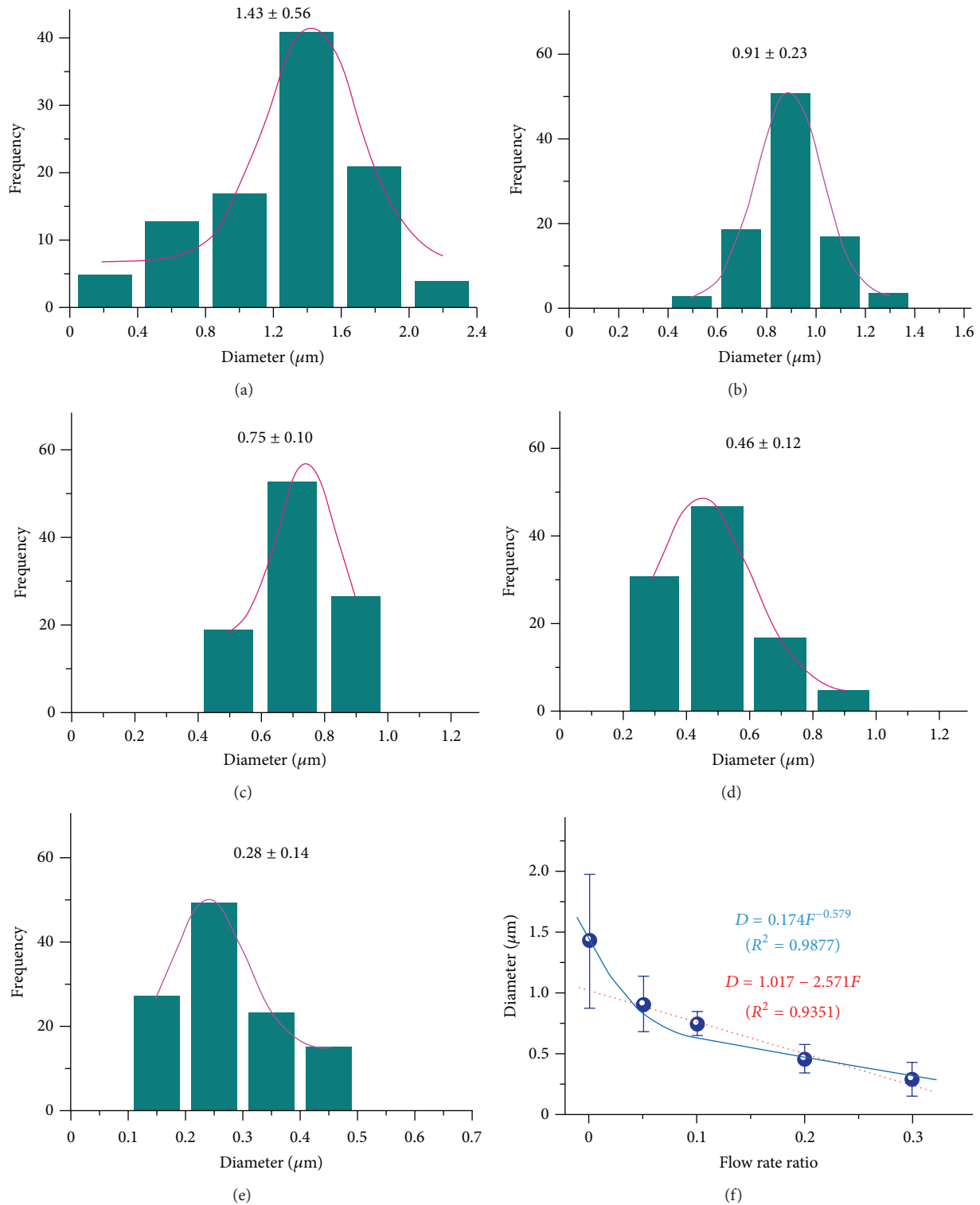
(a)

(b)

(c)

(d)

(e)

(f)

FIGURE 4: The influence of shell salt solutions' flow rate on the size of medicated fibers: ((a)–(e)) diameter distribution of fibers F1 to F5; (f) the relationships between the fibers' diameter and the shell-to-core fluid flow rate ratio.

a linear range from 2 to 50 μg/mL in Figure 7(a). Six times of the detection of the drug content in the nanofibers is 12.2 ± 0.4%, almost the same with the calculated value according to the feed in preparation.

The drug *in vitro* release profiles of the electrospun medicated nanofibers F2 and F4 and the physical mixture are shown in Figure 7(b). Apparently, the medicated nanofibers have altered the drug release behaviors in two aspects. First,
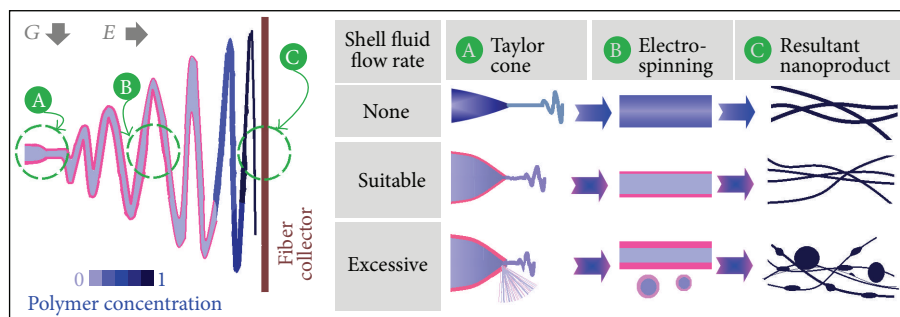
FIGURE 5: A diagram of the mechanism about the sheath fluid flow rate on the formation of polymeric nanofibers. *G* and *E* represent gravity and electrical force, respectively.
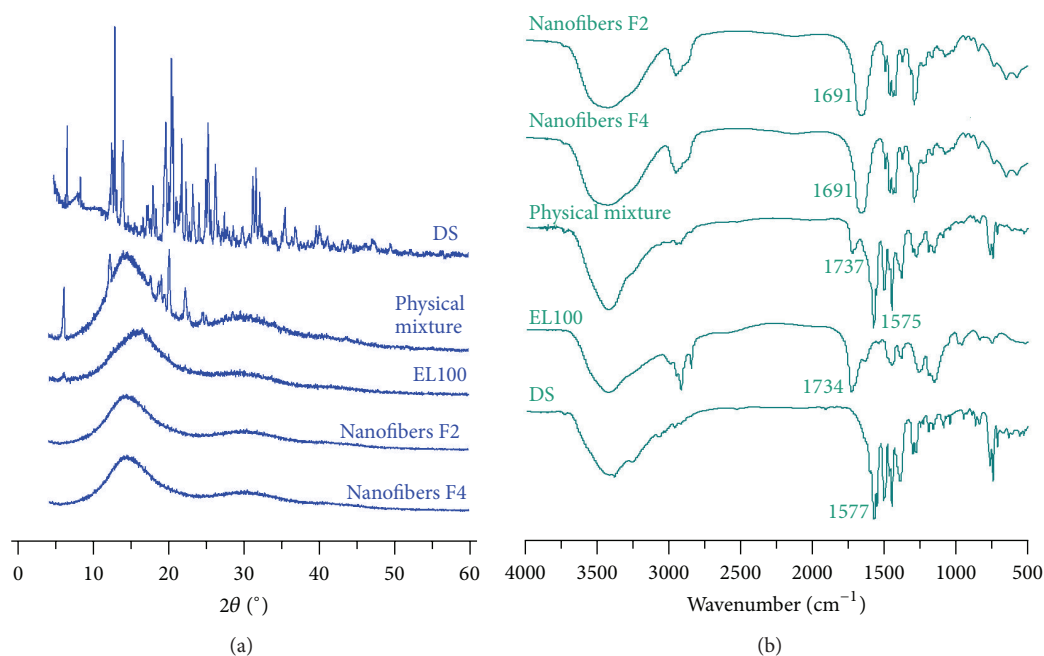

FIGURE 6: Physical forms of components and their compatibility in composite nanofibers: (a) XRD patterns; (b) ATR-FTIR spectra.

as a pH-sensitive polymeric matrix, EL100 has successfully retarded the drug release in an acid environment of pH = 2 at the first two hours. Second, the nanofibers prolonged the drug release time period in the neutral condition. Thus, these medicated nanofibers have the potential applications as oral drug delivery systems that provide a colon-targeted sustained release profile. Nanofibers F4 provided a better drug release profile than nanofibers F2 in that the former has a shorter time period of "tailing-off" release. Many commercial tablets are essentially a physical mixture of drug and polymeric carrier, which is expected to change the drug release behaviors through the polymers' physicochemical properties. However, the effect is often very limited because the physical state of drug is almost the same with the raw drug powders. Shown in Figure 7(c) are the FESEM images of raw DS particles. In the commercial tablets, DS still presents in a cubic crystal format. However, when DS was encapsulated into EL nanofibers, the DS molecules would disperse in the polymeric matrix in an amorphous state (Figure 7(d)).

Accompanied with the polymer physical entanglements, the favorable drug-polymer interactions would play their roles in keeping the stability of the drug-polymer nanocomposites. Thus in the acid condition, the insoluble property of EL100 would protect the loaded DS molecules to retard its release. And in the neutral condition, the slow dissolution of EL100 would gradually release the contained DS in a sustained manner. With the same raw materials, electrospun medicated nanofibers were able to provide a better drug controlled release profile. Thus a more effective drug absorbance and a longer therapeutic blood concentration can be expected after oral administration.

The results of permeation tests on colon membrane are shown in Figure 8. After 12 h, 3.92 ± 0.59, 7.85 ± 0.81, and 8.24 ± 0.73 mg of DS were transmitted into the receptor cells. Although, in the *in vitro* tests, the physical mixture released DS faster than nanofibers F2 and F4, the nanofibers could promote double permeated DS molecules through the colon membrane. This contradictory experimental result

(a)

- ■ Nanofibers F4
- ○ Physical mixture
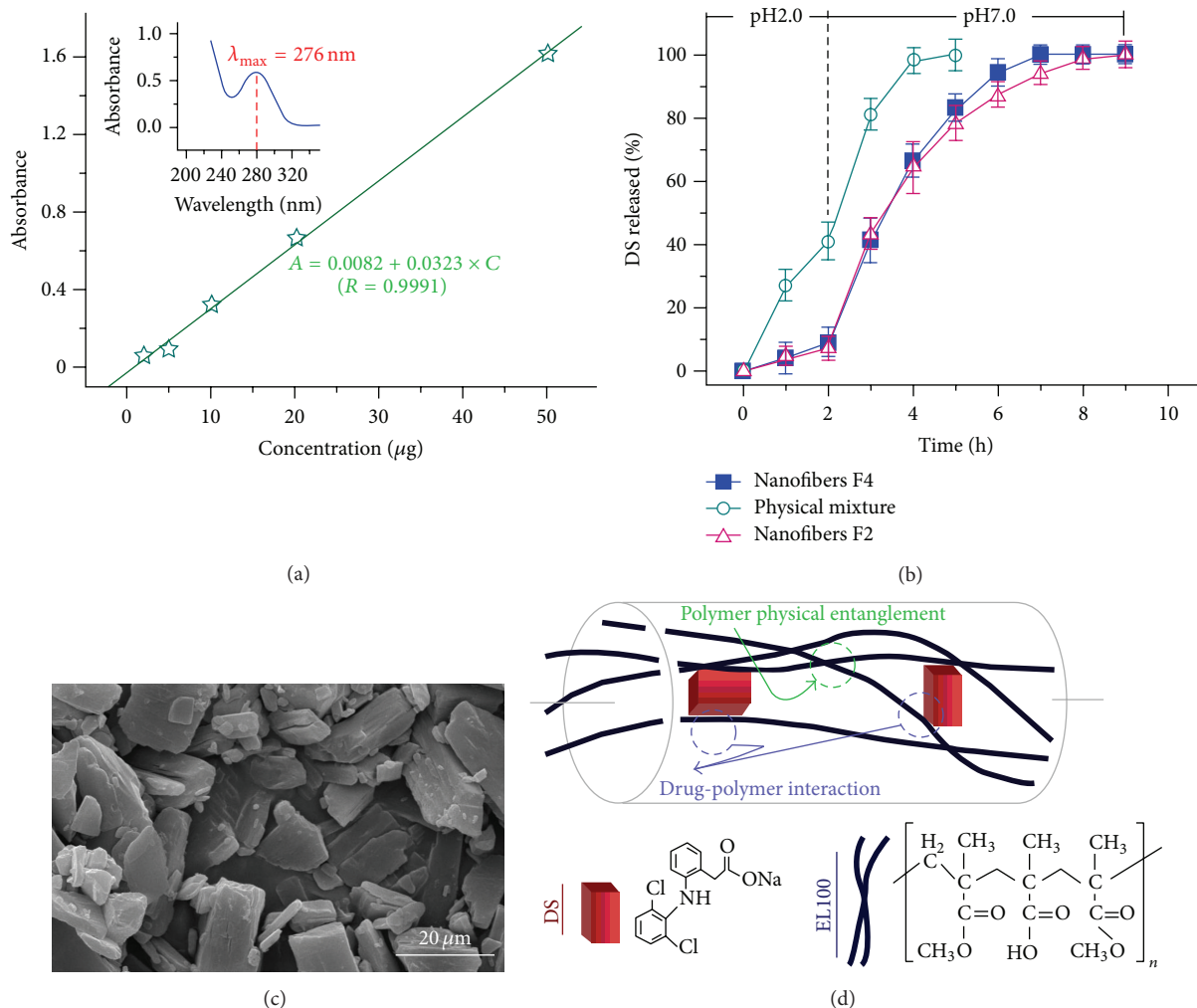- △ Nanofibers F2

(b)

(c)

(d)

FIGURE 7: Functional performance of the composite medicated nanofibers: (a) the standard equation for the detection of DS using UV spectrophotometer; (b) the *in vitro* DS release profiles of nanofibers F2 and F4 and the control samples of physical mixture ($n = 6$); (c) FESEM images of the raw DS particles; (d) a diagram of the distribution of DS molecules in their polymeric matrix.

should be attributed to the different physical state of DS; its amorphous state in the nanofibers made DS molecules easy to be dissolved and permeate through the membrane in the donor cell with very limited dissolution media. In sharp contrast, the crystalline DS powders were difficult in dissolution and permeation when they were put on the colon membrane in the donor cells. Nanofibers F4 showed slightly better permeation results than nanofibers F4, which have a larger diameter. By the way, for potential oral administration, the encapsulation of DS in polymeric carrier should alleviate the potential anaphylactic reaction of drug particles with the digestive tracts.

4. Conclusions

Modified coaxial electrospinning was successfully developed to promote the nanofabrication of medicated fibers, in which salt solutions were employed as sheath fluids. Based on the usage of a homemade concentric spinneret, coaxial electrospinning was implemented under different flow rates of shell solutions. A scaling law between the fibers' diameter (D, μm) and the shell-to-core fluid flow rate ratios (F) was built as $D = 0.174F^{-0.579}$ ($R^2 = 0.9877$). XRD and ATR-FTIR results demonstrated that the electrospun nanofibers were essentially nanocomposites, where the drug had fine compatibility with its polymeric carrier. The coaxial process would not result in drug loss during the preparation. *In vitro* tests verified that the medicated nanofibers were able to release the contained drug in a sustained manner in the neutral condition, appearing better functional performance than their physical mixture. *Ex vivo* permeation studies demonstrated that the nanofibers were able to provide a double permeated amount of drug through the colon membrane compared to the corresponding physical mixture. It is concluded that coaxial electrospinning with a salt solution as a sheath fluid comprises a facile process for producing medicated nanomaterials with tunable diameters and improved functional performance.
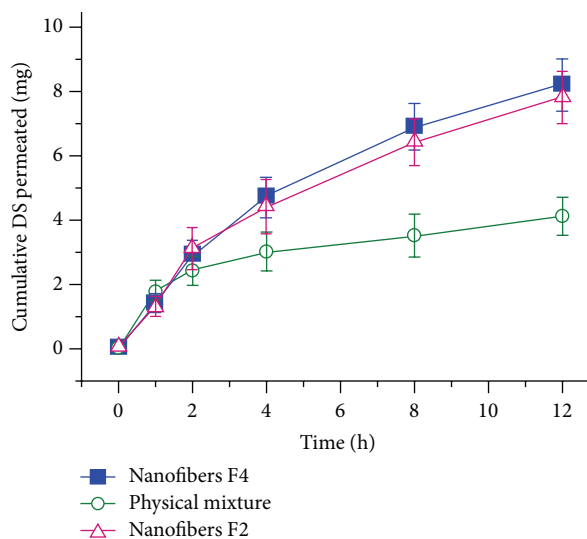
FIGURE 8: *Ex vivo* permeation tests of nanofibers F2 and F4 and the control samples of physical mixture on biomembrane ($n = 3$).

Competing Interests

The authors declare that they have no competing interests.

Acknowledgments

References

[1] M. A. Alam, F. I. Al-Jenoobi, and A. M. Al-Mohizea, "Commercially bioavailable proprietary technologies and their marketed products," *Drug Discovery Today*, vol. 18, no. 19-20, pp. 936–949, 2013.

[2] S. Mitragotri, P. A. Burke, and R. Langer, "Overcoming the challenges in administering biopharmaceuticals: formulation and delivery strategies," *Nature Reviews Drug Discovery*, vol. 13, no. 9, pp. 655–672, 2014.

[3] E. Merisko-Liversidge and G. G. Liversidge, "Nanosizing for oral and parenteral drug delivery: a perspective on formulating poorly-water soluble compounds using wet media milling technology," *Advanced Drug Delivery Reviews*, vol. 63, no. 6, pp. 427–440, 2011.

[4] S. Chakraborty, I.-C. Liao, A. Adler, and K. W. Leong, "Electrohydrodynamics: a facile technique to fabricate drug delivery systems," *Advanced Drug Delivery Reviews*, vol. 61, no. 12, pp. 1043–1054, 2009.

[5] D. I. Braghirolli, F. Zamboni, G. A. X. Acasigua, and P. Pranke, "Association of electrospinning with electrospraying: a strategy to produce 3D scaffolds with incorporated stem cells for use in tissue engineering," *International Journal of Nanomedicine*, vol. 10, pp. 5159–5170, 2015.

[6] K. Siimon, K. Mõisavald, H. Siimon, and M. Järvekülg, "Increasing mechanical strength of electrospun gelatin nanofibers by the addition of aluminum potassium sulfate," *Journal of Applied Polymer Science*, vol. 132, no. 35, pp. 42431–42435, 2015.

[7] K. S. Liu, C. H. Lee, Y. C. Wang, and S. J. Liu, "Sustained release of vancomycin from novel biodegradable nanofiber-loaded vascular prosthetic grafts: in vitro and in vivo study," *International Journal of Nanomedicine*, vol. 10, pp. 885–891, 2015.

[8] T. J. Sill and H. A. von Recum, "Electrospinning: applications in drug delivery and tissue engineering," *Biomaterials*, vol. 29, no. 13, pp. 1989–2006, 2008.

[9] D.-G. Yu, P. Lu, C. Branford-White, J.-H. Yang, and X. Wang, "Polyacrylonitrile nanofibers prepared using coaxial electrospinning with LiCl solution as sheath fluid," *Nanotechnology*, vol. 22, no. 43, Article ID 435301, 2011.

[10] G. Chen, Y. Xu, D.-G. Yu, D.-F. Zhang, N. P. Chatterton, and K. N. White, "Structure-tunable Janus fibers fabricated using spinnerets with varying port angles," *Chemical Communications*, vol. 51, no. 22, pp. 4623–4626, 2015.

[11] S. Agarwal, A. Greiner, and J. H. Wendorff, "Functional materials by electrospinning of polymers," *Progress in Polymer Science*, vol. 38, no. 6, pp. 963–991, 2013.

[12] D. G. Yu, C. Yang, M. Jin et al., "Medicated Janus fibers fabricated using a Teflon-coated side-by-side spinneret," *Colloids and Surfaces B: Biointerfaces*, vol. 138, no. 2, pp. 110–116, 2016.

[13] D.-G. Yu, X.-Y. Li, X. Wang, J.-H. Yang, S. W. A. Bligh, and G. R. Williams, "Nanofibers fabricated using triaxial electrospinning as zero order drug delivery systems," *ACS Applied Materials and Interfaces*, vol. 7, no. 33, pp. 18891–18897, 2015.

[14] C. Yang, D. G. Yu, D. Pan et al., "Electrospun pH-sensitive core-shell polymer nanocomposites fabricated using a tri-axial process," *Acta Biomaterialia*, vol. 35, no. 15, pp. 77–86, 2016.

[15] D.-G. Yu, W. Chian, X. Wang, X.-Y. Li, Y. Li, and Y.-Z. Liao, "Linear drug release membrane prepared by a modified coaxial electrospinning process," *Journal of Membrane Science*, vol. 428, pp. 150–156, 2013.

[16] L. Y. Yeo and J. R. Friend, "Electrospinning carbon nanotube polymer composite nanofibers," *Journal of Experimental Nanoscience*, vol. 1, no. 2, pp. 177–209, 2006.

[17] O. Salata, "Tools of nanotechnology: electrospray," *Current Nanoscience*, vol. 1, no. 1, pp. 25–33, 2005.

[18] A. Balogh, T. Horváthová, Z. Fülöp et al., "Electroblowing and electrospinning of fibrous diclofenac sodium-cyclodextrin complex-based reconstitution injection," *Journal of Drug Delivery Science and Technology*, vol. 26, pp. 28–34, 2015.

[19] X. Li, M. A. Kanjwal, L. Lin, and I. S. Chronakis, "Electrospun polyvinyl-alcohol nanofibers as oral fast-dissolving delivery system of caffeine and riboflavin," *Colloids and Surfaces B: Biointerfaces*, vol. 103, no. 3, pp. 182–188, 2013.

[20] X. Li, L. Lin, Y. Zhu, W. Liu, T. Yu, and M. Ge, "Preparation of ultrafine fast-dissolving cholecalciferol-loaded poly(vinyl pyrrolidone) fiber mats via electrospinning," *Polymer Composites*, vol. 34, no. 2, pp. 282–287, 2013.

[21] Z. K. Nagy, A. Balogh, B. Démuth et al., "High speed electrospinning for scaled-up production of amorphous solid dispersion of itraconazole," *International Journal of Pharmaceutics*, vol. 480, no. 1-2, pp. 137–142, 2015.

[22] D.-G. Yu, Y. Xu, Z. Li, L.-P. Du, B.-G. Zhao, and X. Wang, "Coaxial electrospinning with mixed solvents: from flat to round Eudragit L100 nanofibers for better colon-targeted sustained drug release profiles," *Journal of Nanomaterials*, vol. 2014, Article ID 967295, 8 pages, 2014.

[23] V. Pornsopone, P. Supaphol, R. Rangkupan, and S. Tantayanon, "Electrospun methacrylate-based copolymer/indomethacin fibers and their release characteristics of indomethacin," *Journal of Polymer Research*, vol. 14, no. 1, pp. 53–59, 2007.

[24] H. Wen, C. Yang, D. Yu, X. Li, and D. Zhang, "Electrospun zein nanoribbons for treatment of lead-contained wastewater," *Chemical Engineering Journal*, vol. 290, no. 4, pp. 263–272, 2016.

[25] W. Klairutsamee, P. Supaphol, and I. Jangchud, "Electrospinnability of poly(butylene succinate): effects of solvents and organic salt on the fiber size and morphology," *Journal of Applied Polymer Science*, vol. 132, no. 43, pp. 42716–42726, 2015.

[26] T. Lin and X. Wang, *Encyclopedia of Nanoscience and Nanotechnology*, Edited by H. S. Nalwa, American Scientific, Los Angeles, Calif, USA, 2nd edition, 2011.

[27] W. Qian, D.-G. Yu, Y. Li, X.-Y. Li, Y.-Z. Liao, and X. Wang, "Triple-component drug-loaded nanocomposites prepared using a modified coaxial electrospinning," *Journal of Nanomaterials*, vol. 2013, Article ID 826471, 7 pages, 2013.